1986

Oxidation and reduction reactions of hemerythrin and [mu]-sulfidohemerythrin: mechanism of reduction and implications for electron transfer

Linda Lorraine Pearce
Iowa State University

INFORMATION TO USERS

This reproduction was made from a copy of a manuscript sent to us for publication and microfilming. While the most advanced technology has been used to photograph and reproduce this manuscript, the quality of the reproduction is heavily dependent upon the quality of the material submitted. Pages in any manuscript may have indistinct print. In all cases the best available copy has been filmed.

The following explanation of techniques is provided to help clarify notations which may appear on this reproduction.

1. Manuscripts may not always be complete. When it is not possible to obtain missing pages, a note appears to indicate this.

2. When copyrighted materials are removed from the manuscript, a note appears to indicate this.

3. Oversize materials (maps, drawings, and charts) are photographed by sectioning the original, beginning at the upper left hand corner and continuing from left to right in equal sections with small overlaps. Each oversize page is also filmed as one exposure and is available, for an additional charge, as a standard 35mm slide or in black and white paper format.*

4. Most photographs reproduce acceptably on positive microfilm or microfiche but lack clarity on xerographic copies made from the microfilm. For an additional charge, all photographs are available in black and white standard 35mm slide format.*

***For more information about black and white slides or enlarged paper reproductions, please contact the Dissertations Customer Services Department.**

U·M·I Dissertation Information Service

University Microfilms International
A Bell & Howell Information Company
300 N. Zeeb Road, Ann Arbor, Michigan 48106

Pearce, Linda Lorraine

OXIDATION AND REDUCTION REACTIONS OF HEMERYTHRIN AND MU-SULFIDOHEMERYTHRIN: MECHANISM OF REDUCTION AND IMPLICATIONS FOR ELECTRON TRANSFER

Iowa State University PH.D. 1986

PLEASE NOTE:

In all cases this material has been filmed in the best possible way from the available copy. Problems encountered with this document have been identified here with a check mark __✓__.

1. Glossy photographs or pages _____
2. Colored illustrations, paper or print _____
3. Photographs with dark background _____
4. Illustrations are poor copy _____
5. Pages with black marks, not original copy _____
6. Print shows through as there is text on both sides of page _____
7. Indistinct, broken or small print on several pages __✓__
8. Print exceeds margin requirements _____
9. Tightly bound copy with print lost in spine _____
10. Computer printout pages with indistinct print _____
11. Page(s) _____ lacking when material received, and not available from school or author.
12. Page(s) _____ seem to be missing in numbering only as text follows.
13. Two pages numbered _____. Text follows.
14. Curiing and wrinkled pages _____
15. Dissertation contains pages with print at a slant, filmed as received _____
16. Other _____

_____

_____

University
Microfilms
International

Oxidation and reduction reactions of hemerythrin and μ-sulfidohemerythrin: Mechanism of reduction and implications for electron transfer

by

Linda Lorraine Pearce

A Dissertation Submitted to the
Graduate Faculty in Partial Fulfillment of the
Requirements for the Degree of
DOCTOR OF PHILOSOPHY

Department: Chemistry
Major: Inorganic

Approved:

Signature was redacted for privacy.

In Charge of Major Work

Signature was redacted for privacy.

For the Major Department

Signature was redacted for privacy.

For the Graduate College

Iowa State University
Ames, Iowa

1986

TABLE OF CONTENTS

LIST OF FIGURES

LIST OF TABLES

ABBREVIATIONS

Hr	hemerythrin
P.g. $cytb_5$	Phascolopsis gouldii cytochrome b_5
Mb	myoglobin
cytc	cytochrome c
EPR	electron spin resonance
NMR	nuclear magnetic resonance
MES	2(N-morpholino)ethanesulfonic acid
HEPES	N-2-Hydroethylpiperazine-N'-2ethanesulfonic acid
EPPS	N-(2-hydroxyethyl)piperazine-N'-3propanesulfonic acid
EDTA	ethylene diaminetetraacetate
Tris	tris-hydroxymethyl amino methane
ε_M	molar extinction coefficient, $M^{-1}cm^{-1}$
NLLSQ	nonlinear least squares
LSQ	linear least squares
phen	o-phenanthroline
Glu	glutamic acid
Asp	aspartic acid
His	histidine
Cys	cysteine
pI	isoelectric point
15-ane	1,4,8,12 tetraazacyclopentadecane
$P_{1/2}$	half-saturation power in mW
$metN_3^-$	metazidohemerythrin

μ-S^{2-}semi-metHr	μ-sulfidosemi-methemerythrin
μ-S^{2-}metHr	μ-sulfidomethemerythrin
$(semi\text{-}met)_O$	semi-methemerythrin in the O conformation
$(semi\text{-}met)_R$	semi-methemerythrin in the R conformation
NHE	normal hydrogen electrode
T. zostericola	Themiste zostericola
P. gouldii	Phascolopsis gouldii
redox	oxidation and reduction

DEDICATION

To my parents and my son, David

GENERAL INTRODUCTION

Hemerythrin (Hr) (1,2) is a respiratory protein which can be isolated from several phyla of marine invertebrates. Hr is contained in several species of marine worms, the sipunculids, found on the ocean floor. Unless otherwise stated, Hr in these studies was isolated from the coelomic fluid of the species Phascolopsis gouldii. The function of Hr in sipunculids is to bind oxygen and store it. Apparently, Hr does not act as a transport protein and therefore shows no cooperativity in binding oxygen, nor a Bohr effect (3).

Hr isolated from Phascolopsis gouldii is octameric with a molecular weight of 108,000 Daltons. Each subunit is essentially identical with a molecular weight of 13,500 Daltons, and contains two iron atoms and binds one molecule of oxygen. In each subunit there is one sulfhydryl group from a cysteine residue (4). Modification of this sulfhydryl group by p-hydroxy-mercuribenzoate (5), for example, as well as dilution of the octameric protein results in dissociation of the subunits. Hr contains 113 amino acid residues and is a fairly basic protein with a pI estimated to be from 7.1 to 8.0 (6). Denatured Hr is only sparingly soluble in aqueous solution.

The active site of Hr has been examined using X-ray crystallography (7). The iron atoms have three bridging

ligands; a μ-oxo group and two carboxylate groups from an aspartic acid residue and a glutamic acid residue. One iron atom is coordinated to three imidazoles from histidine residues and the bridging groups, while the other iron atom is ligated to two histidine imidazoles and the bridging groups. The most crystallographically studied structure is that of metazidoHr, where the iron atoms are in the +3 oxidation state and azide ion is bound to the iron atom with only two histidine imidazoles coordinated. The structures for the iron sites in metazidoHr and metHr determined by X-ray crystallography are shown in Figure 1. In oxyHr, the oxygen is thought to coordinate to the site occupied by azide, i.e., to the vacant site on the five-coordinate iron atom of metHr.

The tertiary and quaternary structures of Hr are shown in Figure 2 (7). The majority of amino acid residues are found in four parallel α-helical segments. The iron atoms are buried within these helices and the Fe-Fe axis is approximately perpendicular to the helical axes. The small anions may bind by entering a channel at the end of the subunit and diffusing down the channel formed by the helices to the iron atoms. It has also been suggested that there is a channel which anions may enter on "top" of the iron atoms through a gap between the C and D helices (8). The quaternary structure of Hr is very symmetrical and has been described as a square doughnut. The active sites in the subunits are ~ 30 Å apart.

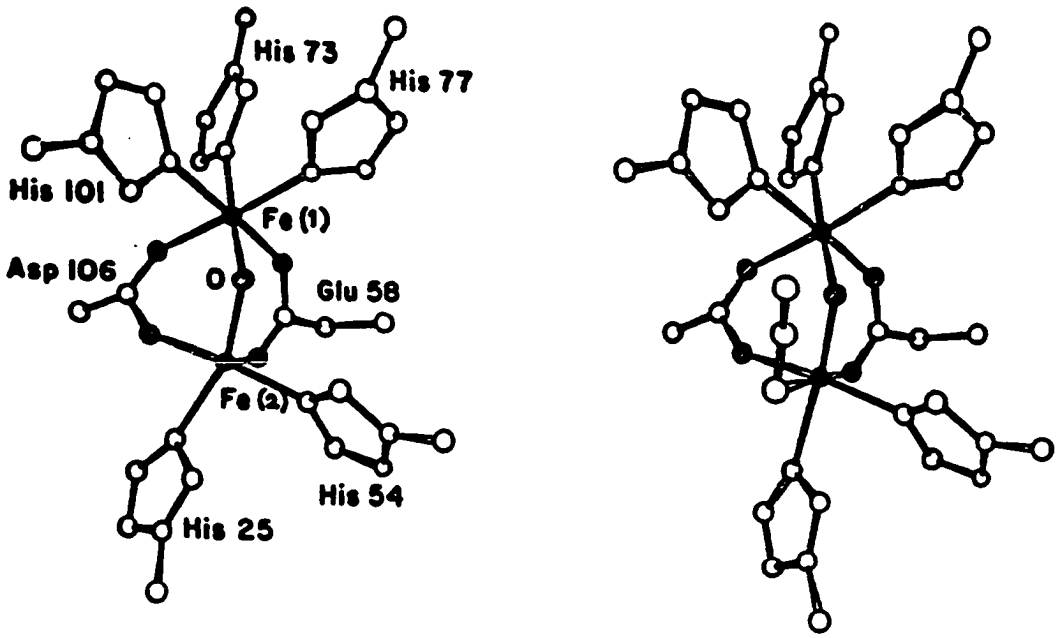

Figure 1. The active site structure of metHr (left) and metazidoHr (right) at 2.0 Å resolution (7)

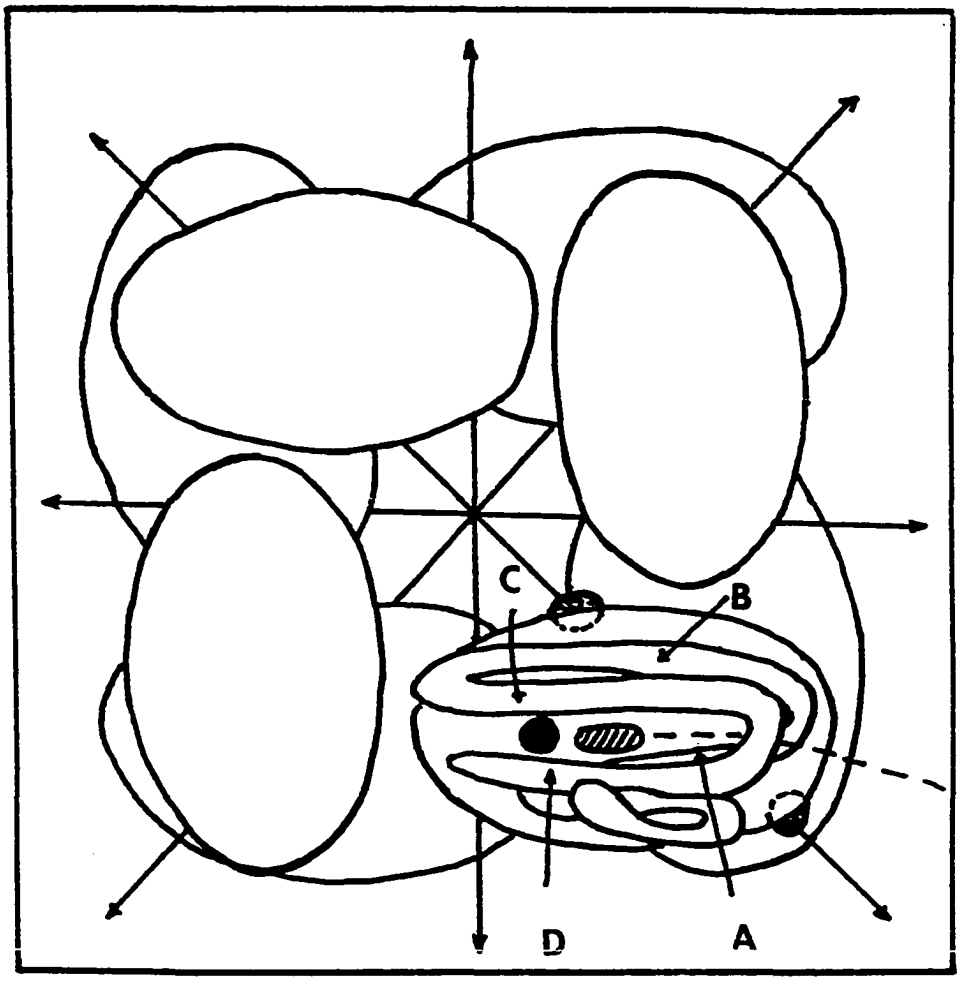

A, B, C, and D label the four parallel helices in each subunit. The solid circle represents the binuclear iron site. The dashed line shows the channel down which anions may diffuse and then bind to the active site. The shaded circles represent binding sites for the perchlorate ion.

Figure 2. Quaternary and tertiary structures of octameric Hr

Hr can reach several oxidation levels. The nomenclature is as follows: MetHr, $[Fe(III),Fe(III)]_8$; oxyHr, $[Fe(III),Fe(III)O_2^{2-}]_8$; deoxyHr, $[Fe(II),Fe(II)]_8$ and semi-metHr, $[Fe(III),Fe(II)]_8$. The iron atoms are high spin and bridged by oxo or hydroxo ions in every case. In all of the derivatives of Hr, the iron atoms are antiferromagnetically coupled. The oxidation states of the iron atoms have been examined by Mössbauer spectroscopy and some representative results are shown in Table 1 (9,10,11,12). ^1H NMR has also been successfully used to determine coupling constants for various derivatives of Hr (13).

The UV-visible absorption spectrum of metHr is pH dependent as shown in Figure 3 and Table 2. The acid-base equilibrium is established slowly (minutes at room temperature) and has a pK_a between 7.0 and 7.4 (14). At higher pH's (pH ~8) it is generally believed that a hydroxide is coordinated to the iron atom at the same site to which azide binds. In the low pH form it is believed that the site where azide binds is open and the iron atom is pentacoordinate. Many small anions other than azide (SCN^-, OCN^-, Cl^- and Br^-, for example) can bind to metHr (15). These anions bind more slowly to the high pH form. Oxygen does not bind to metHr or semi-metHr. Semi-metHr exists in two forms. $(Semi\text{-}met)_O$ is the product of the one-electron oxidation of deoxyHr. $(Semi\text{-}met)_R$ is obtained by one-electron reduction of

Table 1. Mössbauer parameters for Hr derivatives at 77 K[a]

	Fe(III)		Fe(II)		
Derivatives	δ (mm/s)	Δ_{Eq} (mm/s)	δ (mm/s)	Δ_{Eq} (mm/s)	Reference[a]
deoxy			1.19	2.81	9
oxy	0.15	1.93			9
	0.48	1.03			
$metOH_2$	0.46	1.57			9
$metN_3^-$	0.50	1.91			10
μ-S^{2-}met[b]	0.50	0.99			11
μ-S^{2-}semi-met[b]	0.58	1.58	1.14	2.43	12

[a]Isomer shifts are relative to metallic Fe at room temperatures.

[b]Values obtained at 100 K.

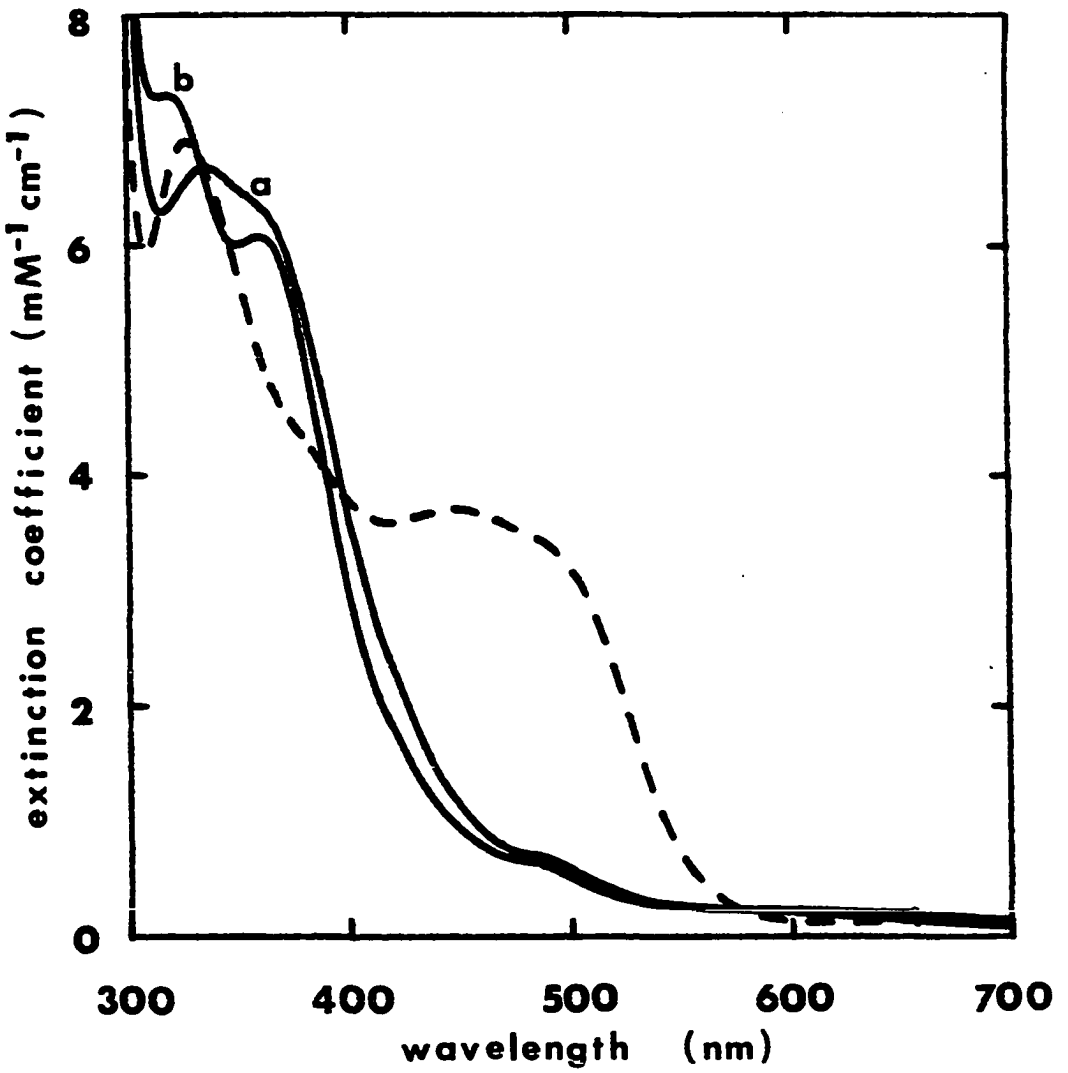

Figure 3. UV-visible absorption spectra of metHr at pH 6.0 (a), pH 8.0 (b) and $metN_3^-$ (---) produced after addition of NaN_3 to (a) or (b)

Table 2. Absorption spectra of hemerythrin derivatives

Hemerythrin Derivatives	LMCT[a] ($O^{2-}\rightarrow Fe$) λ(nm)	ε_M	Exogenous LMCT[a] λ(nm)	ε_M	$^6A_1\rightarrow{}^4T_2(4G)$ λ(nm)	ε_M	$^6A_1\rightarrow{}^4T_2$[b] λ(nm)	ε_M	Reference
oxyHr	330	6800	500	2200	750	200	990	10	15,16
	360	5450							
metHr"hydroxy"	326	6800	480sh	550	597	200	990	8	15,16
high pH form	362	5900							
metHr	355	6400	480sh	600	500sh	200	n.d.		15
low pH form									
$metN_3^-$	326	6750	446	3700	630	190	1010	10.2	15,16
	380	4900							
semi-$metN_3^-$(pH8.2)	315	4400	470	2400	730	~80	920	~20	1,15,16
$(semi\text{-}met)_R$(pH6.2)	350	2000	450	400					1,16
$(semi\text{-}met)_R$(pH8.2)	350	3000	450	460	670	~80	995	~8	15,16

[a]LMCT, ligand to metal charge transfer transition.

[b]Transitions not determined are designated n.d.

metHr. These two forms can be distinguished on the basis of absorption and EPR spectra (Table 3 and Figure 4). The visible spectra of $(semi\text{-}met)_R$ and semi-metazidoHr are shown in Figure 5. The absorption spectrum of $(semi\text{-}met)_R$ is pH dependent. The semi-metHrs exhibit EPR signals due to antiferromagnetic coupling, which produces an S = 1/2 ground state. These EPR signals can be observed near liquid helium temperatures. $(Semi\text{-}met)_O$ has an axially symmetric signal as seen in Figure 4. $(Semi\text{-}met)_R$ has a rhombic EPR signal in which the g-values are pH dependent. The $(semi\text{-}met)_R$ EPR spectrum at pH 6.3 is shown in Figure 4. At pH 8, the signal at g = 1.94 is shifted to g = 1.96. Both $(semi\text{-}met)_O$ and $(semi\text{-}met)_R$ bind azide (as well as other small anions) resulting in a single semi-metazide adduct. The EPR and UV-visible spectra of semi-metazideHr (Table 3 and Figure 4) show little dependence upon pH.

Perchlorate binds to Hr at a secondary site 12 Å away from the iron atoms. Difference electron density maps of T. dyscritum metHr (1,7), with and without perchlorate, show two binding sites. One perchlorate may be hydrogen bonded to an aspartic acid residue near the single cysteine and the other is bound to an ε-amino group of a lysyl residue. The binding of perchlorate causes a decrease in the rate constants for small anion binding. Perchlorate binding also shifts the acid-base equilibrium to the acid form of the protein. X-ray

Table 3. g-values for various semi-methemerythrin derivatives

Species	Derivative	g-values	Reference
octameric P. gouldii	$(semi\text{-}met)_O$, pH 8.2	1.94,1.71	1
octameric P. gouldii	$(semi\text{-}met)_R$, pH 8.2	1.95,1.87,1.65	1
octameric T. zostericola	$(semi\text{-}met)_O$, pH 8.2	1.95,1.72	17
octameric T. zostericola	$(semi\text{-}met)_R$, pH 8.2	1.96,1.88,1.66	17
octameric T. zostericola	$semi\text{-}metN_3^-$, pH 8.2	1.90,1.81,1.49	17
octameric P. gouldii	$semi\text{-}metN_3^-$, pH 8.2	1.90,1.81,1.49	17
octameric P. gouldii	$\mu\text{-}S^{2-}semi\text{-}met$, pH 8.2	1.89,1.70,1.40	12

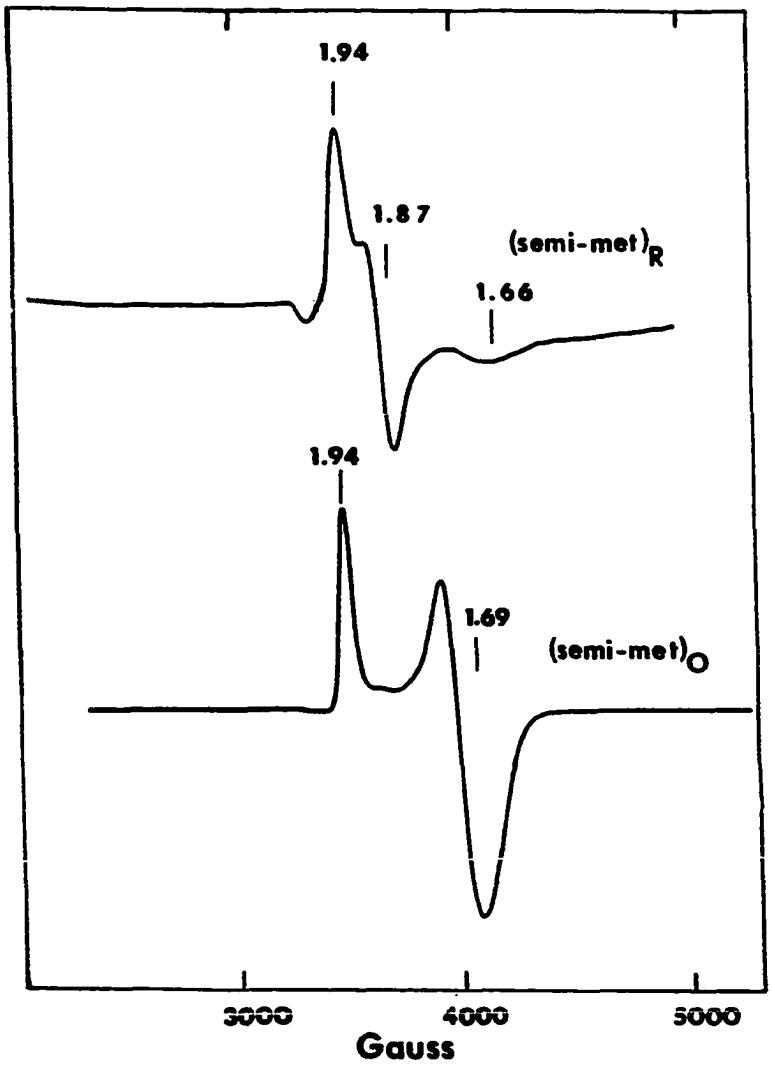

Numbers near signals indicate positions of g values.

Figure 4. $(Semi\text{-}met)_O$ and $(semi\text{-}met)_R$Hr EPR spectra at 4 K, pH 6.3 (50 mM MES)

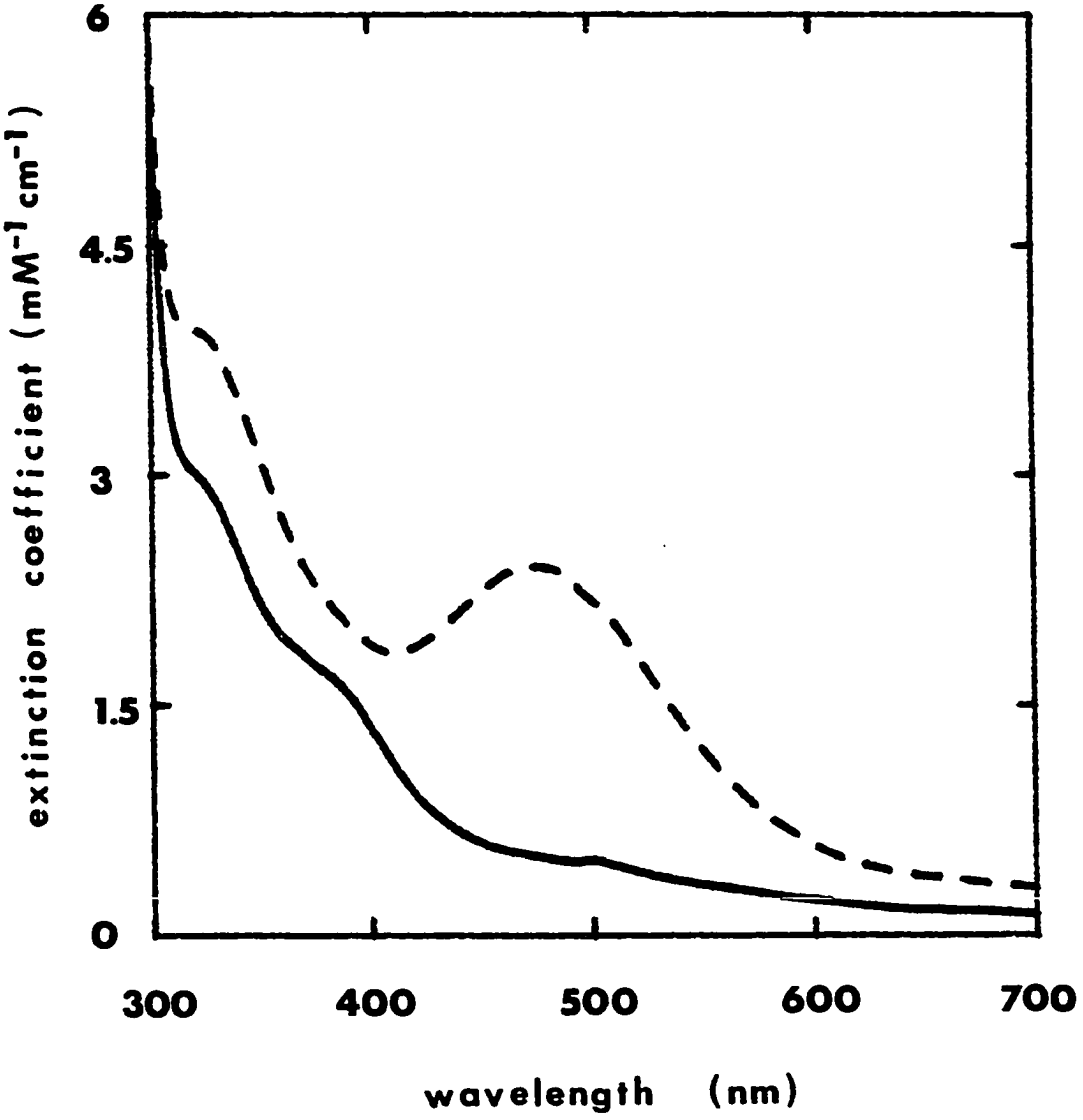

Figure 5. UV-visible absorption spectra of $(semi\text{-}met)_R Hr$ (solid line), and semi-met azideHr (dashed line), the latter obtained after addition of azide to $(semi\text{-}met)_R Hr$ in 50 mM MES, pH 6.3, 0.15 M Na_2SO_4

diffraction results show that perchlorate causes a conformational change.

Small anions bind to the active sites of metHr and the semi-metHrs (6,15). The UV-visible and EPR spectra of these anion adducts (Tables 2 and 3), the most studied of which is the azide adduct, are independent of pH. The extinction coefficients (Table 2) are well known for metazidoHr and semi-metazidoHr and are used routinely to measure concentrations. Anions also assist in the oxidation of oxy- and deoxyHr to the met form (1). In the presence of most anions (Br^-, HCO_2^-, CNO^-, F^- and SCN^-) the reduction of metHr to deoxyHr by dithionite is a single first order process (18).

The most physiologically important forms of Hr are oxy- and deoxyHrs, whose absorption spectra are shown in Figure 6. When oxyHr is converted to metHr it ceases to bind oxygen. Autooxidation of purified oxyHr (Reaction 1) is slow, but

$$2H^+ + [Fe(III),Fe(III)\text{-}O_2^{2-}](oxy) \rightarrow [Fe(III),Fe(III)](met) + H_2O_2 \quad (1$$

does occur. If Cl^- is added (0.3 M), the autooxidation at pH 7 and 25 °C has a half-life of approximately 18.5 hours (1). A cytochrome b_5 has recently been isolated from the erythrocytes of Phascolopsis gouldii (19), which reduces metHr to deoxyHr. Therefore, even though Hr is not an electron

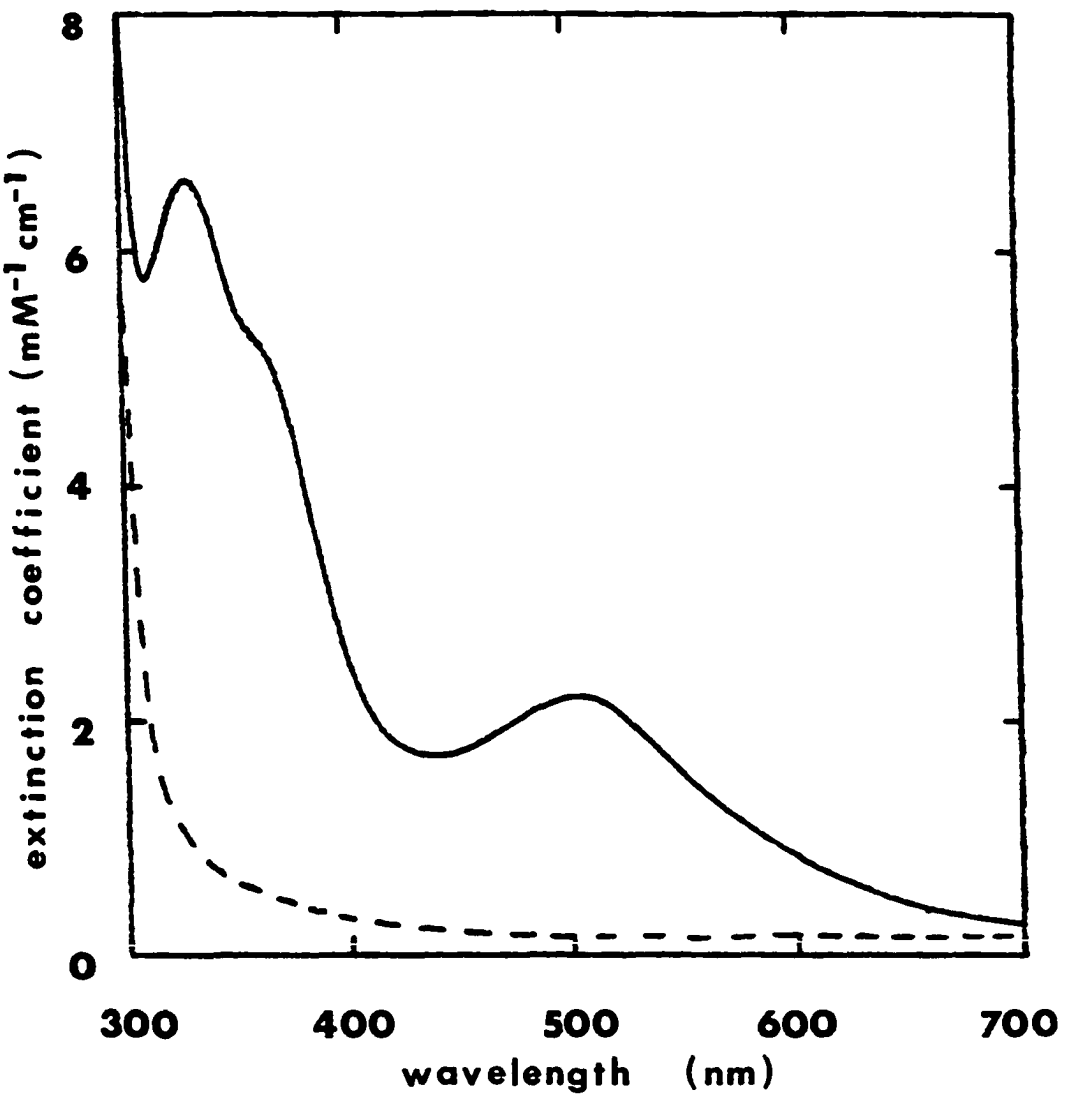

Figure 6. Oxy (solid line) and deoxyHr (dashed line), UV-visible absorption spectra, 50 mM MES, 0.15 M Na_2SO_4, pH 6.3

transfer protein, it must be involved in redox chemistry. Hr must be kept in the reduced state to bind oxygen, and apparently a physiological mechanism exists to keep Hr reduced. The electron transfer properties of Hr are, therefore, of interest. This study examines some of these electron transfer properties using a variety of approaches.

I. THE REDUCTION OF METHEMERYTHRIN TO DEOXYHEMERYTHRIN

Statement of the Problem

The reduction of metHr is of vital interest to the marine organisms that use Hr as their oxygen storage system. There has been some controversy (discussed below) over the mechanism of the reduction of metHr to deoxyHr. As a cytochrome b_5 has been discovered in the erythrocytes of Phascolopsis gouldii (1), which reduces metHr, it is important to understand the mechanism of this reduction. A simpler approach, at least in theory, is one in which small inorganic compounds are used as reducing agents. It is hoped that this study will provide a context within which reduction of metHr by the physiological reducing agent, cytochrome b_5, can be compared.

Previous Work

Dithionite reduction of P. gouldii metHr

Harrington et al. (2) first studied the kinetics of reduction of metHr to deoxyHr by dithionite ion. The reduction seemed to occur in three steps and the semi-met oxidation level was first discovered in this study. The first stage appeared to be reduction of metHr to semi-metHr. This reduction occurred rapidly and was dependent upon

concentration of reductant. The second and third stages were independent of concentration of reductant and were longer in duration ($k_2 \sim 4.4 \times 10^{-4} s^{-1}$ and $k_3 \sim 1 \times 10^{-4}\ s^{-1}$). It was stated, however, that the absorbance changes during the second and third stages did not fit first order kinetic plots very well, although for the third stage this lack of fit may be due to the small absorbance changes associated with this stage. Based on these results, an intramolecular disproportionation mechanism for octameric Hr was proposed for the second stage. This disproportionation and rapid reduction of met subunits can be expressed as steps 1-6:

1) $[Fe(III),Fe(II)]_8 \xrightarrow{k_{disp.}} [Fe(III),Fe(III)]_4[Fe(II),Fe(II)]_4$

semi-met → met + deoxy

2) $[Fe(III),Fe(III)]_4[Fe(II),Fe(II)]_4 \xrightarrow{k_{rered.}} [Fe(III),Fe(II)]_4[Fe(II),Fe(II)]_4$

3) $[Fe(III),Fe(II)]_4[Fe(II),Fe(II)]_4 \xrightarrow{k_{disp.}} [Fe(III),Fe(III)]_2[Fe(II),Fe(II)]_6$

4) $[Fe(III),Fe(III)]_2[Fe(II),Fe(II)]_6 \xrightarrow{k_{rered.}} [Fe(III),Fe(II)]_2[Fe(II),Fe(II)]_6$

5) $[Fe(III),Fe(II)]_2[Fe(II),Fe(II)]_6 \xrightarrow{k_{disp.}} [Fe(III),Fe(III)]_1[Fe(II),Fe(II)]_7$

6) $[Fe(III),Fe(III)]_1[Fe(II),Fe(II)]_7 \xrightarrow{k_{rered.}} [Fe(III),Fe(II)]_1[Fe(II),Fe(II)]_7$

7) $[Fe(III),Fe(II)]_1[Fe(II),Fe(II)]_7 \xrightarrow{k_3} [Fe(II),Fe(II)]_8$

where $k_{disp.}$ is the rate constant for the rate determining disproportionation step and $k_{rered.}$ is the rate for the faster reduction of met subunits produced by disproportionation. The last step (7) is the reduction of the last semi-met subunit, which is unable to disproportionate intramolecularly, and accounts for the third stage. The rates did not appear to be greatly affected by pH (from 6.3 to 8.2).

Reduction kinetics of T. zostericola metHr

Recently, Armstrong et al. have undertaken an extensive study of the reduction kinetics of Themiste zostericola octameric metHr with several synthetic Co(II) and Cr(II) complexes (3). They also found three stages, the latter two being independent of the nature or concentration of reductant. However, the rates for the second stage (Table I-1) were an order of magnitude faster than those reported by Harrington et

al. (2). The second stage product was called a "quarter-met" form by Armstrong et al. (3) and was proposed to contain the following combination of oxidation levels: $[Fe(II),Fe(II)]_4[Fe(III),Fe(II)]_4$. The absorption spectrum for this "quarter-met" form is shown in Figure I-1a. The third stage product is proposed to be deoxyHr. The rate of the second stage of reduction of T. zostericola metHr is pH dependent (Table I-1), while the third stage does not appear to be so, $k_3 = 1.2 \times 10^{-4} s^{-1}$. Interestingly enough, the second stage product does not appear to bind azide as does semi-metHr. Although no explicit mechanism was proposed, Armstrong et al. (3) concluded that the intramolecular disproportionation mechanism of Harrington et al. (2) could not explain the existence of the "quarter-met" form.

In light of these apparently conflicting results, a study of the reduction of P. gouldii metHr by two novel reducing agents has been undertaken. Cr^{2+}/cacodylate and $[Cr(15\text{-ane}N_4)(H_2O)_2]^{2+}$ were used to study the reduction of metHr to deoxyHr. The reduction of metHr by $Na_2S_2O_4$ was also reinvestigated. The reactions were followed using UV-visible as well as EPR and Mössbauer spectroscopies.

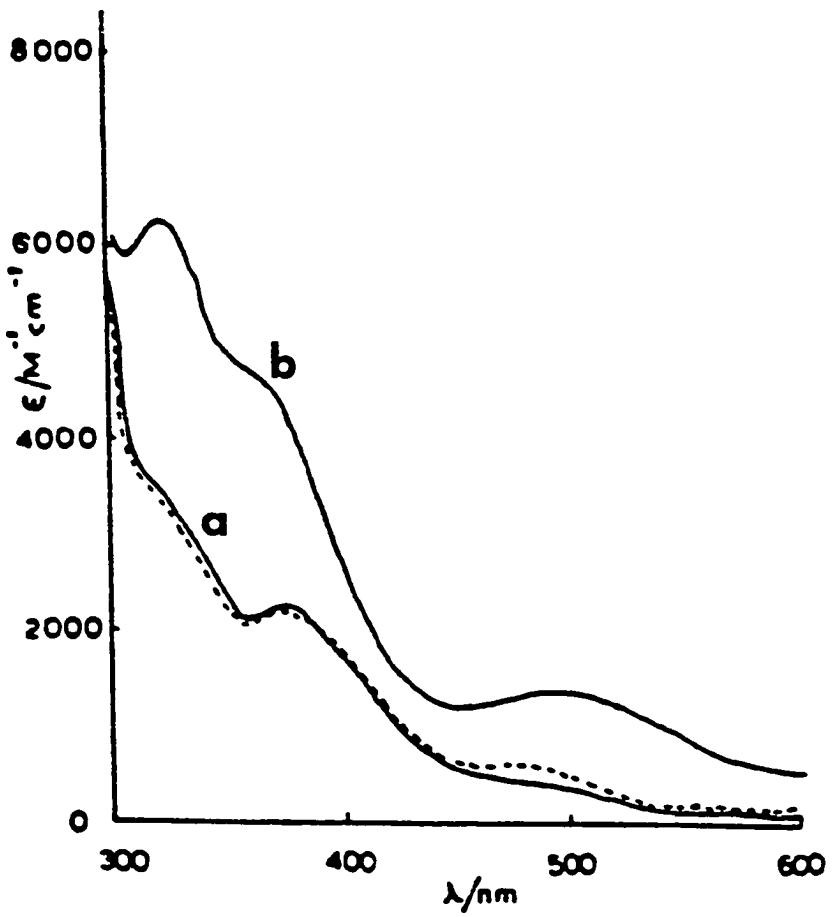

a) after addition of 1.5 reducing equivalents to T. zostericola metHr at pH 6.3, 0.15 M Na_2SO_4. Dashed line is after addition of azide.

b) after exposure of a) to oxygen.

Figure I-1. UV-visible absorption spectra of the second stage product of reduction of T. zostericola metHr (3)

Table I-1. Effect of pH on rate constant, k_{2obs}(25°C) for the second stage of the reduction of T. zostericola metHr (1.2-0.75) x 10^{-5} M, with $[Co(sep)]^{2+}$, I=0.15M (Na_2SO_4) (3)

pH(buffer)	$10^3 k_{2obs}, s^{-1}$	pH(buffer)	$10^3 k_{2obs}, s^{-1}$
9.00(Tris)	3.9	7.28(Tris)	1.77
8.64(Tris)	4.2	6.96(Trismal)	1.32
8.09(Tris)	3.5	6.5 (Mes)	1.65
7.67(Tris)	2.7	6.4 (Mes)	1.80
7.60(Tris)	2.3	6.3 (Mes)	2.05
7.60(Tris)	2.15	6.1 (Mes)	2.63

Experimental

Preparation of P. gouldii metHr

Worms were obtained from the Marine Biological Laboratory, Woods Hole, Massachusetts. The worms were slit and oxyHr crystals were obtained as previously described (4). The Hr crystals were dissolved in 50 mM Tris-acetate or 50 mM phosphate buffer, pH 8.0, containing 150 mM Na_2SO_4 and centrifuged to remove any remaining debris. The protein was then dialyzed at 4 °C against 3-4 mM $K_3Fe(CN)_6$ in 50 mM Tris-acetate. Alternatively, solid $K_3Fe(CN)_6$ was directly added to the protein and allowed to react for several hours. $K_3Fe(CN)_6$ was removed by extensive dialysis at 4 °C. Many changes of buffer were needed to remove the $K_3Fe(CN)_6$. MetHr thus obtained was dialyzed against 50 mM HEPES, MES or EPPS buffer with 0.15 M Na_2SO_4. The concentration of metHr was determined by addition of sodium azide and the use of the extinction coefficient at 446 nm, ε_{446} = 3700 $M^{-1}cm^{-1}$ (5). Concentrations are expressed in terms of subunits (dimeric iron sites).

Preparation of T. zostericola metHr

T. zostericola worms were obtained live from Pacific Biomarine Supply, Venice, California. OxyHr was isolated as previously described (4) without a crystallization step. T.

zostericola metHr was prepared in the same manner as P. gouldii metHr.

Preparation of the inorganic reducing agents

Cr^{2+}/cacodylate $Cr(H_2O)_6^{2+}$ was obtained by oxidation of Cr metal. Chromium metal was obtained from Aldrich Chemical Company, Inc., ~ 100 mesh and 99.9% pure. Approximately 100 mg of Cr metal was placed under a nitrogen atmosphere and ~ 1/2 ml of concentrated HCl was added to start the reaction. Hydrogen evolution was observed immediately. The Cr metal was then washed with 0.25 M $HClO_4$ several times and three to four ml of 0.25 M $HClO_4$ were added. $[Cr(H_2O)_6](ClO_4)_2$ was produced over the period of 30-45 minutes, and the reaction was allowed to proceed until no further hydrogen evolution was observed. The unreacted Cr metal was filtered anaerobically from the Cr^{2+}(aq) solution by use of a Schlenkware frit. The concentration of $[Cr(H_2O)_6](ClO_4)_2$ produced was determined spectrophotometrically by $\varepsilon_{750} = 4.38\ M^{-1}cm^{-1}$ (6). This Cr^{2+}(aq) was then diluted with 0.1 M cacodylic acid (pH 7.0) and used for reduction of Hr. Cr^{2+}/cacodylate concentrations were determined by anaerobic titration with $KMnO_4$ (7).

$[Cr(15\text{-ane}N_4)(H_2O)_2]^{2+}$ 15-ane was obtained from Strem Chemicals, Inc. A 1.5 to two fold excess over Cr^{2+} of 15-ane was deaerated with nitrogen and then diluted with deaerated

buffer (50 mM of MES, HEPES or EPPS) of the desired pH. $[Cr(H_2O)_6](ClO_4)_2$ was then added slowly with stirring. Any precipitated 15-ane was removed by anaerobic centrifugation. The concentration of the $[Cr(15\text{-ane}N_4)(H_2O)_2]^{2+}$ produced was determined using $\varepsilon_{540} = 36.5\ M^{-1}cm^{-1}$ (8).

$Na_2S_2O_4$ $Na_2S_2O_4$ was obtained from BDH Chemicals, Ltd., Poole, England and used without further purification. Solid $Na_2S_2O_4$ was weighed out, deaerated with N_2 and deaerated buffer was added. The concentrations of $Na_2S_2O_4$ were obtained by anaerobic titration of $K_3Fe(CN)_6$, using $\varepsilon_{419} = 1030\ M^{-1}s^{-1}$ for $K_3Fe(CN)_6^{3-}$ (9).

Reactions carried out in D_2O

Reduction reactions using $Fe(EDTA)^{2-}$ were carried out in ~ 90% D_2O. MetHr (~ 1 ml) was dialyzed against ~ 100 ml of buffered D_2O solutions. pD was determined using the equation pD = pH (meter reading) + 0.4. A Beckman 31 pH meter was used for the pH measurements. $Fe(EDTA)^{2-}$ was prepared according to the method of Wherland and Gray in a buffered D_2O solution (10).

Preparation of Mössbauer samples

Mössbauer samples of T. zostericola and P. gouldii Hrs at intermediate stages of reduction at pH 8.2 were prepared using two equivalents of $[Cr(15\text{-ane}N_4)(H_2O_2)]^{2+}$ per dimeric

iron site of metHr. Mössbauer samples of P. gouldii Hr at pH 6.3 were prepared using excess dithionite and frozen when no EPR signal was observable in samples made under comparable conditions. Concentrations of Hr were 5-8 mM. Samples were transferred anaerobically by gas syringe to either 1/2 or 5/8 inch nylon Mössbauer cups in septa-capped, 50 ml or 10 ml disposable syringes. Samples (in the capped syringes) were then frozen in liquid nitrogen. The frozen samples were then shipped to the Department of Physics, University of Illinois at liquid N_2 temperatures using a Minnesota Valley Model BDS-5 biological dry shipper. Mössbauer spectra were run at either 100, 4 or 1.8 K and subjected to a magnetic field of up to 2.2 kgauss.

Preparation of EPR samples for temperature-power saturation study

$(Semi\text{-}met)_R Hr$ was prepared by the addition of one equivalent of dithionite (titrated as previously described) to deaerated metHr (~ 2 mM). Semi-metazidoHr was prepared in the same manner as $(semi\text{-}met)_R Hr$ with subsequent addition of excess NaN_3. $\mu\text{-}S^{2-}$semi-metHr was prepared by dialyzing ~ 1 ml of 2 mM metHr anaerobically against one liter of ~ 3 mM $Na_2S \cdot 9H_2O$ overnight. All of the above samples were prepared in 50 mM MES, pH 6.3, and frozen in EPR tubes by immersion in liquid nitrogen. The tubes were then flame sealed.

Collection of kinetic data

Instrumentation A Perkin-Elmer model 554 UV-visible spectrophotometer was used to obtain kinetic data for reactions slower than 0.1 s^{-1}. Reactions were monitored from 400 to 320 nm. Reactions faster than 0.1 s^{-1} were monitored by use of a stopped flow instrument assembled in this laboratory. The optics were obtained from a Beckman B spectrophotometer and an Aminco-Morrow mixing chamber was installed. Reactions were monitored from 400-380 nm using a Tektronics storage oscilloscope. EPR spectra were obtained using a Bruker model ER-220D spectrometer equipped with an Oxford Instruments liquid helium cryostat. EPR instrument parameters were: frequency, 9.43 GHz; power, 0.2 mW; modulation, 16 gauss at 100 kHz; time constant, 0.1 sec. Gains were 1×10^5 - 1×10^3. EPR spectra were collected at temperatures of 4 to 12K.

Quantitation of number of spins in EPR samples was achieved by double integration of areas of derivative spectra (11). The integrated area of the spectrum of the unknown was compared to those of $CuSO_4 \cdot 5H_2O$ standards of comparable concentrations using Equation 1.

$$[x] = \frac{GN_s MA_s (P_s)^{1/2} (scan_x)^2 g_{ps} Int2_x Y_x [STD]}{GN_x MA_x (P_x)^{1/2} (scan_s)^2 g_{px} Int2_s Y_s} \qquad (1$$

The EPR parameters are abbreviated as follows: GN, reciever gain; MA, modulation amplitude; P, power; scan; Int2, value of the double integral generated by the computer program available with the EPR spectrometer; y, height of integral; [x] and [STD], concentrations of unknown and standard, respectively. The average intensity factor, g_p, was used and calculated for a rhombic EPR spectrum according to Equation 2.

$$g_p = 2/3((g_x^2 + g_y^2 + g_z)/3)^{1/2} + 1/3(g_z + g_y + g_z)/3 \quad (2$$

^{57}Fe Mössbauer spectra were collected by Professor Peter Debrunner in the Department of Physics at the University of Illinois in Champaign-Urbana. A constant acceleration spectrometer equipped with a variable temperature cryostat was used. Velocities are reported relative to Fe metal at 300 K.

Reaction conditions Reactions were carried out under N_2 in an anaerobic cell. Trace oxygen was removed from N_2 using chromous scrubbing towers (see Appendix A). Protein concentrations were maintained at 0.1 mM for all reactions. Reductant concentrations were varied from one to five mM with the exception of Cr^{2+}/cacodylate. Concentrations of Cr^{2+}/cacodylate higher than 2 mM caused protein precipitation. Reactions were also followed by adding sodium azide at various times. Total volume for other than stopped flow reactions was 1.0 ml.

Reactions for EPR spectroscopy were carried out in septum-capped two dram vials, using the reagent concentrations mentioned above. One hundred microliter aliquots were withdrawn anaerobically, using a gas-tight syringe, at various times and placed in four mm o.d. quartz tubing. The samples were then quickly frozen in liquid N_2 and flame sealed. EPR spectra were obtained at a constant temperature near that of liquid helium (from 4 to 10 K).

Measurements of EPR power saturation versus temperature

EPR temperature power saturation data were collected by measuring the EPR absorption derivative signal intensity, I, as a function of incident microwave power, P_0, at temperatures ranging from 4.2 to 10 K. EPR cryostat temperature was calibrated by the method in Appendix B. The signal intensities were measured using g = 1.92, semi-metazidoHr; g = 1.87 (peak to peak), $(semi\text{-}met)_R Hr$; g = 1.89, $\mu\text{-}S^{2-}$semi-metHr. The signal intensities vary as a function of the incident microwave power, P_0, as can be described by Equation 3 (12,13).

$$\log(I/P_{1/2}) = a - b/2\log(P_{1/2} + P) \qquad (3$$

The microwave power was varied at one temperature and a plot of log $(I/\sqrt{P_0})$ versus log P_0 for each sample, over a range of

temperatures was made to obtain $P_{1/2}$, the half-saturation power. When the signal is not saturating (i.e., $P < P_{1/2}$), Equation 1 takes the form of a line with zero slope. When $P > P_{1/2}$, the signal saturates and Equation 1 plots as a line whose slope is -b/2. The intersection of these two lines yields the value of $P_{1/2}$. The values of $P_{1/2}$ were determined for semi-metazido-, $(\text{semi-met})_R$- and μ-S^{2-}semi-metHrs over a range of temperatures using graphical methods.

The power saturation data as a function of temperatures have been well-fitted in other systems by the function in Equation 4, for relaxation by an Orbach process (12,13).

$$\ln P_{1/2} = \ln A - (\Delta/k)(1/T) \qquad (4$$

T is absolute temperature, k is the Boltzmann constant, A is a constant characteristic of the particular system. The value of Δ is a measure of the energy separation between the ground state and the first excited state. Δ is a function of the zero-field splitting energy, D, and the anti-ferromagnetic coupling constant, J, for a binuclear center. A plot of ln $P_{1/2}$ (in mW) versus 1/T (K) was made for semi-metazido-, $(\text{semi-met})_R$- and μ-S^{2-}semi-metHrs. A linear least squares analysis of the linear portion of each plot, generated the slope of the line. The slope of each line is equivalent to $-\Delta/k$.

Calculations of rate constants

Rate constants were determined by fitting absorbance versus time data using the least squares program "Expsum", obtained from the laboratory of Dr. James Espenson, Department of Chemistry, Iowa State University. Rate constants reported are the averages of three to five replicate determinations. Linearity of reductant concentration versus rate constants was determined using a linear least squares program, "LIN" developed in this laboratory by Ron Utecht.

Results

Kinetics

The rate constants for the reductions of *P. gouldii* metHr by excesses of Cr^{2+}/cacodylate, $[Cr(15\text{-ane}N_4)(H_2O)_2)]^{2+}$ and $Na_2S_2O_4$ are reported in Table I-2. In each case we resolve three stages. The first stage is dependent on concentration of reductant while the latter two are not. The third stage is difficult to follow due to the small absorbance change and its length. This third stage does not always go to completion and in some runs incomplete reduction to deoxy occurred. In Figure I-2, the experimental absorbance versus time data for the dithionite reduction of $(semi\text{-}met)_R$Hr to deoxyHr is shown. A non-linear least squares fit of the data using two exponentials gives a better fit of the data than the use of one

Table I-2. Rate constants for reductions of P. gouldii methemerythrin[a]

reducing reagent	$k_1, M^{-1}s^{-1}$	$k_2 \times 10^3, s^{-1}$	$k_3 \times 10^4, s^{-1}$
Cr^{2+}/cacodylate[b]	34(±4)	2.1(±0.2)	1.7(±0.3)
$[Cr(15\text{-ane}N_4)(H_2O)_2]^{2+}$	600(±14)	3.7(±0.2)	2.3(±0.2)
$Na_2S_2O_4$	$1.4(\pm0.1)\times10^5$	2.3(±0.10)	1.7(±0.2)

[a] 50 mM HEPES pH = 7.0, 20°C, I = 0.15 M Na_2SO_4.

[b] 0.1 M cacodylate pH = 7.0, 50 mM $NaClO_4$, 20 °C.

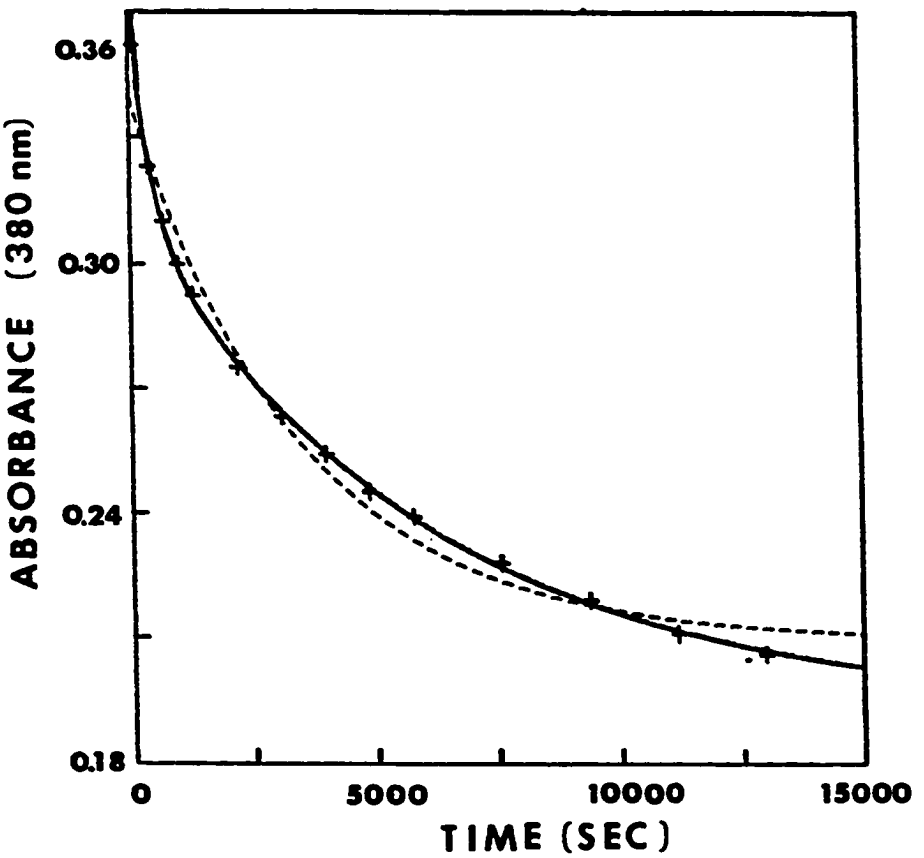

(+) Experimental absorbance versus time data; (---), fit using one exponential; (——), fit using two exponentials. The solid curve corresponds to the values of k_2 and k_3 listed in Table I-2.

Figure I-2. Non-linear least squares fits of the absorbance at 380 nm versus time data for the reduction of 0.1 mM P. gouldii metHr by a 10-fold molar excess of $Na_2S_2O_4$ at pH 7.0 (50 mM HEPES), 0.15 M Na_2SO_4

exponential; k_2 and k_3 are obtained from the two exponential fit. The dependence of k_2 and k_3 upon pH for the reduction with $[Cr(15\text{-ane}N_4)(H_2O)_2]^{2+}$ is shown in Table I-3. A pH of 7.0 was originally chosen for these studies because it appears to be close to the physiological pH as determined by ^{31}P NMR (14). The second stage appears to have some slight dependency upon pH, increasing at pH 6.3 and 8.2, while the third stage is nearly independent of pH. Armstrong et al. noticed a similar trend for T. zostericola Hr as shown in Table I-1 (3).

The reduction of P. gouldii metHr to deoxyHr by $[Cr(15\text{-ane}N_4)(H_2O)_2]^{2+}$ in ~ 95% D_2O was carried out at 20 °C and pH 7.0. No changes in the rate constants were observed for the second and third phases of reduction, i.e., $k_2 = 3.5 \pm 0.4 \times 10^{-3}$ s^{-1}, $k_3 = 2.0 \pm 0.3 \times 10^{-4}$ s^{-1}, in D_2O. The reduction of metHr to semi-metHr using $Fe(EDTA)^{2-}$ was carried out at pH 6.3 (50 mM MES), 0.15 M Na_2SO_4, 20 °C, in ~ 95% D_2O and resulted in a rate constant of 3.8 (± 0.4) $M^{-1}s^{-1}$. In H_2O under the same conditions, the rate was found to be 3.7 (± 0.5) $M^{-1}s^{-1}$. The semi-met nature of the product in D_2O was verified by the absorption spectrum after addition of excess NaN_3.

For the dithionite reduction, the values of k_2 and k_3 in Table I-2 are approximately two to five times those obtained by Harrington et al. (2). We attribute our results to better fits of the data using an NLLS program. Harrington et al. (2)

Table I-3. Dependence of k_2 and k_3 upon pH in $[Cr(15\text{-ane}N_4)(H_2O)_2]^{2+}$ reduction of P. gouldii metHr[a]

pH	$k_2 \times 10^3, s^{-1}$	$k_3 \times 10^4, s^{-1}$
6.3 (50 mM MES)	5.2(±0.1)	2.3(±0.2)
7.0 (50 mM HEPES)	3.7(±0.2)	2.3(±0.2)
8.5 (50 mM EPPS)	5.2(±0.3)	2.3(±0.2)

[a] 0.15 M Na_2SO_4, 20°C.

previously reported nonlinear behavior of data fit to first order kinetic plots, $\ln(A_t - A_\infty)$ versus time.

Product identification

UV-visible absorbance The first stage product, irrespective of reductant, is semi-metHr. Addition of azide results in semi-metazidoHr, which can be quantitated using $\varepsilon_{470} = 2400\ M^{-1}cm^{-1}$ (15). At the end of the first stage, 100% ± 5% of the dimeric iron sites present can be accounted for as semi-metazidoHr. At pH 7.0, the UV-visible absorption spectra of the first and second stage products of reduction of P. gouldii metHr are shown in Figure I-3. The second stage product has a spectrum with shoulders at 330 and 380 nm. When N_3^- is added to this product, very little change in absorbance occurs indicating little or no binding of azide.

The second stage product at pH 6.3, as shown in Figure I-4, gives an absorption spectrum which is similar to that seen at pH 7.0. The feature at 380 nm is more prominent at pH 6.3 than 7.0. Addition of N_3^- to the second stage product results in little change in the absorption spectrum. Addition of oxygen (Figure I-5) to the second stage product results in the spectrum of oxyHr. Using $\varepsilon_{500} = 2200\ M^{-1}cm^{-1}$ (5) indicates that roughly 90% of the dimeric iron sites of the second stage product are in the fully reduced, deoxy, form.

Figure I-3. UV-visible absorption spectra of the products of reduction of 0.1 mM P. gouldii metHr at pH 7.0

Met (——), semi-met (---), second stage product (——), and second stage product + N_3^- (...), third stage product (-.-.-), pH 7.0 (50 mM HEPES), 0.15 M Na_2SO_4, 25°C. Two equivalents of $[Cr(15\text{-}aneN_4)(H_2O)_2]^{2+}$ per monomer were used to reduce metHr to the second and third stage products.

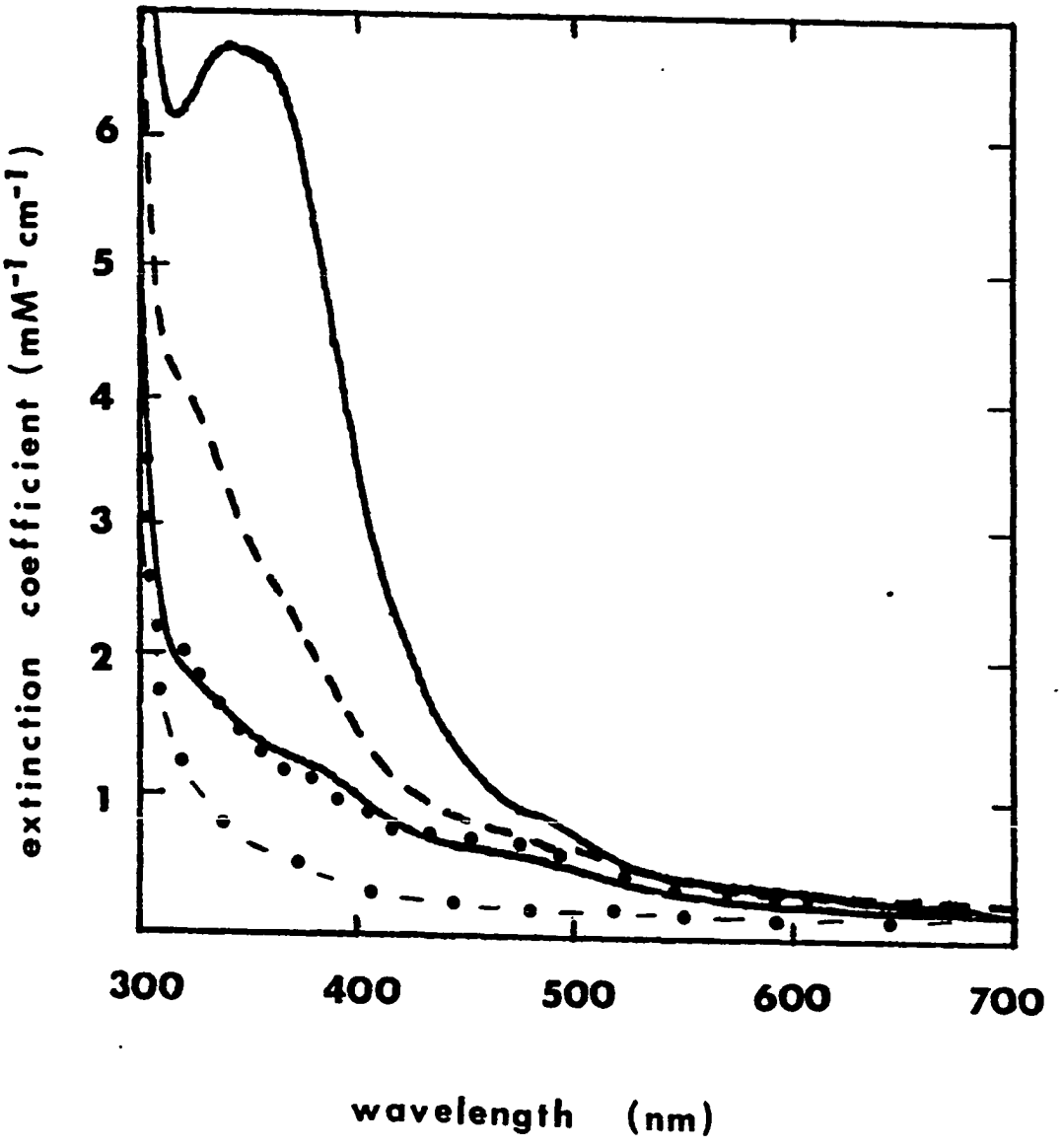
extinction coefficient ($mM^{-1}cm^{-1}$)
6
5
4
3
2
1
300
400
500
600
700
wavelength (nm)

Figure I-4. UV-visible absorption spectra of the products of reduction of 0.1 mM P. gouldii metHr at pH 6.3

Met (——), semi-met (---), second stage product (——), second stage product + N_3^- (...) and third stage product (-.-.-), pH 6.3 (50 mM MES), 0.15 M Na_2SO_4, 25°C. Two equivalents of $[Cr(15\text{-}aneN_4)(H_2O)_2]^{2+}$ per monomer were used to reduce metHr to the second and third stage products.

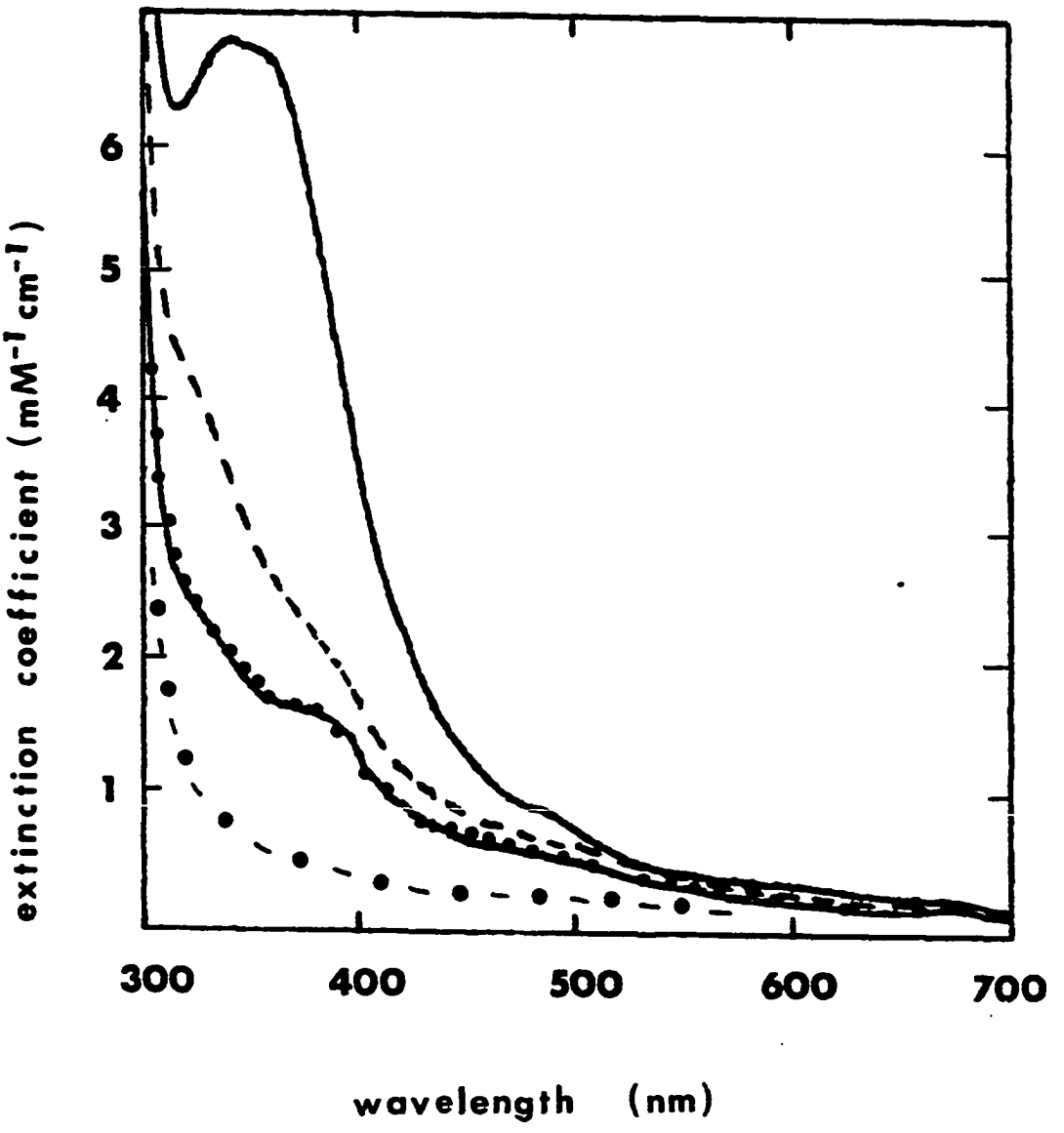
extinction coefficient ($mM^{-1}cm^{-1}$)
6
5
4
3
2
1
300
400
500
600
700
wavelength (nm)

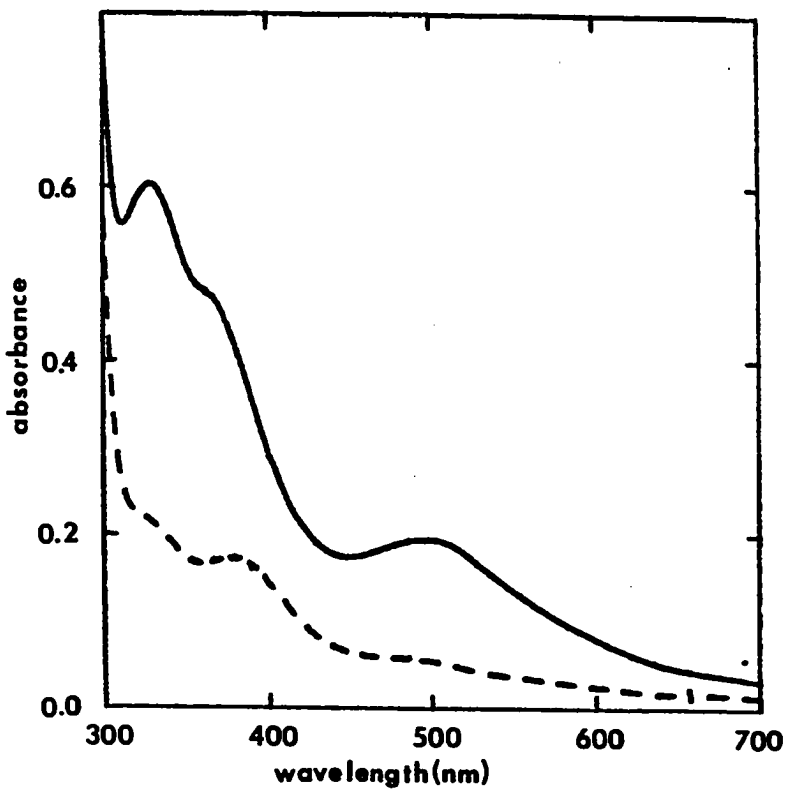

Second stage product (---), pH 6.3, using 2 equivalents of $[Cr(15\text{-ane}N_4)(H_2O)_2]^{2+}$ per monomer; (——) after exposure of second stage product to O_2. One-tenth mM total protein concentration.

Figure I-5. UV-visible spectra of second stage product in the reduction of P. gouldii metHr at pH 6.3 before and after exposure to O_2

The second stage product at pH 8.2 (Figure I-6) has a greater absorbance associated with it than at pH 7.0 or lower. Exposure of the second stage product to oxygen results in 85% ± 5% oxyHr using ε_{500} = 2200 $M^{-1}cm^{-1}$ (5), as can be seen in Figure I-7. Azide addition to the second stage product results in very little change in the absorption spectrum, as shown in Figure I-6.

EPR spectroscopy The reduction of metHr can also be followed by EPR spectroscopy. Only the semi-met form of Hr is known to produce an EPR signal at liquid He temperatures with $g_{avg} \sim 1.84$. In Figure I-8 are shown the EPR spectra for the reduction of P. gouldii metHr with dithionite is shown at pH 7.0. The most intense spectrum is produced immediately and is consistent with ~ 100% of the protein in the $(semi\text{-}met)_R$ form of Hr by double integration (92 (± 20) %). The product of the second stage is represented by the absence of any appreciable EPR spectrum at 100 minutes. The third stage product also has no detectable EPR spectrum. Although the EPR signal intensity decreases during the second stage, no change in EPR line shape occurs. At pH 6.3, the EPR signal intensity during the reduction of P. gouldii metHr with dithionite, Figure I-9, shows a more rapid decrease than at pH 7.0. At ~ 15 minutes, no EPR signal is detectable. The disappearance of the $(semi\text{-}met)_R$ EPR signal is also faster at pH 8.2 than at pH 7.0. In Figure I-10, the EPR spectra of the reduction of

Figure I-6. UV-visible absorption spectra of the products of reduction of 0.1 mM P. gouldii metHr at pH 8.2

Met (——), semi-met(---), second stage product (——), second stage product + N_3^- (....) and third stage product (-.-.-), pH 8.2 (50 mM EPPS), 0.15 M Na_2SO_4, 25 °C. Two equivalents of $[Cr(15\text{-}aneN_4)(H_2O)_2]^{2+}$ per monomer were used to reduce metHr to the second and third stage products.

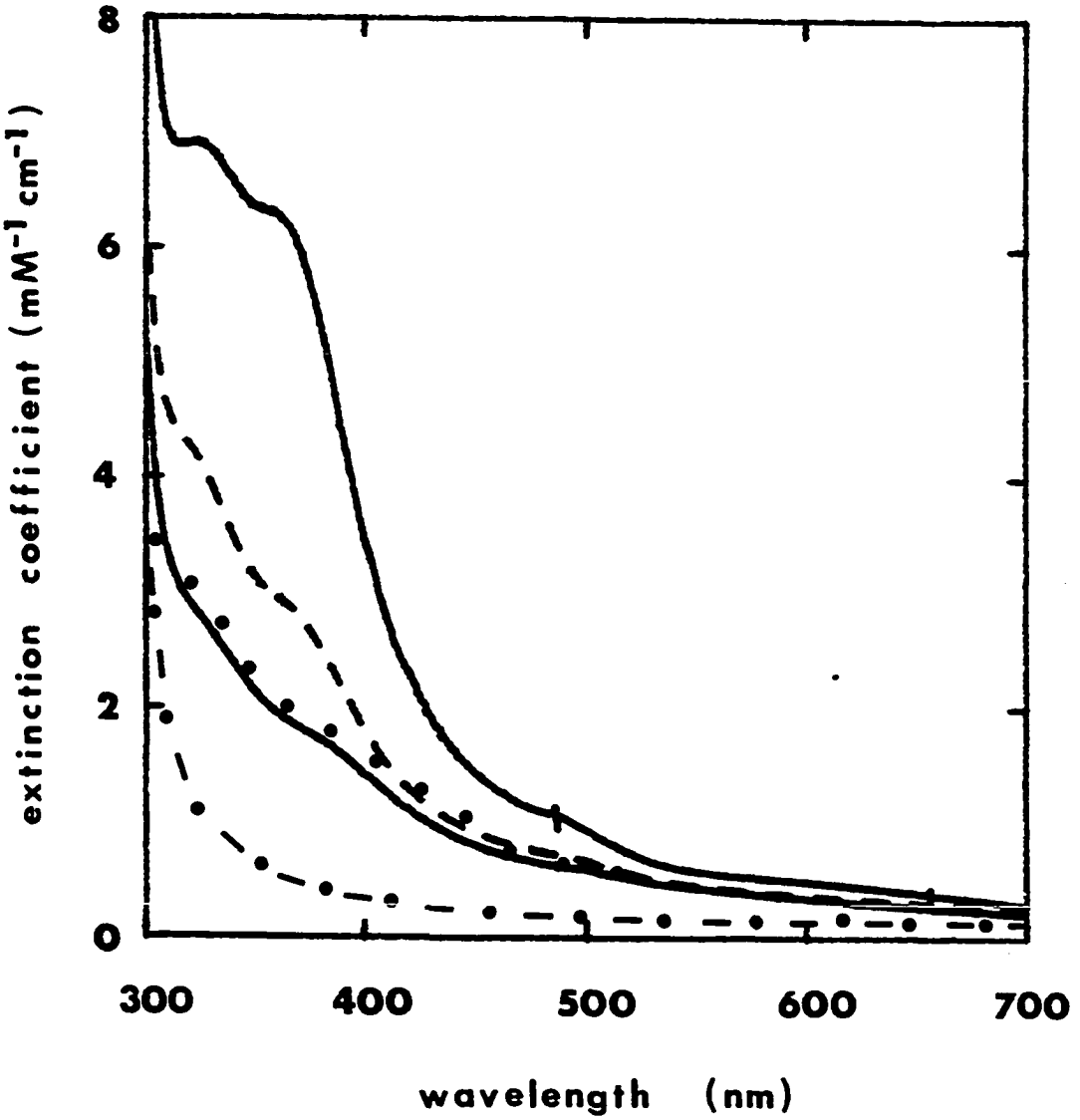
8
6
4
2
0
extinction coefficient ($mM^{-1} cm^{-1}$)
300
400
500
600
700
wavelength (nm)

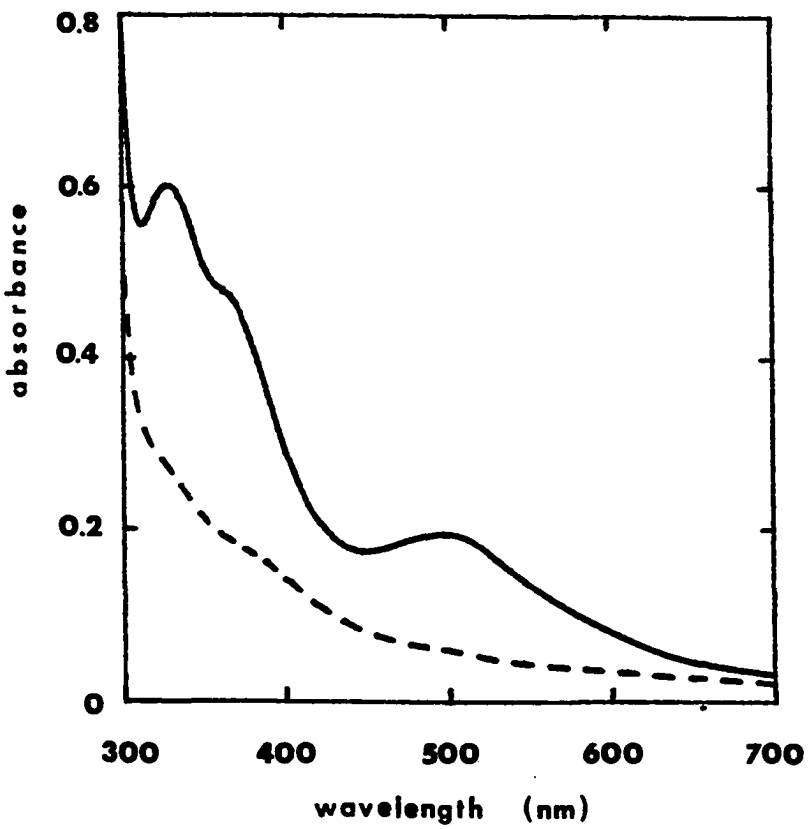

Second stage product (---), pH 8.2, using two equivalents of $[Cr(15\text{-ane}N_4)(H_2O)_2]^{2+}$ per monomer; (——) after exposure of O_2 to second stage product, 0.1 mM total protein concentration.

Figure I-7. UV-visible absorption spectra of the second stage product in the reduction of P. gouldii metHr at pH 8.2 before and after exposure to O_2

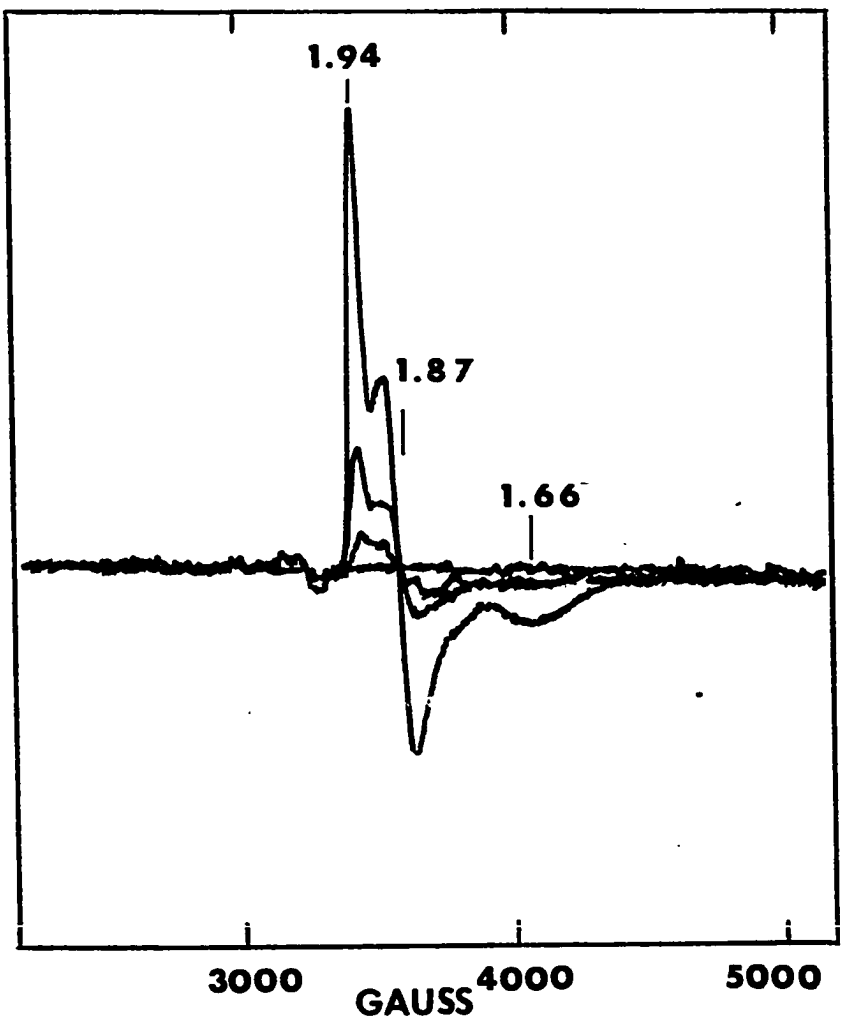

With decreasing intensity, spectra are of samples frozen at ~ 1, 30, 45 and 100 minutes after mixing. Spectra were obtained near 4 K. Numbers near the spectra indicate positions of g values.

Figure I-8. Semi-met EPR signals obtained during reduction of 0.1 mM P. gouldii metHr with a 20-fold molar excess of $Na_2S_2O_4$ at pH 7.0 (50 mM HEPES) and 20 °C

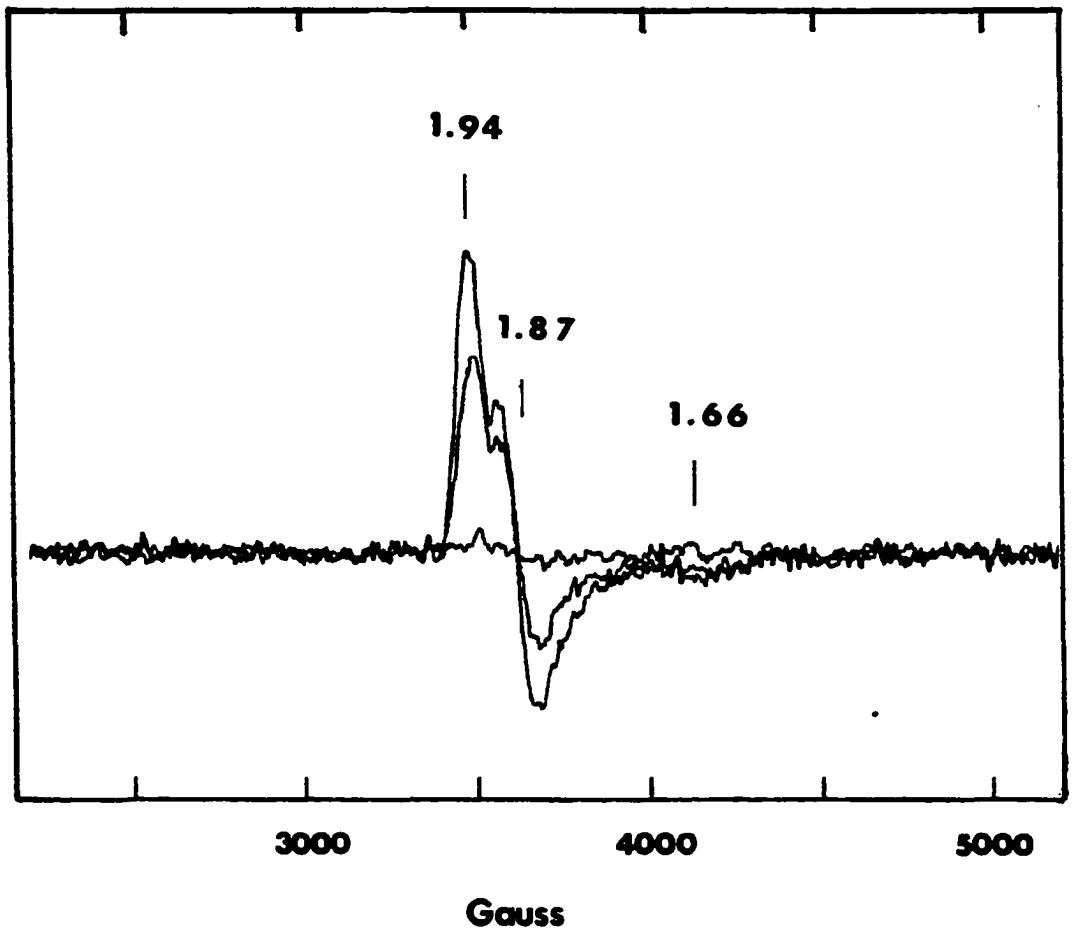

With decreasing intensity, spectra are of samples frozen at ~ 1, 5, and 15 minutes after mixing. Spectra were obtained near 4 K. Numbers near the spectra indicate positions of g values.

Figure I-9. Semi-met EPR signals obtained during reduction of 0.1 mM P. gouldii metHr with a 20-fold molar excess of $Na_2S_2O_4$ at pH 6.3 (50 mM MES) and 20 °C

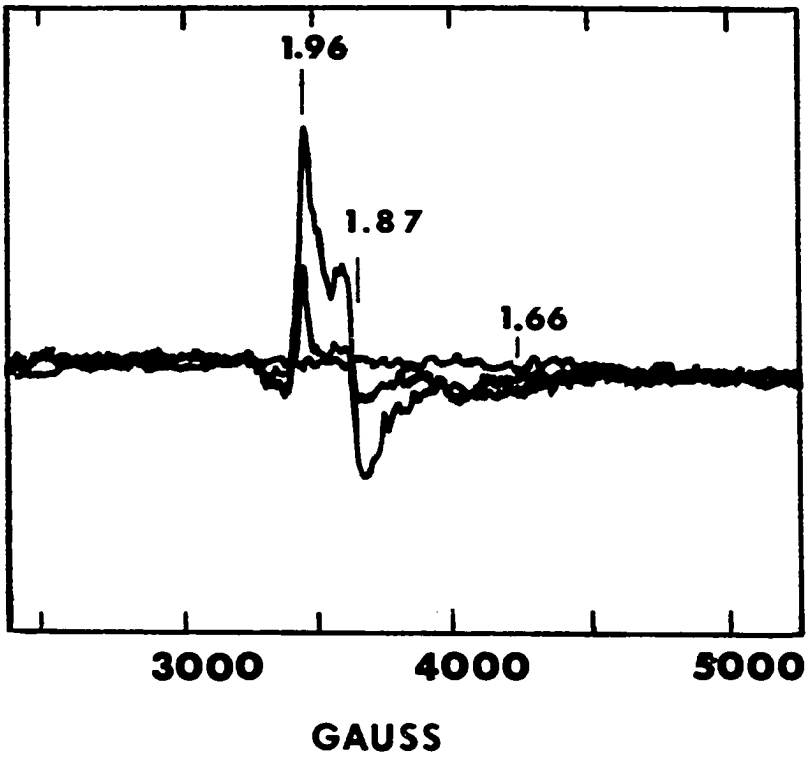

With decreasing intensity, spectra are of samples frozen at ~ 1, 10 and 30 minutes after mixing. Spectra were obtained near 4 K. Numbers near the spectra indicate positions of g values.

Figure I-10. Semi-met EPR signals obtained during the reduction of 0.1 mM P. gouldii metHr with a 20-fold molar excess of dithionite at pH 8.2 (50 mM EPPS) and 25 °C

metHr with dithionite at pH 8.2 are shown.

When the reduction of Themiste zostericola metHr at pH 8.2 is followed by EPR spectroscopy, the spectra shown in Figure I-11 are obtained. In Figure I-11a, the most intense EPR signal is of $(semi\text{-}met)_R$, ~ 100% (double integration of spectra gives values of 95 (± 15) %) at 30 seconds after addition of reductant. At ~ 40 minutes, no EPR signal can be observed and no change in EPR lineshape is observed throughout the reaction. Addition of N_3^- at approximately 1 minute results in EPR signals with g-values of 1.92, 1.82 and 1.5 (Figure I-11b). Previously published EPR spectra of T. zostericola semi-metazidoHr have g-values of 1.90, 1.81 and 1.49 (Table 3) with an EPR lineshape identical with that seen in Figure I-11b. Figure 11 shows that when an EPR signal can be detected, it can be converted to that of semi-metazidoHr. No change in the lineshape of the EPR signal observed in Figure I-11b occurs with time. In addition, a gradual increase in the signal observed at g ~ 13 can be seen. This signal has been previously recognized as resulting from $deoxyN_3^-$ (16).

However, a change in the EPR lineshape of P. gouldii $(semi\text{-}met)_R$Hr is observed when semi-met is prepared using only one equivalent of $Cr^{2+}(aq)$ per dimeric iron (Figure I-12). The same changes are obtained when using one equivalent of $[Cr(15\text{-}aneN_4)(H_2O)_2]^{2+}$ per dimeric iron as shown in

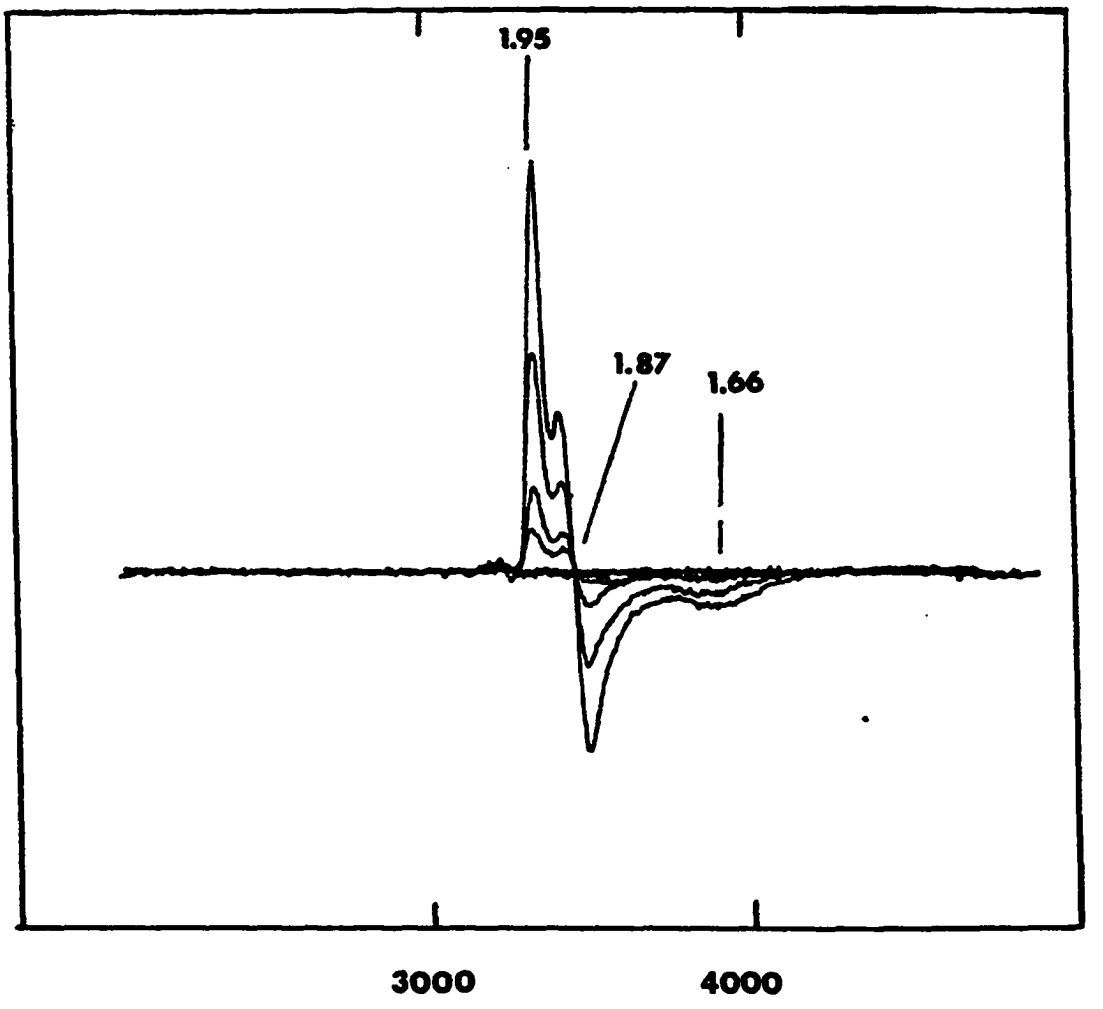

With decreasing intensity spectra were obtained at ~ 30 seconds, 10 minutes, 20 minutes, 30 minutes, 40 minutes after mixing. Kinetic conditions: pH 6.3 (50 mM MES), 0.15 M Na_2SO_4, 25 °C. Numbers near the spectra indicate positions of g values.

Figure I-11a. EPR spectra during reduction of 0.1 mM T. zostericola metHr with a 20-fold molar excess of dithionite

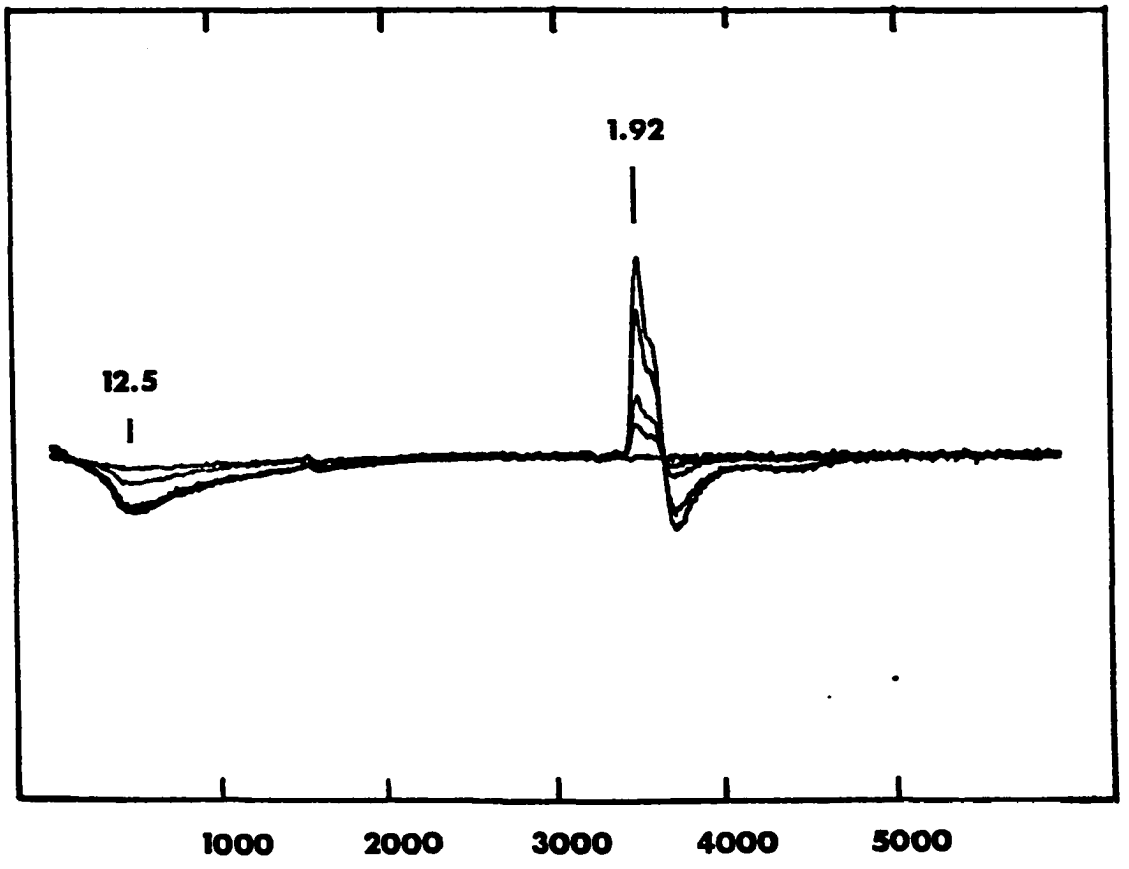

With decreasing intensity at g ~ 1.92 spectra were obtained at ~ 1 minute, 11 minutes, 21 minutes, 31 minutes, 41 minutes. Kinetic conditions: pH 6.3 (50 mM MES), 0.15 M Na_2SO_4, 25 °C. Numbers near the spectra indicate positions of g values.

Figure I-11b. EPR spectra during reduction of 0.1 mM T. zostericola metHr with a 20-fold molar excess of dithionite after addition of 50 mM N_3^-

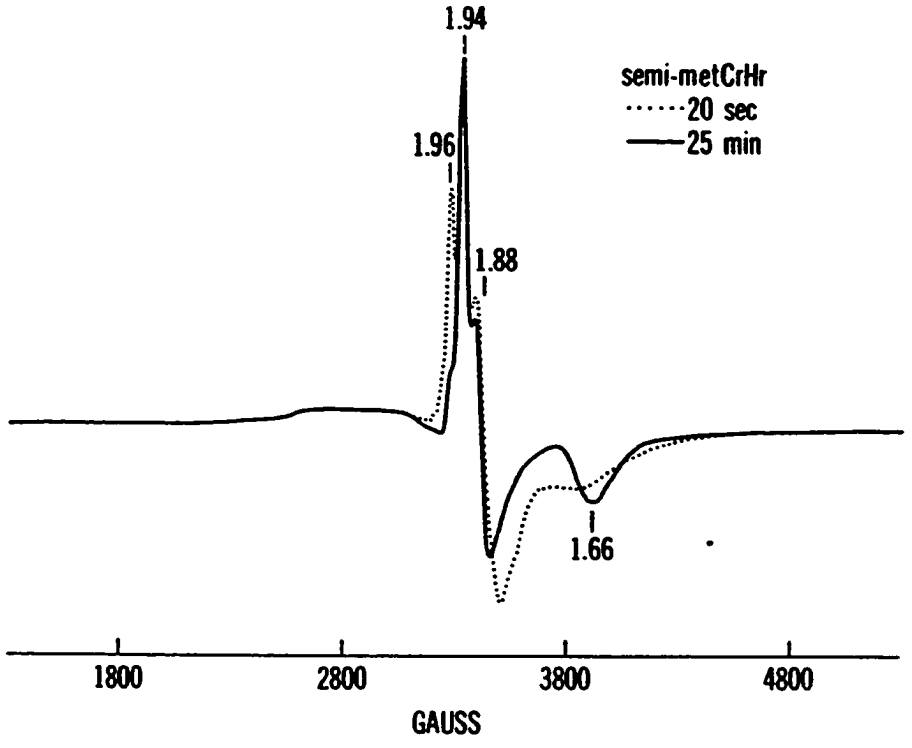

Solutions were incubated for the indicated times at 20 °C. Spectra were obtained near 4 K. Numbers near the spectra indicate positions of g values. Note that the dotted spectrum contains a feature at g = 1.94. The broad feature near 2800 G is due to Cr(III). No further changes in EPR lineshape occur for at least 24 hours.

Figure I-12. Semi-met EPR signals obtained after reduction of 1.0 mM P. gouldii metHr with one equivalent of Cr^{2+}(aq) at pH 7.0 (50 mM HEPES), 0.15 M Na_2SO_4

Figure I-13. The most prominent change is the development of a well resolved feature at g = 1.66.

Mössbauer spectroscopy A ^{57}Fe Mössbauer spectrum obtained at 4.2 K of a concentrated sample (~ 4.5 mM) of the second stage product of the reduction of T. zostericola metHr generated using 1.5 equivalents of $[Cr(15\text{-}aneN_4)(H_2O)_2]^2$ is shown in Figure I-14. The Mössbauer sample was frozen at ~ 40 minutes after incubation of metHr with $[Cr(15\text{-}aneN_4)(H_2O)_2]^{2+}$ at 25 °C. At this time, no EPR signal could be observed in the sample (see Figure I-11a). Three lines are observed in the spectrum which can be attributed to two overlapping quadrupole doublets. The more intense doublet with an isomer shift, δ_{Fe}, of 1.15 mm/sec and a quadrupole splitting, Δ_{Eq}, of 2.94 is consistent with previously published P. gouldii deoxyHr (high spin ferrous) (Table 1, General Introduction). The arrows in Figure I-14 indicate a doublet with δ_{Fe} of 0.60 mm/sec with Δ_{Eq} of 1.84 mm/sec indicative of high spin ferric iron and consistent with spectra previously observed for P. gouldii metHr (Table 1, General Introduction). Mössbauer spectra of T. zostericola Hr derivatives have not been published at this time. In a magnetic field of 2.2 kgauss, no broadening of the spectrum in Figure I-14 is observed indicating lack of any S = 1/2 or S = 3/2 species which might be attributed to a semi-met oxidation

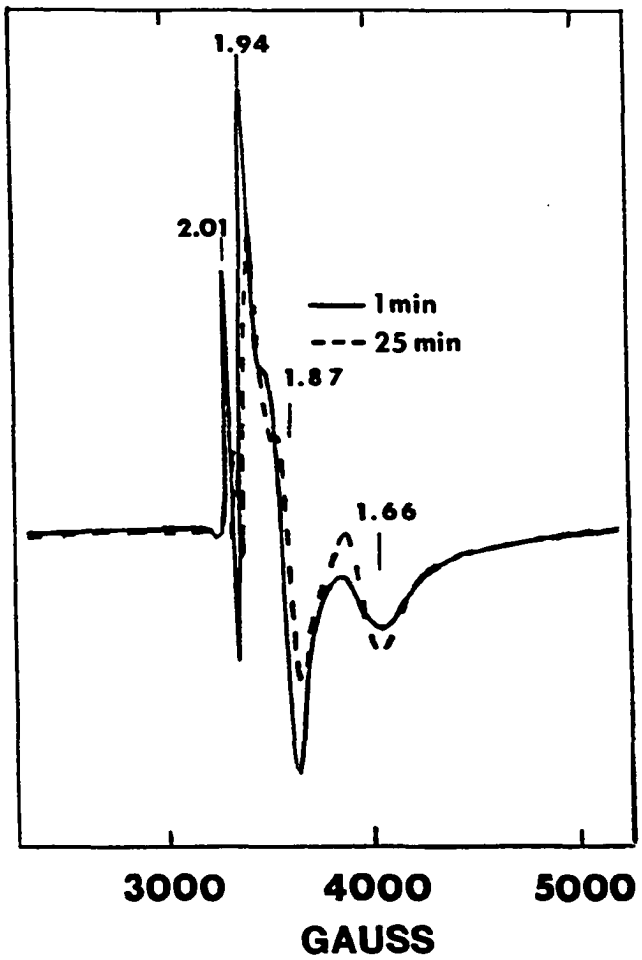

Solutions were incubated for the indicated times at 20 °C. Numbers near the spectra indicate positions of g values. The free radical at g = 2.0 is due to 15-ane.

Figure I-13. Semi-met EPR signals obtained after reduction of 1.0 mM P. gouldii metHr with one equivalent of $[Cr(15\text{-ane}N_4)(H_2O)_2]^{2+}$ at pH 7.0 (50 mM HEPES), 0.15 M Na_2SO_4

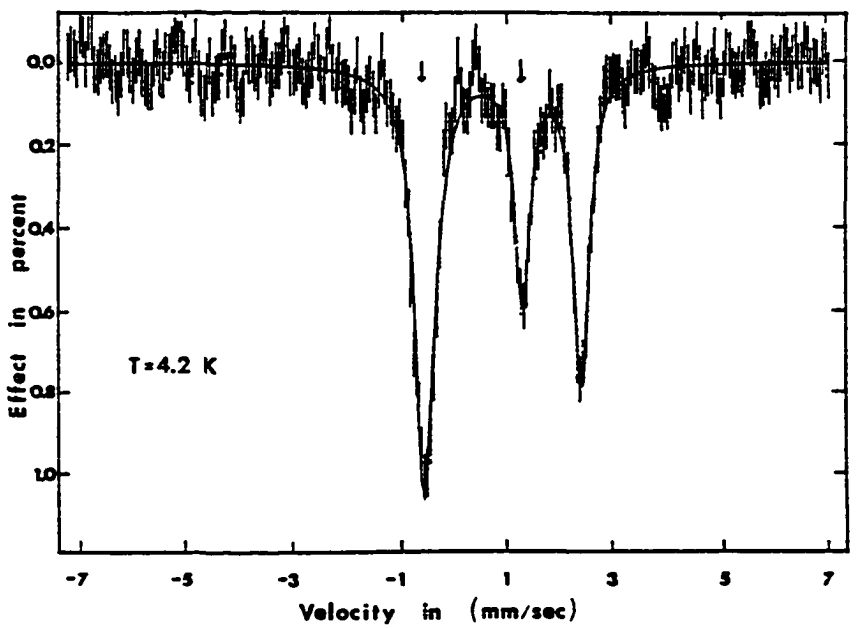

The sample was frozen after incubation at 25 °C for 40 minutes, pH 6.3 (50 mM MES), 0.15 M Na_2SO_4. Arrows indicate absorbances due to metHr (see text for details).

Figure I-14. ^{57}Fe Mössbauer spectrum of the second stage product during the reduction of T. zostericola Hr using 1.5 equivalents of $[Cr(15\text{-}aneN_4)(H_2O)_2]^{2+}$, obtained at 4.2 K in a magnetic field of 2.2 kgauss

level. Spectral simulations of the two doublets (indicated by the solid curve in Figure I-14) show that about 60% of the total protein appears to be at the deoxy oxidation level and ~ 40% at the met oxidation level.

Mössbauer spectra of P. gouldii Hr at 4.2 K were obtained by reducing ~ 5 mM metHr with two equivalents of $[Cr(15\text{-ane}N_4)(H_2O)_2]^{2+}$ and shows ~ 90% deoxyHr and ~ 10% metHr (Figure I-15). The Mössbauer sample in Figure I-15 was frozen after incubation of metHr with $[Cr(15\text{-ane}N_4)(H_2O)_2]^{2+}$ for 15 minutes at 25 °C and represents the second stage product during the reduction of metHr. No EPR signal can be observed for this sample (see Figure I-9). The main quadrupole doublet with δ_{Fe} = 1.19 mm/sec and Δ_{Eq} = 2.84 mm/sec is consistent with high spin ferrous iron previously observed for P. gouldii deoxyHr (Table 1, General Introduction). The arrows in Figure I-15 indicate a trace, ~ 10%, of a quadrupole doublet with δ_{Fe} = 0.46 mm/sec and Δ_{Eq} = 1.91 mm/sec consistent with values previously observed for P. gouldii metHr although the values are slightly different (Table 1, General Introduction). The P. gouldii spectrum was also obtained in a magnetic field of 2.2 kgauss and no broadening of the spectrum was observed at 4.2 K indicating no S = 1/2 semi-met species present. A Mössbauer spectrum of the second stage product during the reduction of metHr at pH 8.2 was also obtained at 100 K and is shown in Figure I-16.

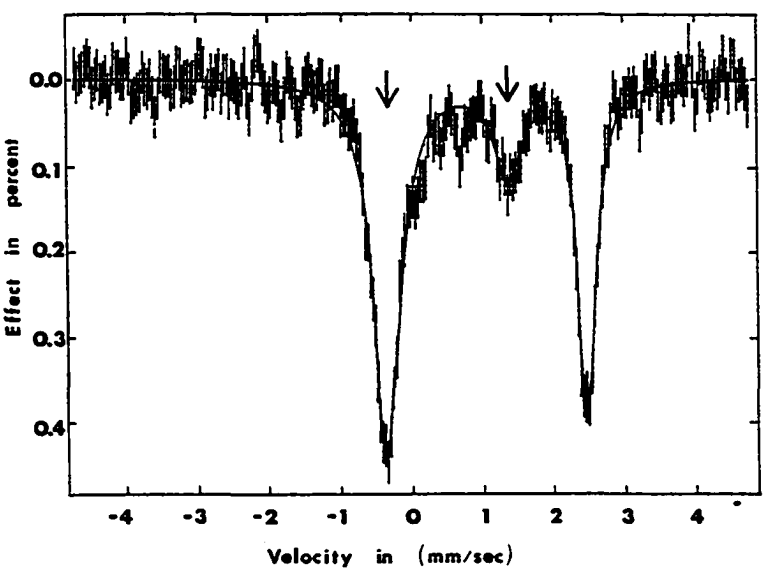

MetHr was incubated with a 10-fold molar excess of dithionite at 25 °C for 15 minutes before freezing. Arrows indicate the absorption due to met'Hr (see text for details).

Figure I-15. Mössbauer spectrum of the second stage product during the reduction of P. gouldii Hr using excess dithionite at pH 6.3 (50 mM MES), 0.15 M Na_2SO_4, obtained at 100 K

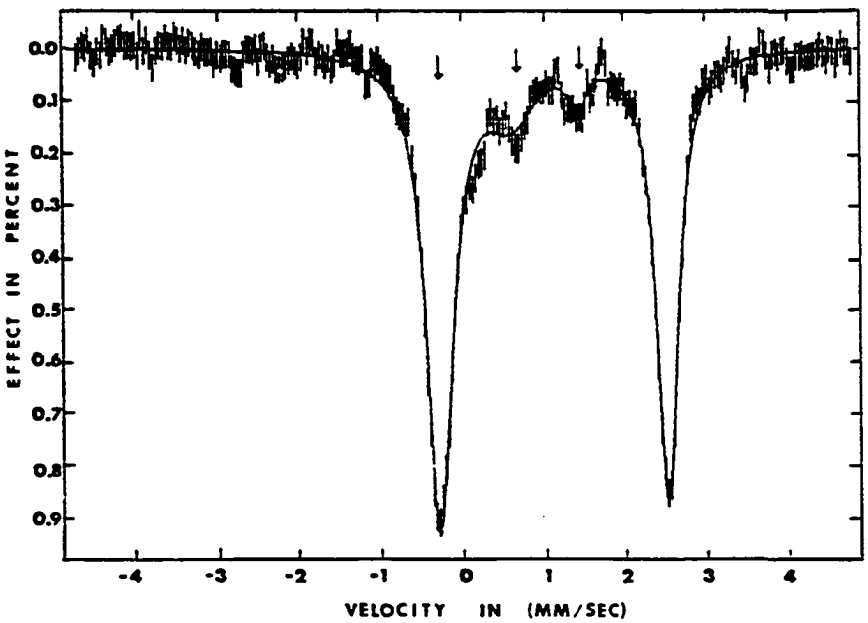

MetHr was incubated with two equivalents of $[Cr(15\text{-ane}N_4)(H_2O)_2]^{2+}$ at 25 °C for 30 minutes before freezing. Arrows indicate the absorption due to met'Hr (see text for details).

Figure I-16. Mössbauer spectrum of the second stage product during the reduction of P. gouldii Hr using two equivalents of $[Cr(15\text{-ane}N_4)(H_2O)_2]^{2+}$, pH 8.2 (50 mM EPPS), 0.15 M Na_2SO_4, obtained at 100 K

The arrows indicate the presence of high spin ferric iron doublets. Attempts to computer fit the high spin ferric iron resonances to oxyHr were not successful and are consistent with these resonances being due to a previously unobserved met species. However, these resonances may also be due to oxyHr in solution at pH 8.2 versus crystalline oxyHr for previously observed spectra (see Table 1, General Introduction).

Determination of Δ from plots of EPR half-saturation power versus time

In Figure I-17, a plot of log P_0 versus log $(I/\sqrt{P_0})$ for semi-metazidoHr at 6.4 K is shown. The half-saturation power ($P_{1/2}$) is determined from the intersection of the two linear portions of the curve using graphical inspection. The lines wtih zero slope (see Figure I-15) were determined by averaging the values of log $(1/\sqrt{P_0})$ (standard deviations were within 10% error). The slopes of the intersecting lines (see Figure I-17) were determined by a linear least squares fit of the data (correlation coefficients were $\geq$ 0.95). The half-saturation powers at various temperatures were determined in this manner for $(semi\text{-}met)_R$-, semi-metazido- and μ-S^{2-}semi-metHrs. In Figure I-18, ln $P_{1/2}$ is plotted versus 1/T for $(semi\text{-}met)_R$-, semi-metazido- and μ-S^{2-}semi-metHrs. The points plotted for $(semi\text{-}met)_R$ and semi-metazidoHrs lie on the same line within experimental uncertainty, while those

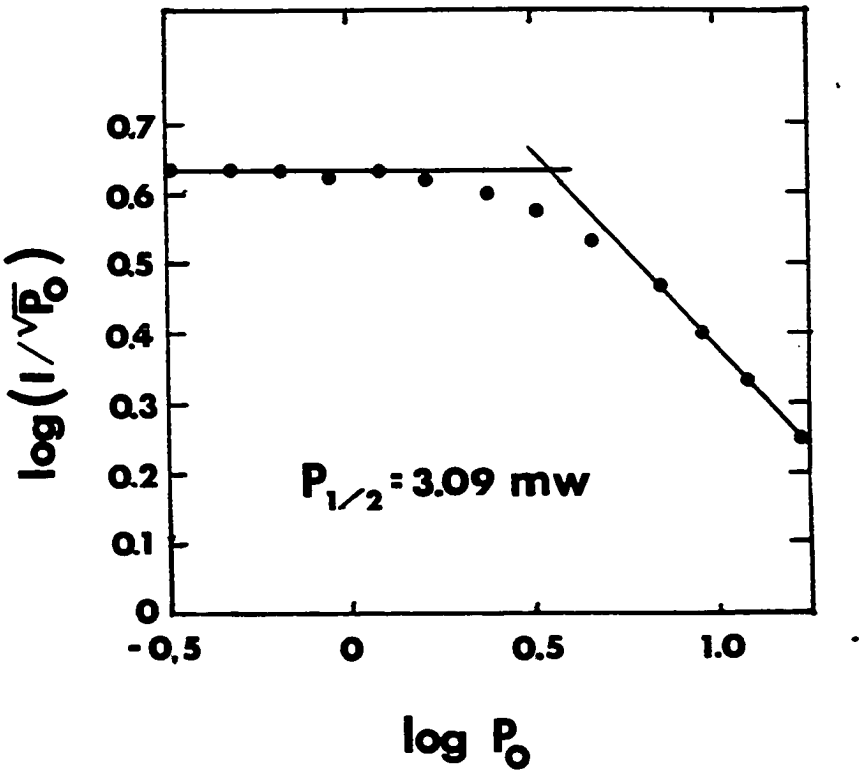

P_0 is measured in mW. Two mM semi-metazidoHr, 50 mM MES, pH 6.3.

Figure I-17. Power saturation of the EPR signal obtained at 6.4 K for semi-metazidoHr

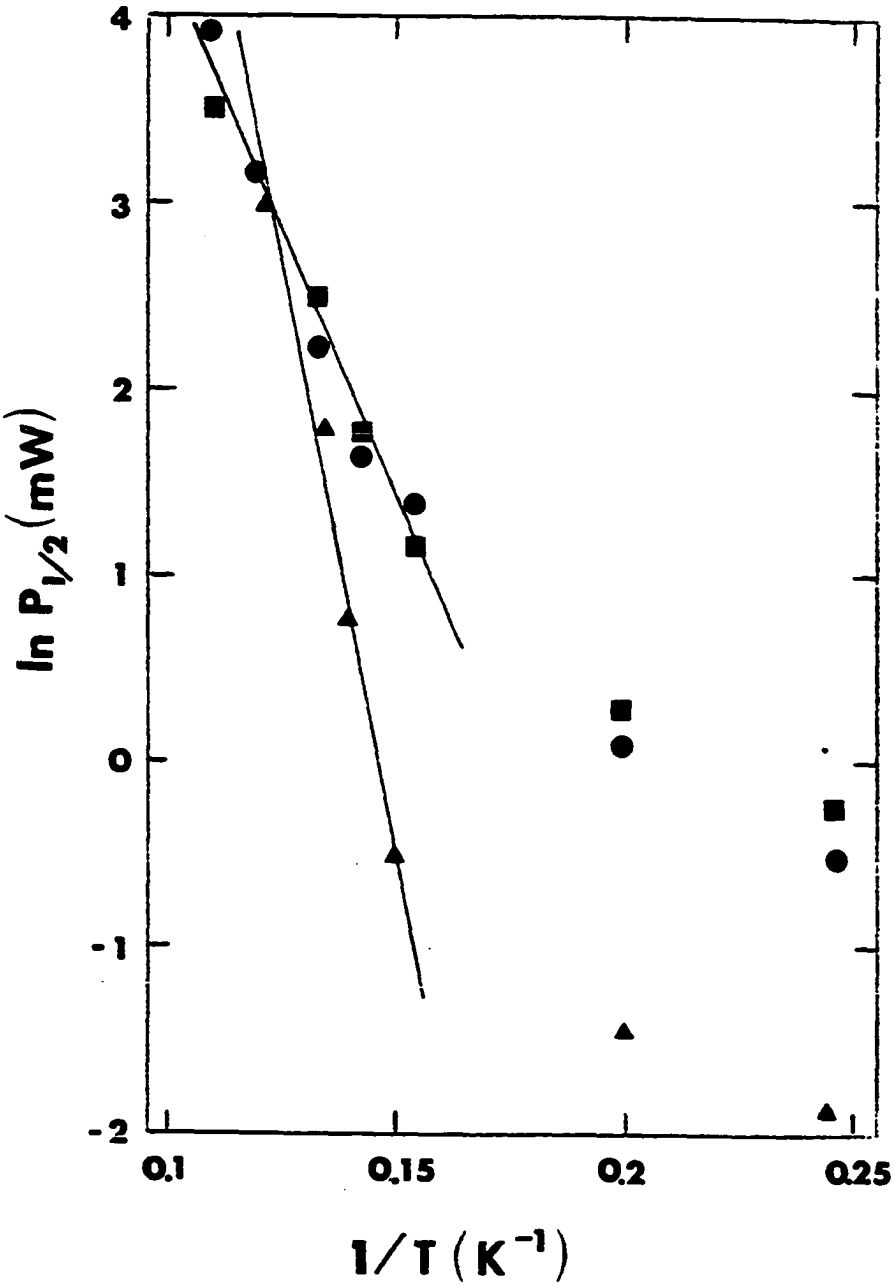

Figure I-18. Temperature dependences of the half-saturation powers for semi-metazidoHr, squares; $(semi\text{-}met)_R Hr$, circles; $\mu\text{-}S^{2-}$semi-metHr, triangles

obtained for μ-S^{2-}semi-metHr lie on a different line. The value of Δ, the energy separation between the ground state and the first excited state, for $(semi\text{-}met)_R$- and semi-metazidoHrs is 45 ($\pm$ 3) cm^{-1} and the value of Δ for μ-S^{2-}semi-metHr is 86 ($\pm$ 4) cm^{-1}. These values were obtained using a least squares fit of the linear portion of the plot in Figure I-18.

Discussion

Rates obtained for stages 2 and 3 during reduction of P. gouldii metHr (Table I-2) are in good agreement with those obtained by Armstrong et al. for reduction of T. zostericola octameric metHr (3). However, the second stage products of the reduction of T. zostericola and P. gouldii metHrs differ in the amount of fully reduced protein obtained. The second stage product of the reduction of P. gouldii metHr is ~ 85% fully reduced [Fe(II),Fe(II)], while the second stage product obtained during the reduction of T. zostericola metHr appears to be ~ 60% fully reduced. The Mössbauer spectra of the second stage product during the reduction of P. gouldii metHr (Figures I-15 and I-16) show ~ 85% fully reduced Hr (deoxy). The Mössbauer spectrum at the same stage of reduction of T. zostericola metHr (Figure I-14) shows ~ 60% deoxyHr. No EPR signal is observed for the second stage product of either T. zostericola or P. gouldii Hrs as shown by Figures I-8 through

I-11. The unreduced product of the second stage for either T. zostericola or P. gouldii is a met form of Hr, [Fe(III),Fe(III)], as shown by Mössbauer spectra in Figures I-14 through I-16, which, unlike normal metHr, shows little or no detectable binding of azide. The two proteins differ in the amount of this met form produced. The second stage product of the reduction of P. gouldii metHr has ~ 10-15% in the met form (Figures I-15 and I-16), while the second stage product obtained during the reduction of T. zostericola (Figure I-14) appears to have ~ 40% of the product in the met form as can be seen by the Mössbauer spectra. In this study, the use of Mössbauer and EPR spectroscopies has been very important in identifying the products during the reduction of metHr. UV-visible absorption spectroscopy is not capable of detecting the differences in products observed by Mössbauer and EPR spectroscopies.

The disproportionation mechanism previously described by Harrington et al. requires the transfer of electrons over distances of 28-30 Å from subunit to subunit within the octamer (17,18). When one equivalent of reducing agent is added to T. zostericola metHr to produce $(semi\text{-}met)_R$, it then disproportionates with a rate constant of 1.2×10^{-4} s^{-1} to give met and deoxyHr. This disproportionation occurs only ~ 10-20% in P. gouldii Hr (17). If the reduction of metHr to deoxyHr occurs via intramolecular disproportionation, then a

decreasing amount of $(\text{semi-met})_R$ is expected until one subunit of $(\text{semi-met})_R$ is left within the octamer, which is then slowly reduced. The data for T. zostericola Hr could be rationalized on the basis of such a mechanism, if it is proposed that the met subunits of the first disproportionation product, $[Fe(III),Fe(III)]_4[Fe(II),Fe(II)]_4$ are quickly reduced to semi-met, giving $[Fe(II),Fe(III)]_4[Fe(II),Fe(II)]_4$. The subsequent disproportionations are slower due to the lower numbers of subunits in the octamer being available to react as follows:

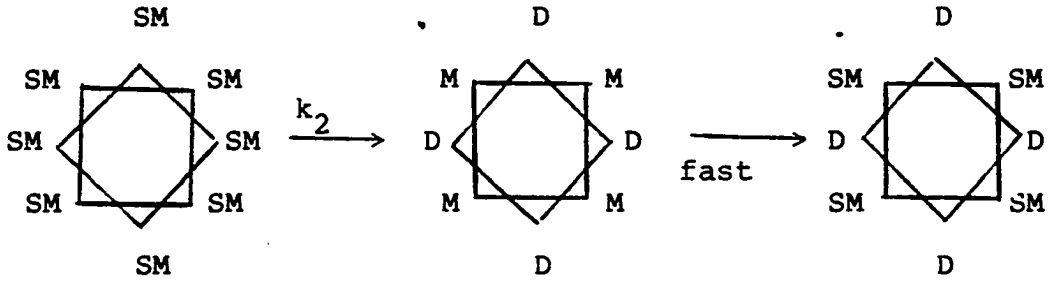

first stage product

second stage product

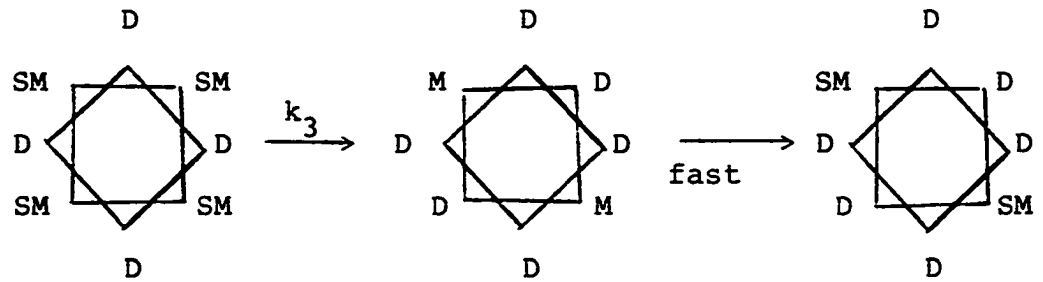

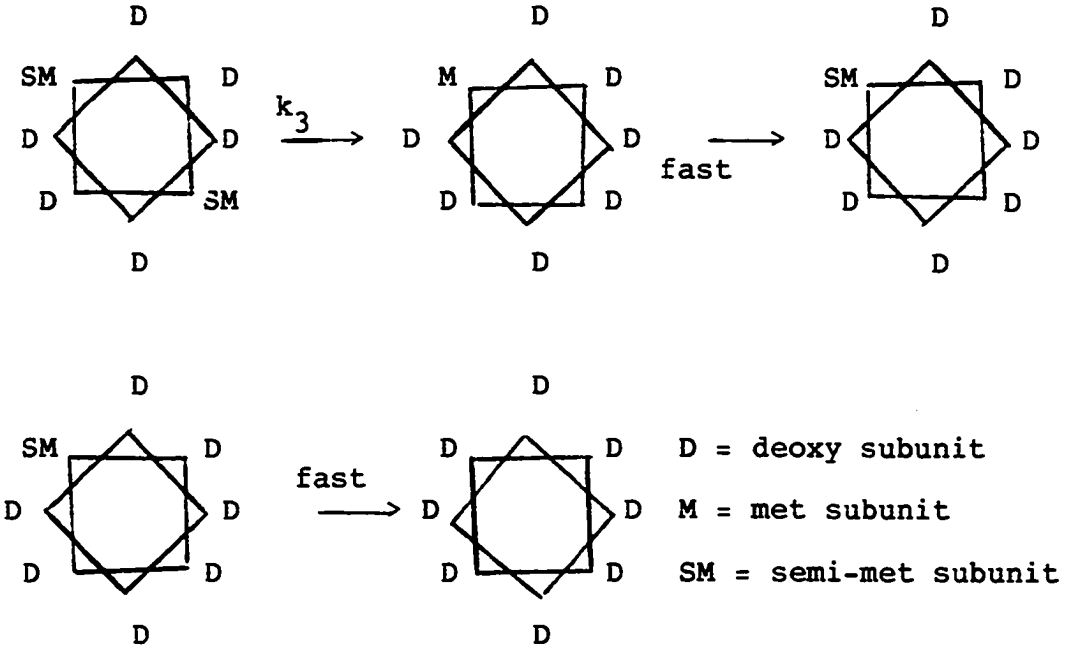

third stage product

If k_3 includes two disproportionation and rereduction steps, as shown above, then this mechanism is consistent with the decreasing rates, k_2 and k_3.

However, in all cases examined in this work, for either T. zostericola or P. gouldii Hr, the second stage product has no EPR signal. According to the scheme above, one should be able to observe a semi-met signal throughout the reduction. Also, for both Hrs, the Mössbauer spectra indicate production of a met form of Hr in addition to deoxyHr. These results seem to rule out simple intramolecular disproportionation as being the rate controlling mechanism throughout the reduction of metHr to deoxyHr. Conformational changes may, therefore,

be important in the reduction mechanism. Evidence for such conformational changes on the time scale of k_2 at the iron site of P. gouldii semi-metHr, without significant disproportionation, is contained in the EPR spectra of Figures I-12 and I-13. The development of a well-resolved feature at g = 1.66 is characteristic of a change towards a $(semi\text{-}met)_O$-type conformation (19). In contrast, only the $(semi\text{-}met)_R$ EPR spectrum is obtained with an excess of reducing agent (Figures I-8-10). These results suggest that a conformational change of the type $(semi\text{-}met)_R \rightarrow (semi\text{-}met)_O$ may be the rate limiting step of the second stage of reduction. Such conformational changes have been invoked previously to explain interconversion between two forms of semi-met obtained as kinetic products. The form obtained upon stoichiometric oxidation of deoxy is termed $(semi\text{-}met)_O$, whereas that obtained upon stoichiometric reduction of met is termed $(semi\text{-}met)_R$. These two forms can be distinguished on the basis of their EPR lineshapes and redox kinetics (1,15,19). $(Semi\text{-}met)_O$ which is produced by a one electron oxidation per monomer of deoxyHr, is known to be rapidly reduced to deoxy (17,18,20). The reduction of monomeric semi-metmyoHr from T. zostericola is also a first order process (3,21), further supporting the idea that the rate controlling step occurs within rather than between subunits. It has been suggested that the difference between the

$(semi\text{-}met)_R$ and $(semi\text{-}met)_O$ forms of Hr is in which iron of the dimeric iron site is reduced. Currently, however, there is no direct evidence to support this proposal.

^1H NMR by Maroney et al. (22) has recently shown that the magnitude of the antiferromagnetic coupling between the irons of the active site in several P. gouldii semi-metHr anion adducts is consistent with a μ-hydroxo bridge between the iron atoms as is the ^1H NMR and MCD of deoxyHr (22,16). The values of Δ, the energy difference between the ground state and the first excited state, have now been determined for $(semi\text{-}met)_R$-, semi-metazido- and $\mu\text{-}S^{2-}$semi-metHrs using EPR temperature power saturation data (Figure I-18). For binuclear compounds, the magnitude of Δ is a function of both the zero field splitting energy, D, and the antiferromagnetic coupling energy, J. Since the relationship between D and J is unknown in these mixed valent Hr derivatives, D and J cannot be calculated. However, for antiferromagnetic coupling between Fe(II) (S = 2) and Fe(III) (S = 5/2) giving a ground spin state S = 1/2, the energy separation between the ground state and first excited spin state (S = 3/2) is equal to 3J, where J is the antiferromagnetic coupling constant (23). If $D << J$, then Δ is essentially equal to 3J. From this analysis, J can be calculated from values of Δ for $(semi\text{-}met)_R$-, semi-metazido- and $\mu\text{-}S^{2-}$semi-metHrs. The value of J is similar for $(semi\text{-}met)_R$- and semi-metazidoHrs, ~ -15 cm^{-1}.

The value of J for μ-S^{2-}semi-metHr is ~ -30 cm^{-1}. The values of J, determined by Maroney et al. (22), from the temperature dependences of ^1H NMR resonances of the N_3^-, F^-, Cl^-, CN^-, and OCN^- adducts of semi-metHr and of μ-S^{2-}semi-metHr are listed in Table I-4. These values compare very well with those calculated from Δ and support the assumption that D << J. Readily interpretable ^1H NMR spectra of $(semi\text{-}met)_R Hr$ are unavailable, but the value of Δ determined from EPR temperature versus power saturation indicates that the magnitude of antiferromagnetic coupling in $(semi\text{-}met)_R$ is consistent with the presence of a μ-hydroxo bridge rather than a μ-oxo bridge. The magnitudes of Δ and J for μ-S^{2-}semi-metHr may be attributed to the persistence of the sulfido bridge in this derivative (as opposed to a hydrosulfido bridge). The ^1H NMR spectra of T. zostericola semi-metHr anion adducts are very similar to those of P. gouldii Hr, suggesting similar magnitudes of antiferromagnetic coupling (20).

The reduction of metHr to the semi-met level must then be accompanied by the protonation of the μ-oxo bridge present in metHr. Using $Fe(EDTA)^{2-}$ as the reductant, kinetic studies carried out in D_2O show no change in the rate of reduction of P. gouldii metHr to $(semi\text{-}met)_R Hr$, 3.8 ($\pm$ 0.4) $M^{-1}s^{-1}$ (H_2O) versus 3.7 ($\pm$ 0.5) $M^{-1}s^{-1}$ (D_2O), indicating that a proton is probably not involved in the rate determining step. It is possible, however, that the proton is tranferred to the μ-oxo

Table I-4. Antiferromagnetic coupling constants for P. gouldii Hr complexes (22)[a]

Hr derivatives	-J (cm^{-1})
semi-metN_3^-	18-20
semi-metF^-	18-23
semi-metCl^-	16-20
semi-metCN^-	23
semi-metOCN^-	18
μ-S^{2-}semi-met	30-36
deoxy	15

[a]Values of -J were calculated from the temperature dependences of the ^1H NMR resonances of the various derivatives.

bridge in a fast step either before or after reduction of the iron has occurred. Therefore, if a conformational change occurs during the reduction of $(semi\text{-}met)_R$Hr to deoxyHr, protonation of the μ-oxo bridge is unlikely to be involved.

The kinetic data available for T. zostericola and P. gouldii Hrs along with the physical characterizations of the kinetic products can be rationalized in the context of Scheme I-1. The reduction of P. gouldii metHr involves a conformational change during the second stage (k_2), as evidenced by the EPR spectra in Figures I-12 and I-13. If this conformational change is of the $(semi\text{-}met)_R \rightarrow (semi\text{-}met)_O$ type, it may be accompanied by a reversal of the iron oxidation states (i.e., $Fe^{2+}Fe^{3+} \rightarrow Fe^{3+}Fe^{2+}$). The iron which is closest to the surface in the Hr subunit (the six-coordinate Fe of Figure 2 in the General Introduction) is the one which is reduced when met is reduced to the semi-met level as shown by ^{1}H NMR (22), kinetic studies of T. zostericola metHr (3) and the kinetic studies reported in Section II. If this iron is oxidized via an intrasubunit electron transfer from the iron farther away from the surface (i.e., the five coordinate iron shown in Figure 2 of the General Introduction) reduction of the resulting iron (III), now closer to the surface, by external reducing agents may be more facile. During the reduction of semi-metHr, some disproportionation must occur in order to explain the

Scheme I-1

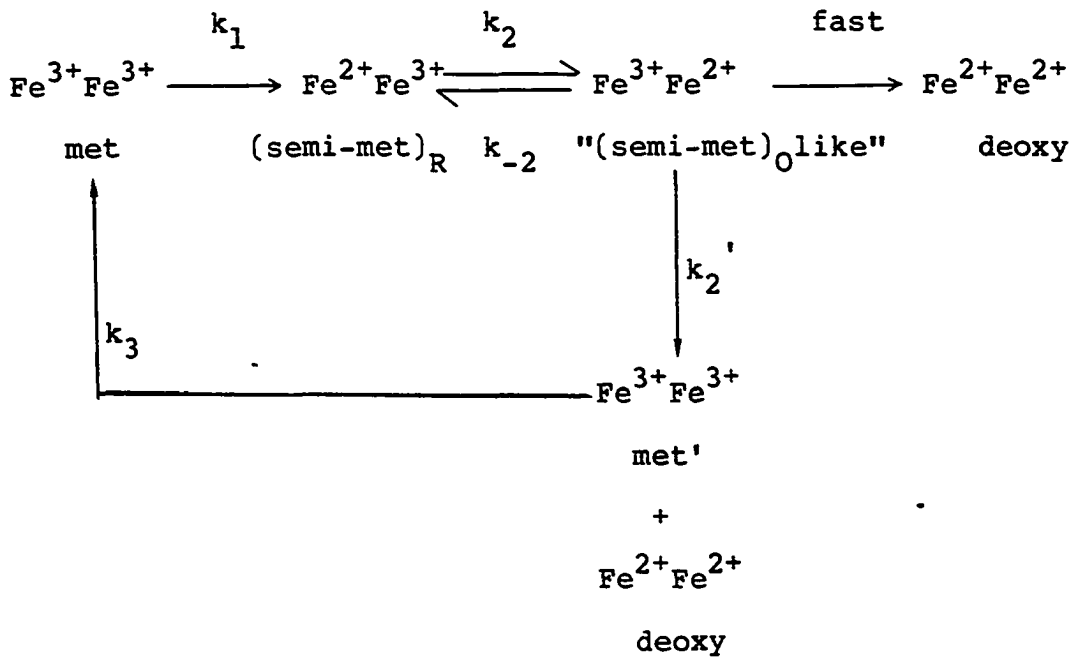
k1
k2
fast
Fe3+Fe3+
Fe2+Fe3+
Fe3+Fe2+
Fe2+Fe2+
met
(semi-met)R
k-2
"(semi-met)Olike"
deoxy
k2'
k3
Fe3+Fe3+
met'
+
Fe2+Fe2+
deoxy

production of metHr seen in the Mössbauer spectra. It is proposed that this disproportionation occurs via step k_2' yielding a form of metHr labelled met'. The rate determining step of the third stage, k_3, is proposed to be the conformational change of met' to the "normal" met form as indicated in Scheme I-1. It is interesting to speculate about the nature of met'. It may include a μ-hydroxo bridge as found in semi-met- and deoxyHrs as well as a conformation similar to that of $(\text{semi-met})_o$. The Fe(2) in Figure 1 of the General Introduction is known to coordinate hydroxide at high pH in metHr but this coordination site is vacant at low pH (24,25). Perhaps the met' form has a water molecule coordinated at the vacant position on Fe(2). The rate determining step for the third stage of reduction would then consist of the dissociation of the water to give the "normal met". Coordination of a water molecule at the innermost iron atom (Fe(2) in Figure 1 of the General Introduction) could aid in the conformational change of the type R → O in stage two, perhaps involving reversal of the oxidation states, i.e., $Fe^{2+}Fe^{3+} \rightarrow Fe^{3+}Fe^{2+}$, by making the innermost iron six-coordinate. This iron becomes Fe^{2+} if the conformational change in stage two involves reversal of the oxidation states. The proposed rate determining step of stage three, dissociation of the water molecule, is consistent with the kinetics of reduction of metHr anion adducts (26). For

example, the reduction of met SCN^-Hr with dithionite is uniphasic with the rate determining step consisting of the dissociation of SCN^- from metHr as follows:

$$\text{metSCN}^- \xrightarrow{k_{obs}} \text{met} \longrightarrow \text{semi-met} \longrightarrow \text{deoxy.}$$

The reduction of T. zostericola metHr can be explained by the same Scheme I-1 with the disproportionation step, k_2', now more effectively competing with the reduction of the "$(\text{semi-met})_o$-like" second stage product. Again, the slow stage, k_3, is the conformational change of the met' form to metHr which is then reduced via the faster steps k_1 and k_2. The amount of the met' form of Hr produced during the reduction of T. zostericola Hr is ~ 40%. If k_2' is nearly equal to the rate of direct reduction of the "$(\text{semi-met})_o$-like" form of Hr, then ~ 33% met' would be produced, so it appears that these rates may be quite similar for T. zostericola Hr, while the smaller proportion of met' for P. gouldii Hr indicates that k_2' is less than that of the "fast" step in Scheme I-1. The rate of disproportionation of T. zostericola $(\text{semi-met})_o$, which may correspond to k_2' in Scheme I-1, has been previously measured and found to have a rate constant of ~ 3×10^{-3} s^{-1} at pH 8.2 (18). The conformational change proposed to occur during the second stage of reduction with rate constant k_2 (~ $3.5 \times 10^{-3} s^{-1}$ at

pH 8.0, Table I-1) is slightly faster than the disproportionation of T. zostericola Hr. To explain our observations, one would prefer $k_2' > k_2$ in Scheme I-1. Thus, the changes we see (Figures I-12 and I-13), although similar, may not be identical to an R → O conformational change.

In conclusion, it can be said that P. gouldii and T. zostericola Hrs have similar mechanisms of reduction from the met form to the deoxy form. The main difference lies in the amount of disproportionation of each species. As previously noted, the $(\text{semi-met})_R$ form of P. gouldii Hr disproportionates only 10-20% while for T. zostericola, the $(\text{semi-met})_O$ or $(\text{semi-met})_R$ form, disproportionates completely to a product containing 1/2 metHr and 1/2 deoxyHr (17,18). These previously published observations are completely consistent with the present results showing a smaller amount of met' (using the terminology of Scheme I-1) for P. gouldii versus T. zostericola Hr. The reduction of T. zostericola monomeric metmyoHr to the deoxy level, studied by Armstrong and Sykes (19), also has three rate constants similar to those obtained for octameric P. gouldii and T. zostericola Hrs (3) indicating that similar conformational changes are occuring within the monomeric species and that the third stage in this case, is also a conformational change of met' produced via intermolecular disproportionation. Armstrong and Sykes have suggested that in the reduction of metmyoHr the third stage,

with a rate constant of ~ 2 x 10^{-4} s^{-1}, consists of a conformational change of deoxy' → deoxy (19). Again, our Mössbauer spectra of the octameric protein are more consistent with a met' → met conformational change and this may well be the case for myoHr also. The similar kinetic data for metmyoHr, k_2, ~ 2 x 10^{-3} s^{-1}; k_3, 2 x 10^{-4} s^{-1}, would indicate that perhaps intermolecular rather than intramolecular disproportionation is also the case for the octameric Hrs.

References

1. Utecht, R. E.; Kurtz, D. M., Jr. Inorg. Chem. 1985, 24, 4458-4459.

2. Harrington, P. C.; deWaal, D. J.-A.; Wilkins, R. G. Arch. Biochem. Biophys. 1978, 191, 444-451.

3. Armstrong, G. D.; Ramasami, T.; Sykes, A. G. Inorg. Chem. 1984, 24, 3230-3234.

4. Klotz, I. M.; Klotz, T. A.; Fiess, H. A., Arch. Biochem. Biophys. 1957, 68, 284-294.

5. Garbett, K.; Darnall, D. W.; Klotz, I. M.; Williams, R. J. P. Arch. Biochem. Biophys. 1969, 135, 419-434.

6. Tanabe, Y.; Sugano, S. J. Phys. Soc. Japan 1954, 9, 766-779.

7. Dawson, J. W.; Gray, H. B.; Holwerda, R. A.; Westhead, E. W. Proc. Nat. Acad. Sci. USA 1972, 69, 30-33.

8. Adzamli, I. K.; Henderson, R. A.; Sinclair-Day, J. D.; Sykes, A. G. Inorg. Chem. 1984, 23, 3069-3073.

9. Irwin, M. J.; Duff, L. L.; Shriver, D. F.; Klotz, I. M.; Arch. Biochem. Biophys. 1983, 224, 473-478.

10. Wherland, S.; Holwerda, R. A.; Rosenberg, R. C.; Gray, H. B. J. Am. Chem. Soc. 1975, 97, 5260-5262.

11. Eaton, S. S.; Eaton, G. R. Bull. of Mag. Reson. 1979, 1, 130-137.

12. Rutter, R.; Hager, L. P.; Dhonau, H.; Hendrich, M.; Valentine, M.; Debrunner, P. Biochemistry 1984, 23, 6809-6816.

13. Yim, M. B.; Kuo, L. C.; Makinen, M. W. J. Magn. Reson. 1982, 46, 247-256.

14. Robitaille, P.; Kurtz, D. M., Jr. "^{31}P-NMR studies of erythrocytes isolated from the sipunculids, Phascolopsis gouldii and Themiste zostericola", Iowa State University, Ames, Iowa, manuscript in preparation.

15. Loehr, J. S.; Loehr, T. M.; Mauk, A. G.; Gray, H. B. J. Am. Chem. Soc. 1980, 102, 6992-6996.

16. Reem, R. C.; Solomon, E. I. J. Am. Chem. Soc. 1984, 106, 8323-8325.

17. Babcock, L. M.; Bradić, Z.; Harrington, P. C.; Wilkins, R. G.; Yoneda, G. S. J. Am. Chem. Soc. 1980, 102, 2849-2850.

18. Harrington, P. C.; Wilkins, R. G. J. Am. Chem. Soc. 1981, 103, 1550-1556.

19. Armstrong, G.; Sykes, A. G. submitted to Inorg. Chem.

20. Wilkins, R. G.; Harrington, P. C. Adv. Inorg. Biochem. 1983, 5, 51-85.

21. Harrington, P. C.; Muhoberac, B. B.; Wharton, D. C.; Wilkins, R. G. Biochemistry 1981, 20, 6134-6139.

22. Maroney, M. J.; Kurtz, D. M., Jr.; Nocek, J. M.; Pearce, L. L.; Que, L., Jr. submitted to J. Am. Chem. Soc.

23. Palmer, G. in "Iron Sulfur Proteins, Vol. 2" Lovenberg, W. Ed. 1973, Academic Press, N. Y., p. 286-325.

24. Stenkamp, R. E.; Sieker, L. C.; Jensen, L. H.; Sanders-Loehr, J. Nature 1981, 291, 263-264.

25. McCallum, J. D.; Shiemke, A. K.; Sanders-Loehr, J. Biochemistry 1984, 23, 2819-2825.

26. Olivas, E.; deWaal, J. A.; Wilkins, R. G. J. Inorg. Biochem. 1979, 11, 205-212.

II. COMPARISONS OF THE OXIDATION AND REDUCTION KINETICS OF HEMERYTHRIN AND μ-SULFIDOHEMERYTHRIN

Introduction

The sulfide derivative of Hr

When sodium sulfide is added to metHr, a one electron reduction occurs and sulfide is inserted into a bridging position between the irons replacing the μ-oxo bridge. This derivative was found to be at the semi-met oxidation level using Mössbauer and EPR spectroscopy (1) (see Tables 2 and 3 in the General Introduction). Resonance Raman spectroscopy of μ-S^{2-}semi-metHr contains a strong peak at 444 cm^{-1} assigned to the symmetric stretch of an Fe-S-Fe species. Recently, it has been found that μ-S^{2-}semi-metHr can be oxidized with ferricyanide to μ-S^{2-}metHr and this latter derivative has been extensively characterized (2,3,4). Mössbauer spectroscopy has confirmed that the active site is at the met oxidation level (Table 2 in the General Introduction). The peak near 500 cm^{-1} due to the Fe-O-Fe species found in all resonance Raman spectra of metHr anion adducts is absent in spectra of μ-S^{2-}metHr. The resonance Raman spectrum of μ-S^{2-}metHr is much more complicated than that of μ-S^{2-}semi-metHr but is quite consistent with the presence of an Fe-S-Fe species.

The absorption spectra of μ-S^{2-}metHr and μ-S^{2-}semi-metHr

are shown in Figure II-1. On the basis of the excitation profile of the resonance Raman spectrum, it has been suggested that the absorption band present at 464 nm in μ-S^{2-}metHr contains much $S^{2-} \rightarrow$ Fe charge transfer character (2). The absorption spectrum of μ-S^{2-}metHr is characterized by a lack of any well resolved bands in the near UV due to a μ-oxo bridge as seen in other metHr anion adducts.

The reduction potential of the μ-S^{2-}semi-metHr/μ-S^{2-}metHr couple has been determined at pH 8.0 with and without sodium perchlorate by equilibration with ferri- and ferrocyanide (3). The potential changes slightly upon addition of perchlorate. In Tris-acetate buffer, the potential is somewhat dependent upon whether the ferri/ferrocyanide titration is started from μ-S^{2-}semi-metHr or μ-S^{2-}metHr. The average potential for the μ-S^{2-}semi-metHr/μ-S^{2-}metHr couple in 50 mM Tris-acetate (pH 8.0, I = 0.15 M) was determined to be 298 ($\pm$ 21) mV versus NHE (25 °C). When the titration was performed in 50 mM Tris-perchlorate (pH 8.0, I = 0.15 M) no dependence of potential upon starting species was observed and the potential was determined to be 295 ($\pm$ 5) mV versus NHE (25 °C).

The reduction potential of the $(\text{semi-met})_R$Hr/metHr couple has been previously determined using dichloroindophenol. The potential was determined to be 110 mV versus NHE (5) (pH 8.2, I = 0.15 M and 25 °C). Thus, when the μ-oxo bridge in metHr

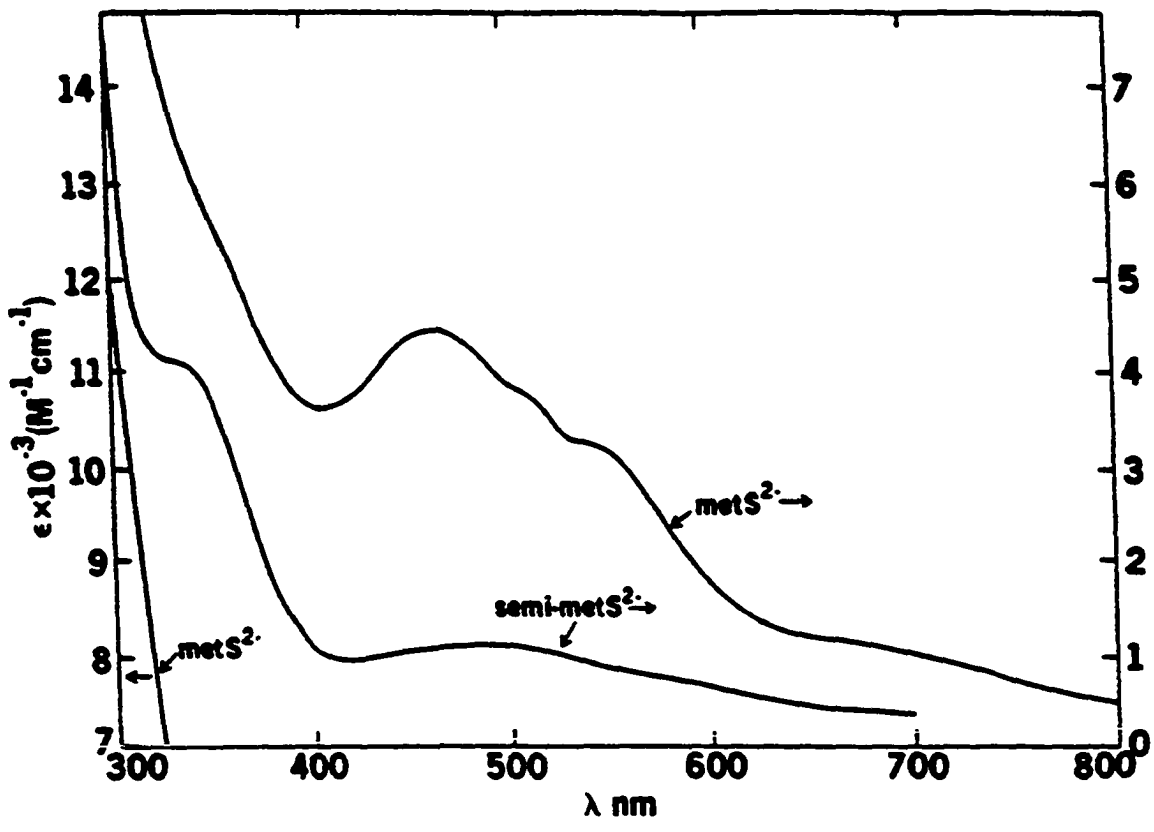

Figure II-1. UV-visible absorption spectra of μ-S^{2-}metHr and μ-S^{2-}semi-metHr in anaerobic Tris/acetate pH 8.0 (4)

is replaced by a μ-sulfido bridge the reduction potential is increased by ~ 200 mV as shown in Figure II-2.

The Marcus relation

Marcus theory (6,7) has been applied both successfully and unsuccessfully to electron transfer reactions of metal sites in proteins with inorganic complexes as well as to protein-protein electron transfer reactions (8). The Marcus relation is an attempt to predict the rates of bimolecular outer-sphere electron transfer. An outer-sphere mechanism has been defined, for small molecules, as one in which the reactants do not form an intermediate with bridging groups that provide a pathway for electron transfer (9). The Marcus relation can be described by the following equations:

$$k_{12} = (k_{11}k_{22}K_{12}f_{12})^{1/2} \qquad (1$$

$$f_{12} = \frac{(\log K_{12})^2}{4 \log (k_{11}k_{22}/Z^2)} \qquad (2$$

where k_{12} is the cross reaction rate constant, K_{12} the equilibrium constant for the cross reaction, k_{11} and k_{22} are the self-exchange rate constants. In the expression for f_{12}, Z is the diffusion-controlled rate of collision between

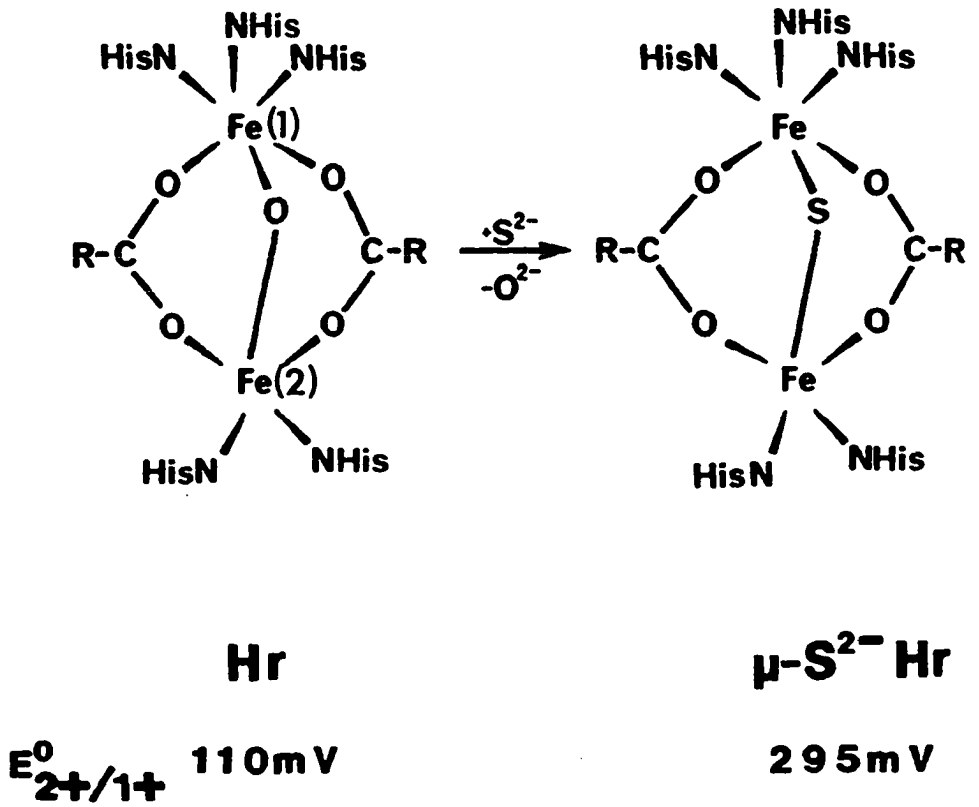

Figure II-2. Active site of metHr (left) and proposed active site of μ-S^{2-}metHr (right) (4)

uncharged particles. f_{12} is a usually taken to be unity, and thus only Equation 1 is normally used.

Statement of the Problem

The rates of reduction of μ-S^{2-}metHr or oxidation of μ-S^{2-}semi-metHr have not been previously determined. It seems intuitively obvious that, since the potential of μ-S^{2-}metHr has been raised ~ 200 mV versus that of metHr, the rates of reduction should increase and conversely the rates of oxidation should decrease. If outer sphere reagents are used, the Marcus relation can be applied to predict the ratio of rate constants using Equation 3, and assuming the values of

$$k_{12}\mu\text{-}S^{2-}\text{metHr}/k_{12}\text{met} = \frac{(K_{12}\mu\text{-}S^{2-}\text{met})^{1/2}}{(K_{12}\text{met})^{1/2}} \qquad (3$$

k_{11} for μ-S^{2-}metHr and metHr are essentially the same. The values of the equilibrium constants, K_{12}, can be calculated from the known reduction potentials of met- and μ-S^{2-}metHrs and the ratio of rates thus calculated can be compared to the experimentally determined ratio of rates. The increase in reduction potential observed when the μ-oxo bridge is replaced by a μ-sulfido bridge presents a unique opportunity to examine

the effect on kinetics of electron transfer of increasing the reduction potential of a metal center in a protein, while leaving the protein matrix virtually unchanged. The Marcus theory predicts an increase in the rate of electron transfer for μ-S^{2-}metHr over met Hr. The ratio of rate constants, $k_{12}\mu$-S^{2-}met/k_{12}met, should be ~ 40 according to the Marcus relation for the reduction of met- and μ-S^{2-}metHrs. Conversely, Marcus theory predicts the ratio of rate constants, $k_{12}(\text{semi-met})_R/k_{12}\mu$-$S^{2-}$semi-met to be ~ 40 for the oxidation of $(\text{semi-met})_R$ and μ-S^{2-}semi-metHrs.

$Fe(EDTA)^{2-}$ has been previously used as an outer sphere reducing agent, as it has no ionizable groups with pK's in the range of pH 6-8 (10). Therefore, the rates of reduction of metHr and μ-S^{2-}metHr were determined using $Fe(EDTA)^{2-}$. The rates of reduction using Cr^{2+}/cacodylate and $[Cr(15\text{-ane}N_4)(H_2O)_2]^{2+}$ have also been determined and the results applied to the Marcus theory. The rates of reduction of metHr and μ-S^{2-}metHr by two heme proteins, Mb and P.g. $cytb_5$, have also been examined as have the rates of oxidation of metHr and μ-S^{2-}metHr by $Fe(CN)_6^{3-}$ and by $[Co(phen)_3]^{3+}$.

Experimental

Preparation of metHr

Live worms of the species Phascolopsis gouldii were purchased from Marine Biological Laboratories, Woods Hole, Massachusetts and oxyHr was isolated from the coelomic fluid and crystallized by a literature proceedure (11). Crystals of oxyHr were frozen in liquid nitrogen for storage. OxyHr was prepared by dissolving oxyHr crystals into 50 mM Tris/acetate. MetHr was prepared by dialysis of solutions of oxyHr against 50 mM HEPES, pH 7.0, containing 2 mM $K_3Fe(CN)_6$ at 4 °C. Excess ferricyanide was removed by extensive dialysis against the buffer of choice. Typically ~ 5 ml of metHr were dialyzed against 3-4 one liter changes of buffer over a 24 hour period. Concentrations of metHr were determined by the addition of sodium azide and the use of $\varepsilon_{446} = 3700\ M^{-1}cm^{-1}$ (12). All concentrations are expressed in terms of binuclear iron sites. Most solutions of metHr were frozen and stored at liquid nitrogen temperatures, then thawed before use.

Preparation of $(semi\text{-}met)_R Hr$

Oxygen was removed from metHr either by anaerobic dialysis or by alternate evacuation and flushing with N_2 several times for a few hours. One equivalent of $[Cr(15\text{-}aneN_4)(H_2O)_2]^{2+}$ was added to metHr in an anaerobic

cuvette and reduction was judged complete by monitoring the absorbance at 380 nm. Reactions were complete within one minute at room temperature. $(Semi\text{-}met)_R Hr$ was used within a few minutes of preparation.

Preparation of μ-S^{2-}metHr

All operations were carried out under N_2 unless otherwise noted. MetHr (~ 1 mM) was dialyzed against 3-5 mM $Na_2S \cdot 9H_2O$ in 50 mM HEPES, pH 7, for ~ 10 hours. The resulting μ-S^{2-}semi-metHr was dialyzed against buffer containing 3-4 mM $K_3Fe(CN)_6$ for several hours. The resulting μ-S^{2-}metHr was passed rapidly by centrifugation over small "dry" Sephadex G-25 columns in 5 ml disposable plastic syringe barrels (aerobically) and then dialyzed anaerobically against the appropriate buffer for several hours to remove any remaining $K_3Fe(CN)_6$ prior to use. Protein concentrations were determined using $\varepsilon_{464} = 4500\ M^{-1}s^{-1}$ (2). Solutions of μ-S^{2-}metHr were frozen and stored in liquid nitrogen before use.

Preparation of μ-S^{2-}semi-metHr

MetHr was dialyzed against sulfide as described above and excess sulfide removed by anaerobic dialysis or by use of the small "dry" Sephadex G-25 columns described above. μ-S^{2-}semi-metHr was also prepared by the addition of one

equivalent of $Na_2S_2O_4$ to μ-S^{2-}metHr. Concentrations of $Na_2S_2O_4$ were determined by titration with $K_3Fe(CN)_6$ solutions, whose concentrations were determined using ε_{420} = 1030 $M^{-1}cm^{-1}$ (13). The concentrations of μ-S^{2-}semi-metHr were determined using ε_{500}=1100 $M^{-1}cm^{-1}$ (2). Concentrations are expressed as binuclear iron sites. Solutions of μ-S^{2-}semi-metHr were frozen and stored in liquid nitrogen before use.

Preparation of deoxyMb

Sperm whale Mb was obtained from Sigma Chemical Co. and passed over a Sephadex G-25 column equilibrated with 10 mM phosphate, pH 7.0, before use. DeoxyMb was prepared by anaerobic titration with sodium dithionite immediately before use. DeoxyMb solutions prepared in this manner were used within a few minutes, otherwise autooxidation occured. Concentrations of deoxyMb were obtained spectrophotometrically using ε_{560} = 1.2 x $10^4 M^{-1}cm^{-1}$ (14).

Preparation of reduced P.g. $cytb_5$

P.g. $cytb_5$ was isolated from the erythrocytes of Phascolopsis gouldii obtained from Marine Biological Laboratories, Woods Hole, Massachusetts, as described elsewhere (15). The cytochrome was reduced by anaerobic titration with sodium dithionite or by anaerobic photochemical reduction in the presence of 1 μM riboflavin and ~ 1 mM EDTA.

Concentrations of P.g. $cytb_5$ were determined using ε_{412} = 1.15 x 10^5 $M^{-1}cm^{-1}$ for the oxidized form of P.g. $cytb_5$ (15). The reduction potential of P.g. $cytb_5$ was determined by anaerobic titration with methylene blue at pH 7.0 and I = 0.5 M Na_2SO_4. Full details will be described elsewhere (15,16).

Preparation of inorganic reagents

Solutions of Cr^{2+}/cacodylate were prepared by oxidation of Cr metal, obtained in powder form from Aldrich, anaerobically with $HClO_4$. Cr^{2+}(aq) was prepared anaerobically in a Schlenkware filter equipped with a glass frit. Typically, 3-4 ml of 0.25 M $HClO_4$ were added to ~ 100 mg of Cr metal after activating the Cr metal with ~ 1/2 ml of concentrated HCl (HCl was removed by anaerobically washing the metal with 3-4 ml portions of $HClO_4$ several times). When the reaction was complete, ~ 30 minutes, (no further evolution of H_2 was observed) the Cr^{2+}(aq) was pulled through the frit (by use of a vacuum) into a round bottom flask leaving the unreacted Cr metal on the frit above. The resulting Cr^{2+}(aq) was then diluted with 0.1 M cacodylate, pH 7.0, 50 mM $NaClO_4$. $NaClO_4$ was added as it is an effector of Hr and some ClO_4^- was present as the counter ion of Cr^{2+}. The Cr(II) concentrations were determined by titration with sodium permanganate using ε_{545} = 2340 $M^{-1}cm^{-1}$ (17). $[Cr(15\text{-ane}N_4)(H_2O)_2]^{2+}$ was prepared by addition of Cr^{2+}(aq) to a solution containing a

slight excess of 1,4,8,12-tetraazacyclopentadecane (15-ane) obtained from Strem Chemical Co. Some precipitation of 15-ane occured and the precipitate was removed by anaerobic centrifugation of the solutions. The concentration of $[Cr(15\text{-ane}N_4)(H_2O)_2]^{2+}$ was determined using ε_{540} = 36.5 $M^{-1}cm^{-1}$ (18). $Fe(EDTA)^{2-}$ was prepared anaerobically by the method of Wherland et al. (10). $[Co(phen)_3]Cl_3$ was prepared by a literature method and ε_{330} = 4680 $M^{-1}cm^{-1}$ was used to determine its concentrations in solution (19).

Determination of pI

The pI's of met- and μ-S^{2-}metHrs were determined using an LKB Bromma 2117 Multiphor isoelectric focusing instrument with a 50-50 mixture of LKB Ampholine pH 3-10, pH 5-8 as the ampholite solution. Met- and μ-S^{2-}metHrs were run on adjacent gels which were 2.6% crosslinked. Both proteins migrated the same distance and direction; an identical pI of 7.8 was determined for met- and μ-S^{2-}metHrs.

Kinetic measurements for reactions of Hr with inorganic reagents

Reactions were run with 0.1 mM concentrations of protein and a 10-fold or greater molar excess of inorganic reagent except in the case of the oxidation of μ-S^{2-}semi-metHr by $K_3Fe(CN)_6$ where 0.05 mM concentrations of protein (expressed

as subunits) were used. Concentrations of Cr^{2+}/cacodylate greater than 2 mM caused protein precipitation. All reactions were performed under N_2 which had been scrubbed with chromous scrubbing towers to remove traces of O_2 (see Appendix A). Reactions were initiated using either stopped-flow or conventional mixing techniques and were monitored from 320 to 500 nm. The stopped flow instrument was equipped with an Aminco-Morrow mixing chamber and absorbance traces were displayed on a Tektronix Model 5150 storage oscilloscope. Reactions slower than the stopped-flow time scale were monitored on a Perkin-Elmer Model 554 spectrophotometer. The absorbance versus time data were fit to an exponential function using nonlinear least squares analysis or by a $\ln(A_t - A_\infty)$ versus time plot and the use of least squares analysis. The reactions were followed to at least 80% completion. The rate constants reported are the average of 3-5 replicate determinations.

Kinetic measurements for protein-protein reactions

Reactions were monitored by the use of a Perkin-Elmer Model 554 spectrophotometer. All reactions were carried out under N_2 in an anaerobic cuvette. Concentrations of deoxyMb for all reactions were between 10 and 30 μM. A 10-fold or larger molar excess of metHr or μ-S^{2-}metHr (calculated on the basis of subunits) over deoxyMb was used in each reaction.

Oxidations of deoxy Mb were monitored at either 560 nm or 430 nm. Oxidations of P.g. $cytb_5$ were followed at 422 nm (λ_{max} for reduced P.g. $cytb_5$). The concentration of P.g. $cytb_5$ was 1 μM in all reactions. Concentrations of met- and μ-S^{2-}metHrs ranged from 10 - 1000 μM. Rate constants were calculated using NLLS analysis or from linear least squares analysis of $\ln(A_t - A_\infty)$ versus time plots. Reactions were followed for at least 85% of the total reaction time. The rate constants reported are the average of 3-5 replicate determinations.

Kinetic measurements in D_2O

About one ml of metHr was dialyzed against ~ 100 ml of buffered D_2O solution. Buffered D_2O solutions were adjusted to the required pD (pD = pH(meter reading) + 0.4). Reactions were carried out with $Fe(EDTA)^{2-}$ and $[Co(phen)_3]Cl_3$ made in buffered D_2O solutions. Kinetic measurements were carried out as described above.

Results and Discussion

Reduction kinetics

In Table II-1, the reduction kinetics of met- and μ-S^{2-}metHrs with Cr^{2+}/cacodylate, $[Cr(15\text{-ane}N_4)(H_2O)_2]^{2+}$ and $Fe(EDTA)^{2-}$ are reported. The observed first order rate constants are linearly dependent upon reductant concentration

Table II-1. Second order rate constants for the reductions of met- and μ-S^{2-}metHrs by various reducing agents

reductant	k_{12}(met)$M^{-1}s^{-1}$	k_{12}(μ-S^{2-}met)$M^{-1}s^{-1}$	k_{12}(μ-S^{2-}met)/ k_{12}(met)
$Fe(EDTA)^{2-}$ [a]	3.8 (± 0.1)	292 (± 6)	77
Cr^{2+}/cacodylate [b]	34 (± 4)	922 (± 90)	27
$[Cr(15\text{-}aneN_4)(H_2O)_2]^{2+}$ [c]	950 (± 90)	3.23 (±0.38)x10^4	34

[a] pH 6.3 (50 mM MES) 0.15 M Na_2SO_4, 20 °C.

[b] pH 7.0, 0.1 M cacodylate, 50 mM $NaClO_4$, 20 °C.

[c] pH 6.3 (50 mM MES) 0.15 M Na_2SO_4, 20 °C.

in all cases as shown in Figures II-3 through II-8 for the reductions of met- and μ-S^{2-}metHrs with $Fe(EDTA)^{2-}$, Cr^{2+}/cacodylate, and $[Cr(15\text{-ane}N_4)(H_2O)_2]^{2+}$, respectively. In the case of metHr, Cr^{2+}/cacodylate and $[Cr(15\text{-ane}N_4)(H_2O)_2]^{2+}$ can reduce metHr to deoxyHr. As shown in Section I, the reduction of metHr to semi-metHr is usually much faster than the subsequent reduction of $(semi\text{-}met)_R$Hr to deoxyHr. Thus, the reduction to $(semi\text{-}met)_R$ is easily separated from subsequent reduction. Further reduction of μ-S^{2-}semi-metHr was not observed in any of these studies. This observation is consistent with previous studies using dithionite as reducing agent (3,4).

The pH dependence of the $Fe(EDTA)^{2-}$ reduction of metHr is shown in Figure II-9 and the data are tabulated in Table II-2 and II-3. As $Fe(EDTA)^{2-}$ does not have an ionizable functional group with a pK_a in this pH range, the changes in rates must be associated either with the ionization of a functional group in metHr or with a conformational change in the protein. Armstrong et al. (20) have noted similar changes in the rates of reduction of T. zostericola metHr with pH, which notably were obtained with positively charged reagents. They suggested that the iron atom being reduced is not the one that binds hydroxide at high pH, but is instead the six coordinate iron. This conclusion is lent additional support by our results on the pH dependence of the second order rate

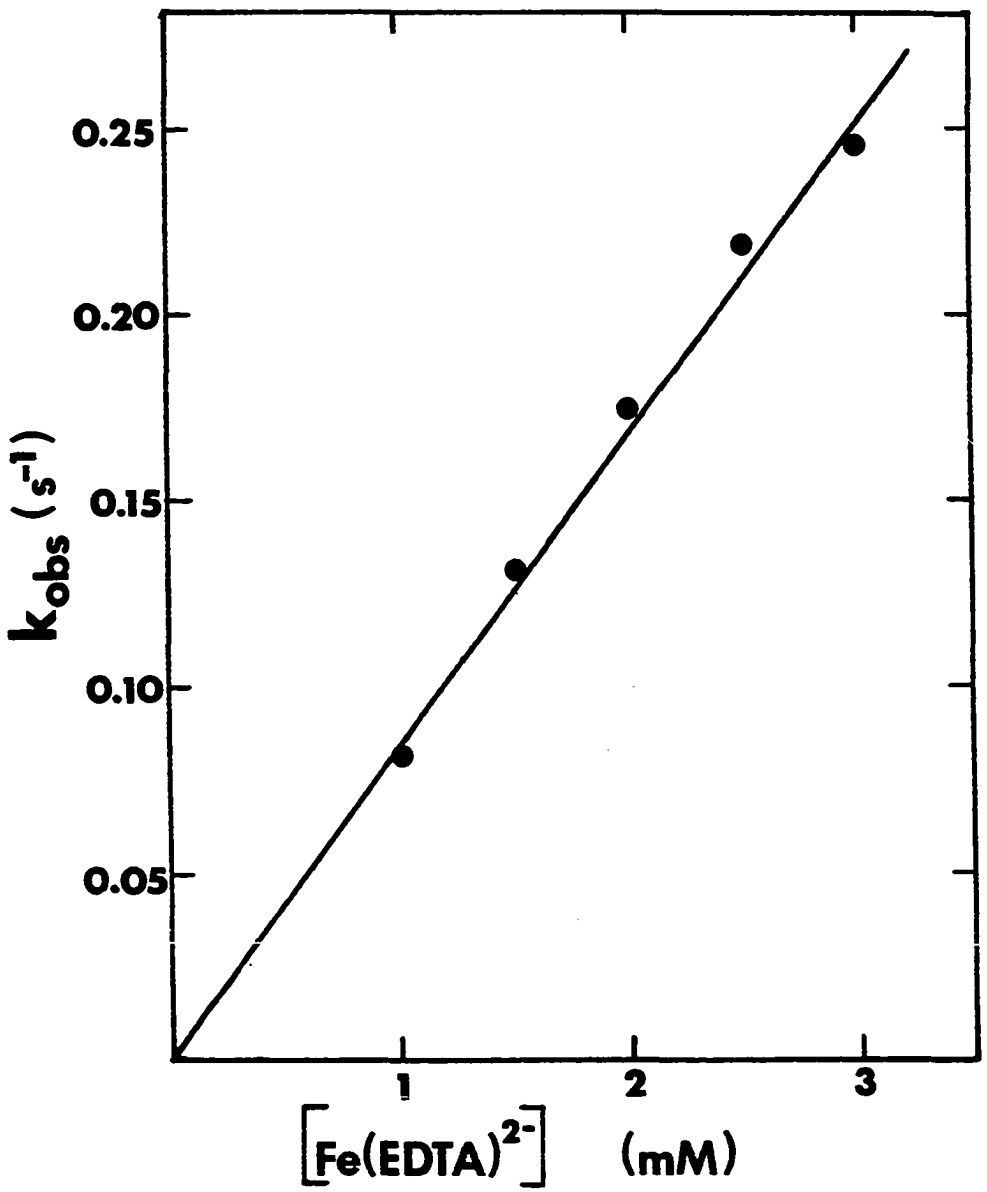

Figure II-3. Linear dependence of observed first order rate constant upon $Fe(EDTA)^{2-}$ during the reaction with 0.1 mM μ-S^{2-}metHr, pH 6.3, (50 mM HEPES) 0.15 M Na_2SO_4, 25 °C

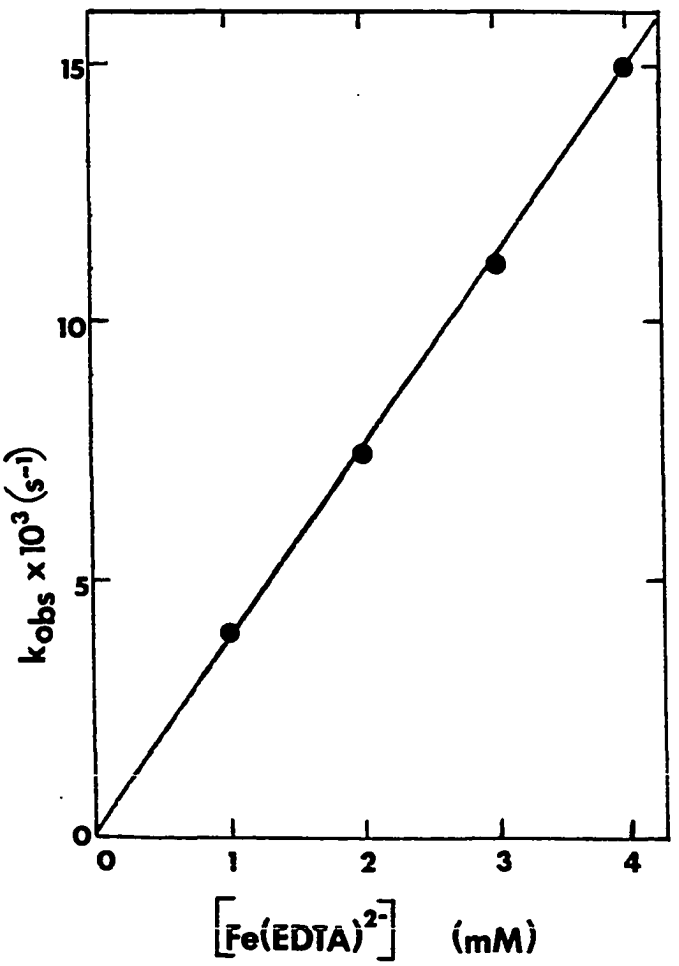

Figure II-4. Linear dependence of observed first order rate constant upon $Fe(EDTA)^{2-}$ concentration in the reaction with 0.1 mM metHr, pH 8.2, 50 mM EPPS, 0.15 M Na_2SO_4, 20 °C

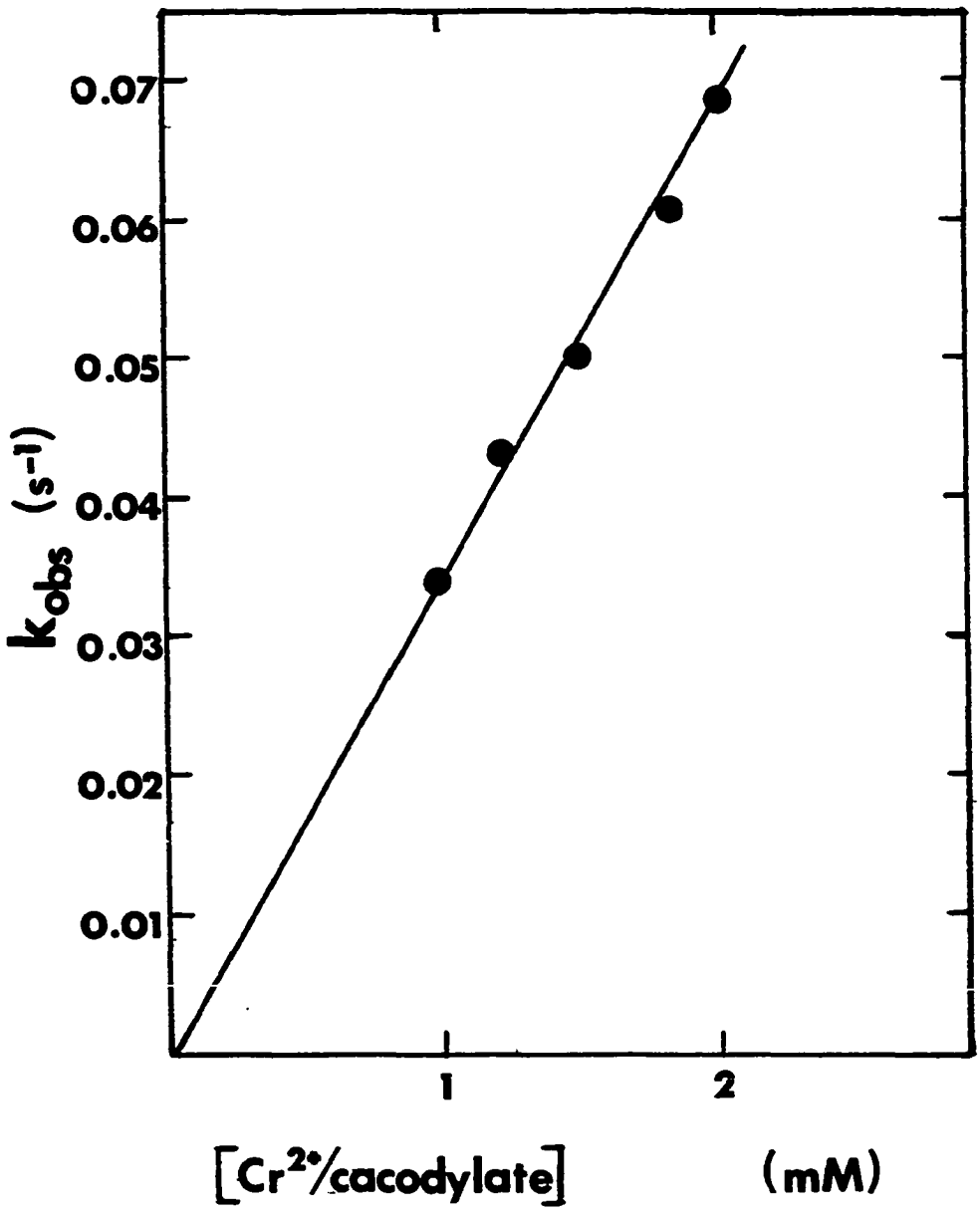

Figure II-5. Linear dependence of observed first order rate constant upon Cr^{2+}/cacodylate in the reaction with 0.1 mM metHr, pH 7.0, 50 mM $NaClO_4$, 20 °C

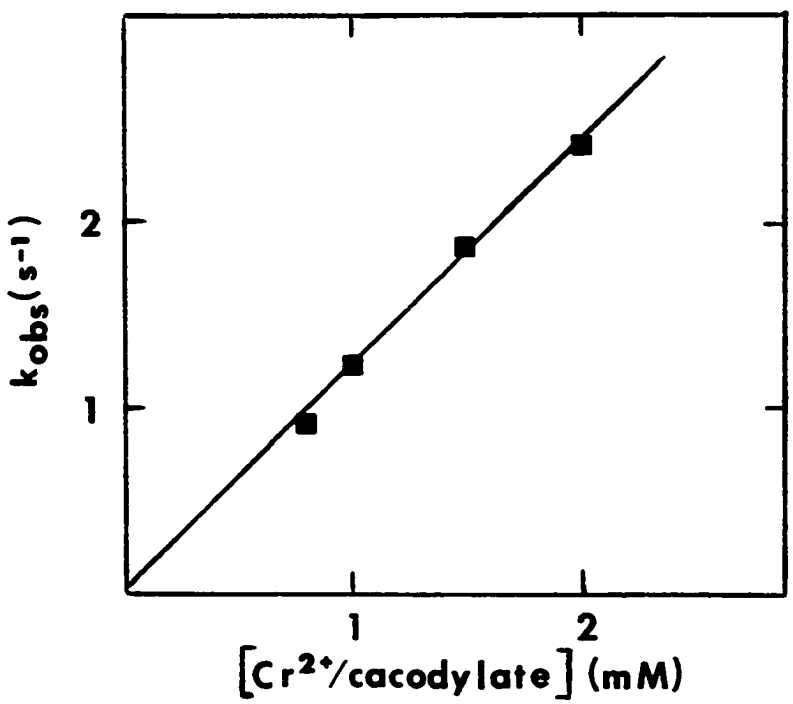

Figure II-6. Linear dependence of observed first order rate constant upon concentration of Cr^{2+}/cacodylate in the reaction with 0.1 mM μ-S^{2-}metHr, pH 7.0, 50 mM $NaClO_4$, 30 °C

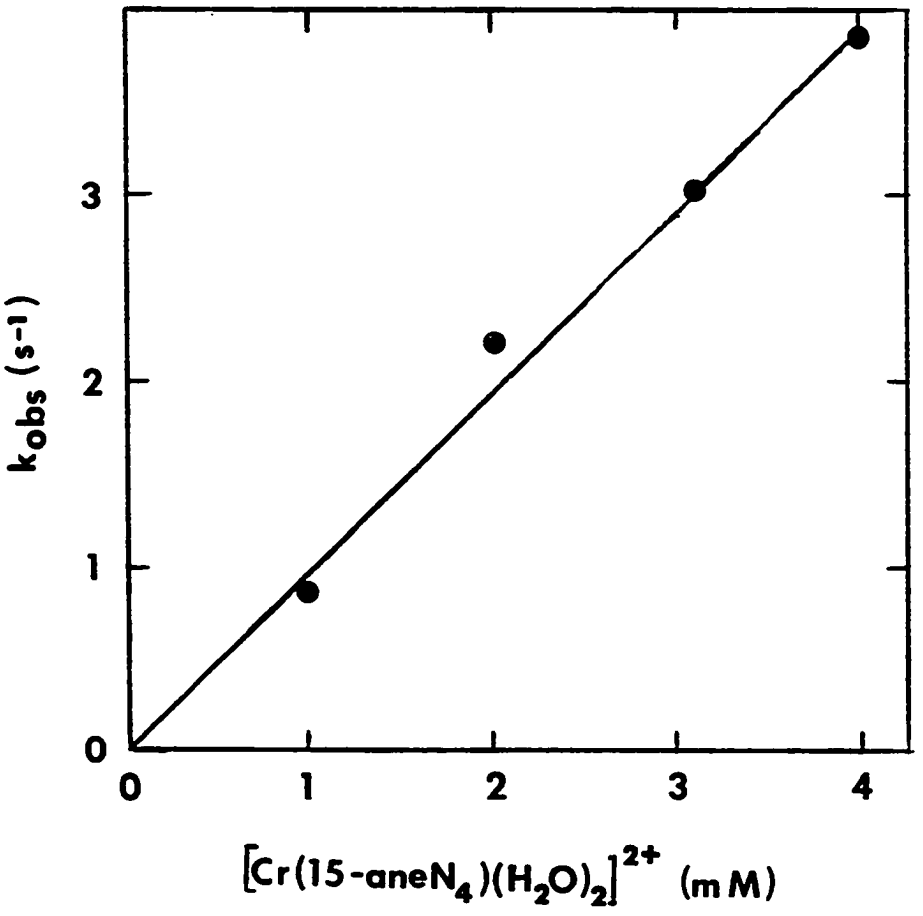

Figure II-7. Linear dependence of obseved first order rate constant upon concentration of $[Cr(15\text{-}aneN_4)(H_2O)_2]^{2+}$ in the reaction with 0.1 mM metHr, pH 6.3, (50 mM MES), 0.15 M Na_2SO_4, 20 °C

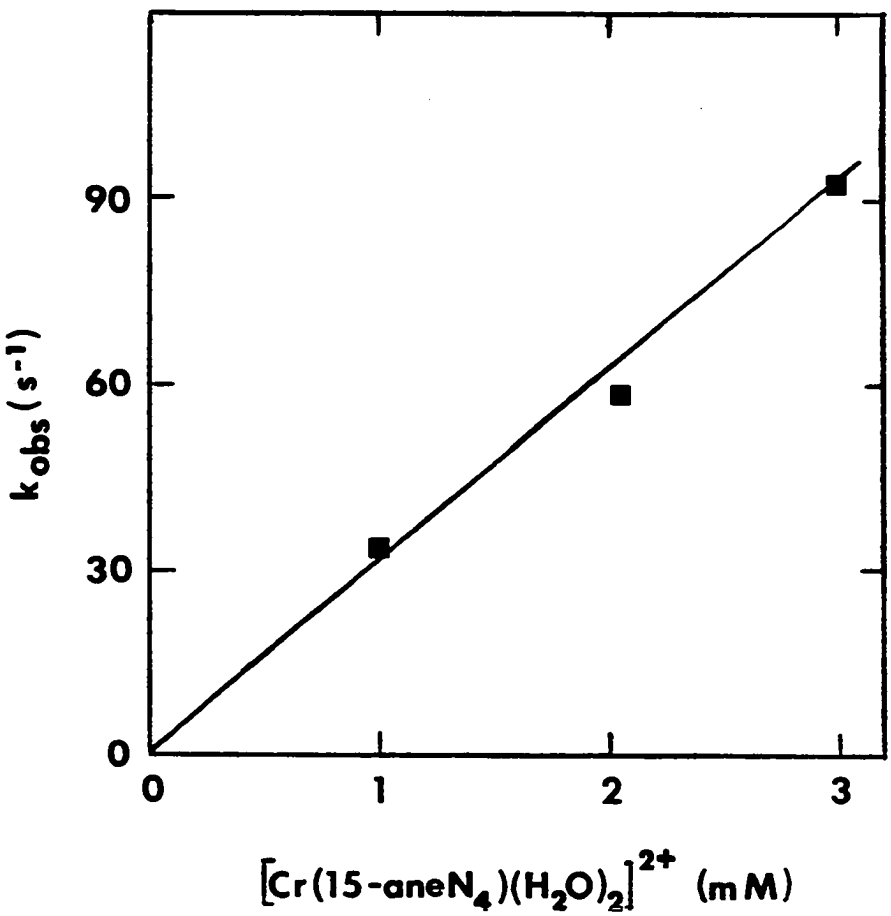

Figure II-8. Linear dependence of the observed first order rate constant upon concentration of $[Cr(15\text{-}aneN_4)(H_2O)_2]^{2+}$ in the reaction with 0.1 mM μ-S^{2-}metHr, pH 6.3, (50 mM MES), 0.15 M Na_2SO_4, 20 °C

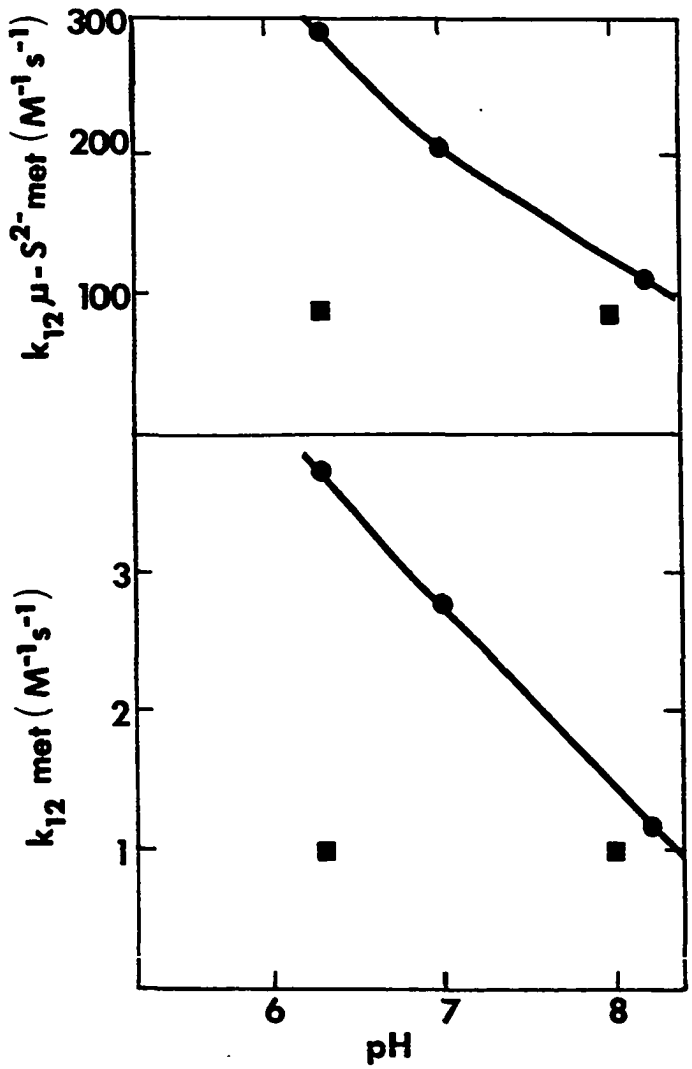

Squares represent reactions in the presence of 50 mM $NaCl_4$. Fifteen hundredths M Na_2SO_4, 25 °C, 50 mM MES, HEPES, or EPPS at pHs 6.3, 7.0 and 8.2, respectively. Solid curves do not represent any theoretical fit of the data.

Figure II-9. The dependence of the rates of reduction of met and $\mu\text{-}S^{2-}$metHr with $Fe(EDTA)^{2-}$ upon pH

Table II-2. pH dependence of the second order rate constants for the reduction of μ-S^{2-}metHr with $Fe(EDTA)^{2-}$. I = 0.15 M (Na_2SO_4), 20°C. Values in parentheses are standard deviations

pH	$[NaClO_4]$ (mM)	$k(M^{-1}s^{-1})$
6.3	50	89.0(± 2.8)
6.3	--	292(± 6)
7.0	--	207(± 2)
8.0	50	83.2(± 2.9)
8.2	--	110(± 2.4)

Table II-3. pH dependence of the second order rate constants for the reduction of metHr with $Fe(EDTA)^{2-}$, I = 0.15 M Na_2SO_4, 20°C, values in parentheses are standard deviations

pH	$[NaClO_4]$(mM)	$k(M^{-1}s^{-1})$
6.3	50	1.00(± 0.06)
6.3	--	3.8(± 0.1)
7.0	--	2.93(± 0.04)
8.0	50	1.00(± 0.04)
8.2	--	1.14(± 0.14)

constants for reduction of μ-S^{2-}semi-metHr, also shown in Figure II-9. Previous studies (2-4) have given no indication of any hydroxide binding to the iron site in μ-S^{2-}metHr, yet the pH dependence exhibited by the reduction kinetics of μ-S^{2-}metHr is very similar to that for metHr. We conclude, as do Armstrong et al. (20), that the iron atom which binds hydroxide is probably not reduced and that changes at this iron atom do not change the rate of reduction of the iron site to any great extent. Further insight on this point can be obtained from the reduction of μ-S^{2-}metHr and metHr with $Fe(EDTA)^{2-}$ in the presence of $NaClO_4$. Structural studies indicate that the perchlorate anion binds to the outer surface of the Hr octamer and that the conformation of the iron site is affected by the binding of the perchlorate anion (21,22). As shown in Figure II-9, the rate of reduction of metHr at pH 8.0 in the presence of $NaClO_4$, is slightly lower than the rate of reduction at pH 8.2 in the absence of $NaClO_4$, 1.1 $M^{-1}s^{-1}$. At pH 6.3, the rate of reduction of metHr in the presence of $NaClO_4$ is virtually unchanged from its value at pH 8.0. A similar situation is found for the reduction of μ-S^{2-}metHr with $Fe(EDTA)^{2-}$ in the presence of $NaClO_4$, as shown in Figure II-9. The presence of $NaClO_4$ appears to "lock" both the metHr and μ-S^{2-}metHr into similar conformations at pH 6.0 and 8.0 as evidenced by the reduction kinetics of both species. Thus, we conclude that the influence of pH and an allosteric effector,

$NaClO_4$, on the reduction kinetics of met- and μ-S^{2-}metHrs are very similar to each other and therefore, that the differences in rates of reduction between metHr and μ-S^{2-}metHr are due to intrinsic differences in the redox properties of the iron site, rather than to differences in water or hydroxide binding to the iron atom, or to differences in the protein matrix. There also appear to be no significant differences in the protein surface charges of met- and μ-S^{2-}metHr as the pI's are identical, ~ 7.8. This value is close to that measured previously for metHr (23).

Table II-1 shows that the rates of reduction by Cr^{2+}/cacodylate, $[Cr(15\text{-ane}N_4)(H_2O)_2]^{2+}$ and $Fe(EDTA)^{2-}$ are 30-80 times higher for μ-S^{2-}metHr than metHr. Assuming that the electron self-exchange rate constants are identical for metHr and μ-S^{2-}metHr, simple Marcus theory predicts that the ratio of second order rate constants for reduction of μ-S^{2-}met- and metHrs should obey Equation 3 (6). Based on the ~ 200 mV potential difference between the two derivatives of Hr, Marcus theory predicts that the rate of reduction of μ-S^{2-}metHr should be ~ 40 fold faster than the rate of reduction of metHr. Table II-1 also shows the ratios of rate constants, $k_{12}\mu$-S^{2-}met/k_{12}met. It appears that for all three reagents, Equation 3 is fairly well obeyed. Note that in the case of Cr^{2+}/cacodylate, agreement with the calculated ratio is good even in the presence of the allosteric effector,

perchlorate. The ratio of rate constants for $Fe(EDTA)^{2-}$ appears to be somewhat higher than expected. Negatively charged reagents, such as $Fe(CN)_6^{3-}$, appear to bind to Hr. It is possible that $Fe(EDTA)^{2-}$ differs slightly in its interactions with μ-S^{2-}metHr and metHrs and this difference may cause deviations from Equation 3. $Fe(EDTA)^{2-}$ is also not spherically symmetric, having hydrophobic and hydrophilic faces (8). This asymmetry may accentuate whatever slight conformational differences may exist between μ-S^{2-}metHr and metHr.

Activation parameters for the reduction of μ-S^{2-}met and metHrs with $Fe(EDTA)^{2-}$ and Cr^{2+}/cacodylate were determined from Eyring plots as shown in Figures II-10 and II-11 using data in Table II-4. The values of $\Delta H^{\ddagger}$ and $\Delta S^{\ddagger}$ are reported in Table II-5. The activation enthalpies of these reactions are all very similar, although somewhat lower values are obtained for reductions of μ-S^{2-}metHr. The differences in activation entropies between μ-S^{2-}met- and metHr are larger than expected (25), but apparently reflect the differences in reorganization of the two iron sites necessary to reach the transition state. We do not believe these differences in activation parameters reflect large mechanistic differences for the reduction of μ-S^{2-}metHr versus metHr.

Using $Fe(EDTA)^{2-}$ as the reductant, values of the electron self-exchange constant, k_{11}, for metHr and for μ-S^{2-}metHr can

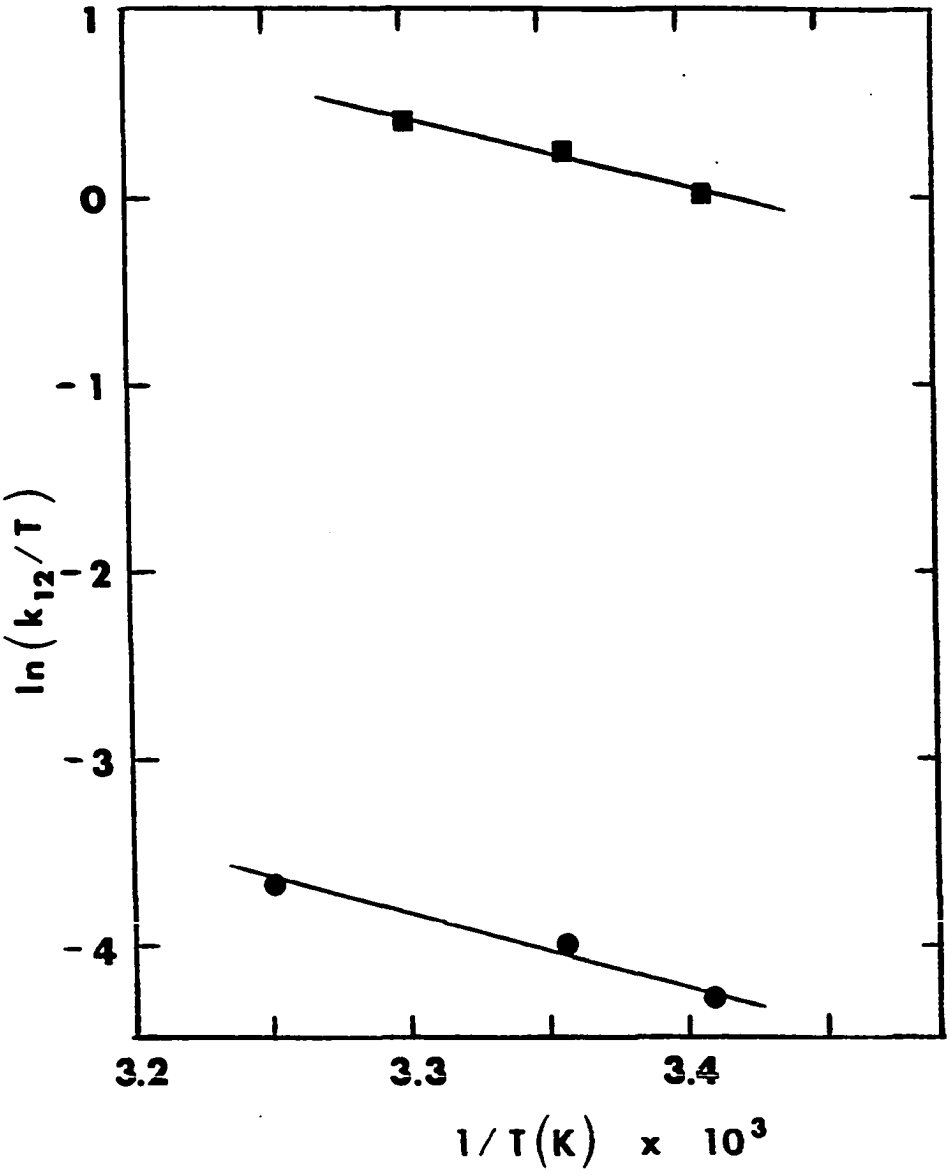

Figure II-10. ln (k_{12}/T) versus 1/T is plotted for the $Fe(EDTA)^{2-}$ reaction with metHr (circles) and μ-S^{2-}metHr (squares) pH 6.3, (50 mM MES), 0.15 Na_2SO_4

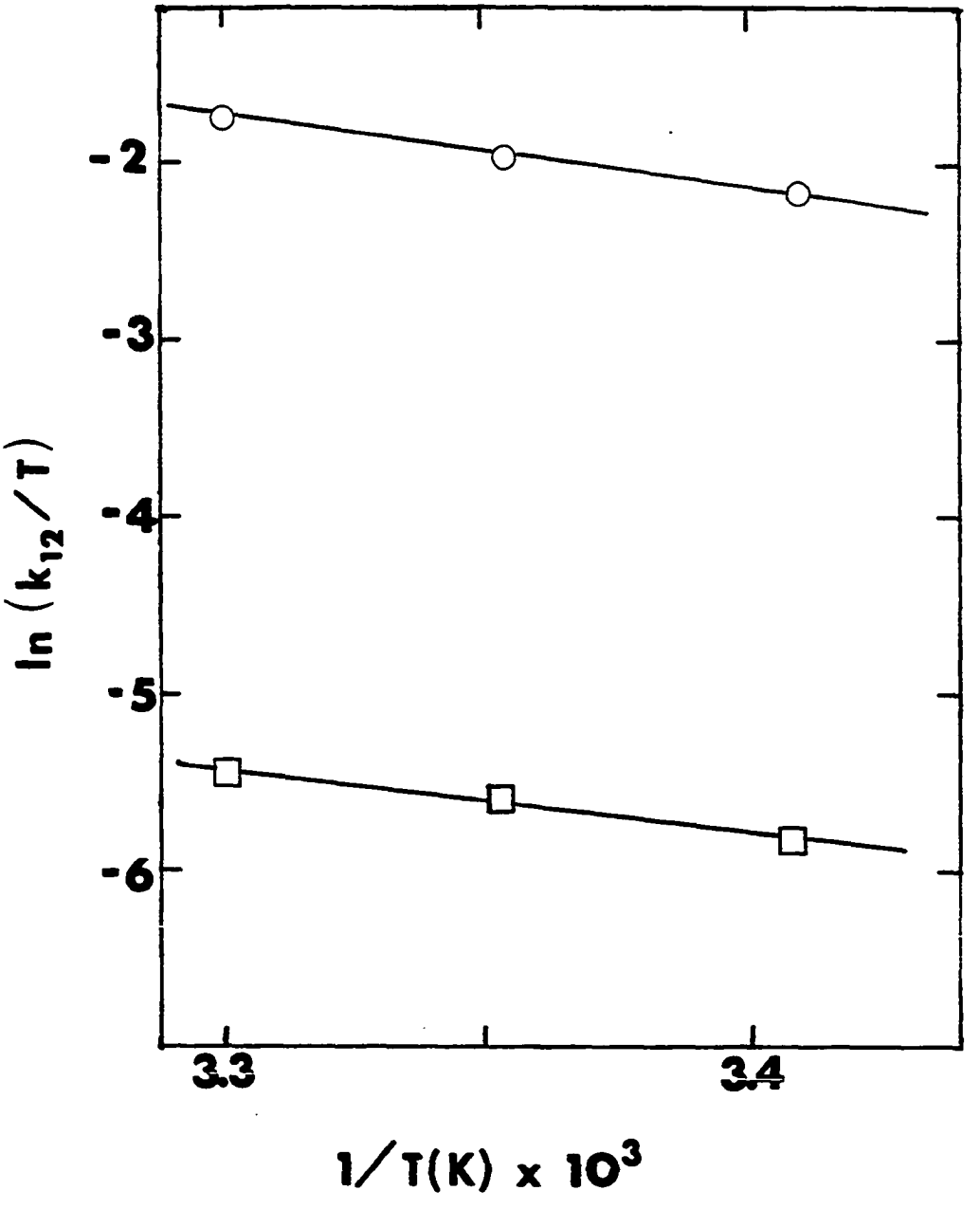

Figure II-11. ln (k_{12}/T) versus 1/T is plotted for the Cr^{2+}/cacodylate reaction with metHr (open circles) and μ-S^{2-}metHr (open squares) pH 7.0, 0.1 M cacodylate, 50 mM $NaClO_4$

Table II-4. Temperature dependent rate constants for the reduction of met and μ-S^{2-}metHrs using $Fe(EDTA)^{2-}$ and Cr^{2+}/cacodylate

$Fe(EDTA)^{2-}$	pH 6.3,(50mM MES), 0.15 M Na_2SO_4	
T(°C)	k_{12}met($M^{-1}s^{-1}$)	k_{12}μ-S^{2-}metHr($M^{-1}s^{-1}$)
20	3.8(±0.1)	292(±6)
25	5.4(±0.1)	350(±3)
30.5		442(±12)
35	7.1(±0.4)	

Cr^{2+}/cacodylate	pH 7.0,0.1 M cacodylate,50 mM $NaClO_4$	
T(°C)	k_{12}met($M^{-1}s^{-1}$)	k_{12}μ-S^{2-}met($M^{-1}s^{-1}$)
20	34(±4)	922(±90)
25	42(±4)	1062(±90)
30	51(±5)	1200(±120)

Table II-5. Activation parameters for the reduction of metHr and μ-S^{2-}metHr by $Fe(EDTA)^{2-}$ and Cr^{2+}/cacodylate

	$\Delta H^{\ddagger}$(kJ/mole)	$\Delta S^{\ddagger}$(J/mol·K)
	μ-S^{2-}metHr	
$Fe(EDTA)^{2-}$ [a]	23.0 (± 0.2)	-71.6 (± 0.7)
Cr^{2+}/cacodylate[b]	20 (± 5)	-72 (± 17)
	metHr	
$Fe(EDTA)^{2-}$ [a]	28.2 (± 0.3)	-137 (± 2)
Cr^{2+}/cacodylate[b]	27.3 (± 0.3)	-122 (± 3)

[a] pH 6.3, (50 mM MES), 0.15 M Na_2SO_4.

[b] pH 7.0, 0.1 M cacodylate, 50 mM $NaClO_4$.

be calculated from the Marcus relation. The values of k_{11} for met and μ-S^{2-}metHr are 5×10^{-4} and 1×10^{-3} $M^{-1}s^{-1}$, respectively at pH 6.3, 25 °C. These values agree fairly well with those previously established for Hr (14,24). Again, the evidence suggests that the increases in rates for the sulfide derivative are due to the increase in reduction potential at the iron site rather than to an increase in intrinsic ability of the surrounding protein to transfer electrons or to a different iron being reduced. In a study of the comparison of the reduction kinetics of metmyoglobin and metsulfmyoglobin, Lim and Mauk also concluded that the intrinsic electron transfer ability of myoglobin did not undergo any changes which could not be accounted for by the use of Equation 1 when the heme group was modified with sulfur (26). However, our comparison represents a much larger difference in reduction potential of the metal site and also is the first such comparison for non-heme proteins.

Oxidation kinetics

The kinetics of oxidation of $(semi\text{-}met)_R$Hr has been previously studied by Wilkins et al. using $Fe(CN)_6^{3-}$ (24,28a). In the present study, the oxidation of μ-S^{2-}semi-metHr and $(semi\text{-}met)_R$Hr by $[Co(phen)_3]Cl_3$ was carried out as well as the oxidation of μ-S^{2-}semi-metHr by $Fe(CN)_6^{3-}$. The oxidation of $(semi\text{-}met)_R$Hr by $Fe(CN)_6^{3-}$ was reexamined, using a different

method of preparation of $(semi\text{-}met)_R$ than used by previous workers. Simple Marcus theory (Equation 3) predicts that the rate of oxidation of $(semi\text{-}met)_R$Hr should be 40-fold faster than the rate of oxidation of μ-S^{2-}semi-metHr. In Table II-6, the second order rate constants for the above reactions are shown. The dependence of rates upon the concentration of $[Co(phen)_3]Cl_3$ for the oxidations of μ-S^{2-}semi-metHr and $(semi\text{-}met)_R$Hrs are shown in Figure II-12. The presence of ~ 100 mM Cl^- does not appreciably affect the rates of oxidation of μ-S^{2-}semi-met- and $(semi\text{-}met)_R$Hrs by $[Co(phen)_3]Cl_3$. The dependence of rates upon the concentration of $Fe(CN)_6^{3-}$ for the oxidations of μ-S^{2-}semi-metHr and $(semi\text{-}met)_R$Hr are shown in Figure II-13. A typical absorbance versus time plot with an NLLS fit of the experimental absorbance versus time data for the oxidation of $(semi\text{-}met)_R$Hr by $Fe(CN)_6^{3-}$ is shown in Figure II-14. The value of the second order rate constant obtained for the oxidation of $(semi\text{-}met)_R$Hr by $Fe(CN)_6^{3-}$ is ~ 50 times the value obtained for the oxidation of μ-S^{2-}semi-metHr by $Fe(CN)_6^{3-}$ (Table II-6). This increase in rate for the oxidation of $(semi\text{-}met)_R$Hr agrees well with the value of 40 predicted using the Marcus relation. $Fe(CN)_6^{3-}$ is known to bind to both met and μ-S^{2-}metHrs (27). The good agreement with Marcus theory for the ratio of rate constants for oxidations of the two derivatives of Hr suggests that the

Table II-6. Kinetic data for oxidations of $(semi\text{-}met)_R$ and $\mu\text{-}S^{2-}$semi-metHrs by $Co(phen)_3^{3+}$ and $Fe(CN)_6^{3-}$, pH 8.2 (50 mM EPPS), 0.15 M Na_2SO_4, 25 °C

Oxidant	$k_{12}(semi\text{-}met)_R$ $(M^{-1}s^{-1})$	$k_{12}\mu\text{-}S^{2-}$semi-met Hr $(M^{-1}s^{-1})$	$k_{12}(semi\text{-}met)_R / k_{12}\mu\text{-}S^{2-}$semi-met
$Co(phen)_3^{3+}$	1.3 (± 0.2)	8.2 (± 0.4)	0.12
$Fe(CN)_6^{3-}$	$1.6(\pm 0.3)\times 10^4$	326 (± 10)	49

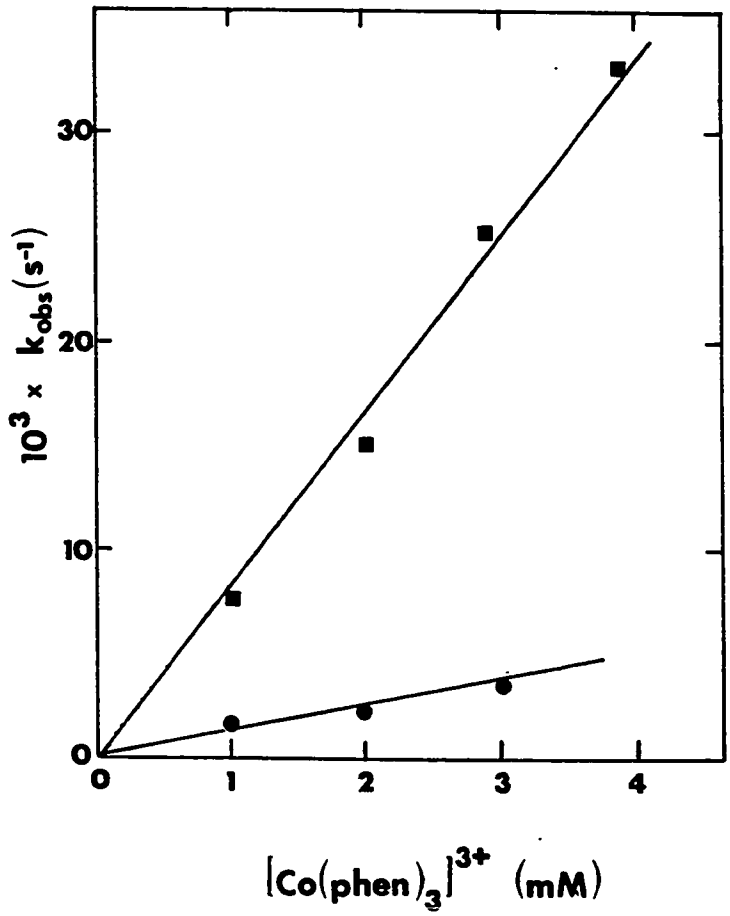

pH 8.2, (50 mM EPPS), 0.15 M Na_2SO_4, 25 °C; 0.1 mM $(semi\text{-}met)_R Hr$ (circles), 0.1 mM $\mu\text{-}S^{2-}$semi-metHr (squares).

Figure II-12. The dependence of the observed first order rate constants for oxidations of $(semi\text{-}met)_R Hr$ and $\mu\text{-}S^{2-}$semi-metHr upon the concentration of $Co(phen)_3^{3+}$

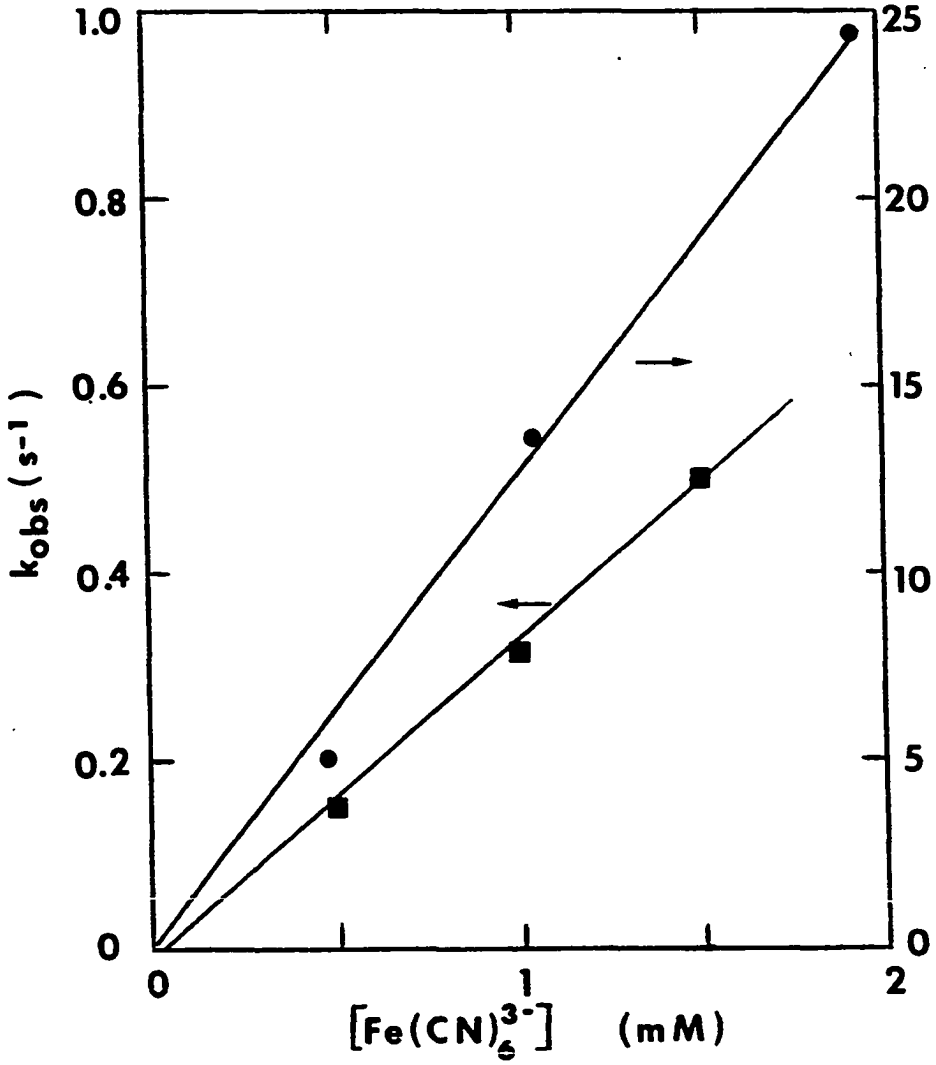

pH 8.2 (50 mM EPPS), 0.15 M Na_2SO_4, 25 °C; 0.05 mM $(semi\text{-}met)_R Hr$ (circles), 0.05 mM $\mu\text{-}S^{2-}$semi-metHr (squares).

Figure II-13. The dependence of the observed first order rate constants for $(semi\text{-}met)_R Hr$ and $\mu\text{-}S^{2-}$semi-metHr upon the concentration of $Fe(CN)_6^{3-}$

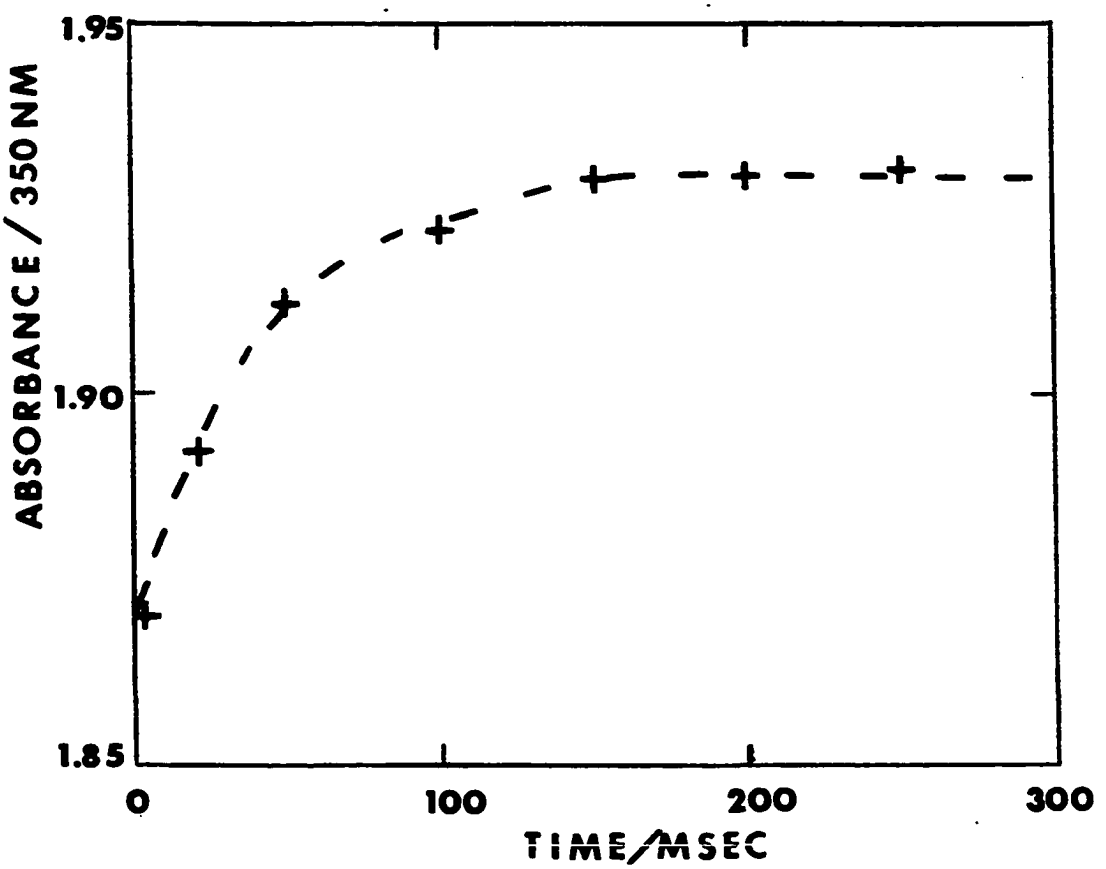

Figure II-14. (---) one exponential fit of (+) experimental absorbance (350 nm) versus time data of the oxidation of 0.05 mM (semi-met)$_R$Hr by 2.0 mM $Fe(CN)_6^{3-}$ at pH 8.2 (50 mM EPPS), 0.15 M Na_2SO_4, 25 °C

binding sites for $Fe(CN)_6^{3-}$ are most likely the same.

The rates of oxidation using $[Co(phen)_3]Cl_3$ do not obey Marcus theory as can be seen by the ratios of rates in Table II-6. The activation parameters for the oxidations by $[Co(phen)_3]Cl_3$, obtained from Eyring plots (Figure II-15), using data in Table II-7, indicate that different mechanisms are operating for oxidations of the two derivatives of Hrs by $[Co(phen)_3]Cl_3$. For the oxidation of μ-S^{2-}semi-metHr by $[Co(phen)_3]Cl_3$, $\Delta H^{\ddagger}$ = 30.0 (± 0.2) kJ/mol and $\Delta S^{\ddagger}$ = -80 (± 1) J/K·mol, pH 8.2. Activation parameters obtained for the oxidation of metHr by $[Co(phen)_3]Cl_3$ are: $\Delta H^{\ddagger}$ = 76 (± 1) kJ/mol and $\Delta S^{\ddagger}$ = 59 (± 3) J/K·mol, pH 8.2.

The use of $Co(phen)_3^{3+}$ to oxidize other metalloproteins, such as the blue copper proteins, resulted in higher calculated values of k_{11} than those obtained using other redox reagents (8). The hydrophobic phenanthroline ligands in $Co(phen)_3^{3+}$ may well be involved in the penetration of protein surfaces. Differential interaction of $Co(phen)_3^{3+}$ with the surfaces of μ-S^{2-}semi-metHr and $(semi\text{-}met)_R$Hrs may be important in the failure of the Marcus relation to predict the ratio of rate constants for the oxidations of μ-S^{2-}semi-metHr and $(semi\text{-}met)_R$.

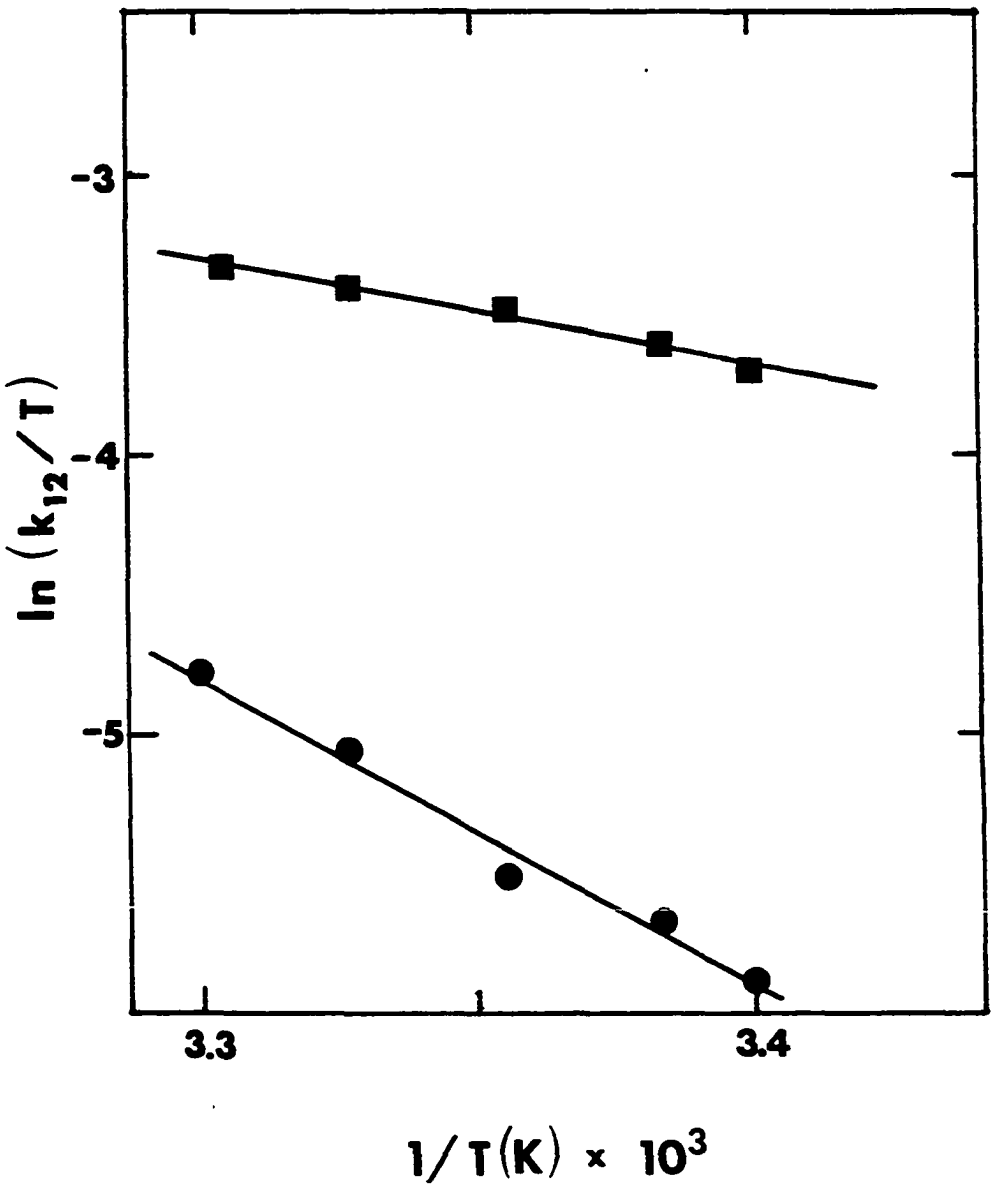

Figure II-15. ln (k_{12}/T) versus 1/T is plotted for the $Co(phen)_3^{3+}$ reaction with $(semi\text{-}met)_R Hr$ (circles) and $\mu\text{-}S^{2-}$semi-metHr (squares), pH 8.2, (50 mM EPPS), 0.15 M Na_2SO_4

Table II-7. Temperature dependent rate constants for the oxidation of $(semi\text{-}met)_R$ and $\mu\text{-}S^{2-}$semi-metHrs using $Co(phen)_3^{3+}$

T(°C)	$k_{12}(semi\text{-}met)_R(M^{-1}s^{-1})$	$k_{12}\mu\text{-}S^{2-}semi\text{-}met(M^{-1}s^{-1})$
20	0.8(±0.1)	7.2(±0.3)
23	1.0(±0.1)	7.8(±0.4)
25	1.3(±0.2)	8.2(±0.4)
27	1.8(±0.3)	10.8(±0.4)
30	2.4(±0.2)	11.2(±0.3)

Differences in the iron sites of $(semi\text{-}met)_R$ and $\mu\text{-}S^{2-}$semi-metHrs

Recent ^1H NMR studies have established that the magnitude of antiferromagnetic coupling found in the semi-met anion adducts is consistent with the protonation of the μ-oxo bridge in metHr to form a μ-hydroxo bridge in semi-metHr anion adducts (28,29). While ^1H NMR of either $(semi\text{-}met)_O$ or $(semi\text{-}met)_R$ has not been feasible thus far, it is reasonable to assume on the basis of similar temperature dependences of the half-saturation powers of the EPR spectra of semi-metN_3^- and $(semi\text{-}met)_R$ (described in Section I of this thesis), that a μ-hydroxo bridge exists in $(semi\text{-}met)_R$Hr also. The magnitude of antiferromagnetic coupling in $\mu\text{-}S^{2-}$semi-metHr is somewhat larger than that found in the anion adducts of $(semi\text{-}met)_R$Hr and the larger coupling has been attributed to the preservation of the μ-sulfido bridge in $\mu\text{-}S^{2-}$semi-metHr versus the μ-hydroxo bridge proposed for $(semi\text{-}met)_R$Hr. Conversely, ^1H NMR indicates that met and $\mu\text{-}S^{2-}$metHrs have similar coupling constants. The fact that conformational changes and protonation of the μ-oxo bridge need not be invoked to explain the behavior of the oxidation or reduction kinetics of native Hr or the sulfide derivative of Hr may indicate that these changes occur rapidly after electron transfer. However, in order to investigate this possibility,

a search for deuterium isotope effects on the rates of oxidation and reduction was undertaken.

Redox kinetics in D_2O

The reduction of metHr by $Fe(EDTA)^{2-}$ was carried out in ~ 95% D_2O. A rate constant of 3.7 $M^{-1}s^{-1}$ (± 0.5) was obtained, which is, within experimental error, the same as found in H_2O (Table II-1). The oxidation of $(semi\text{-}met)_R Hr$ by $Co(phen)_3^{3+}$ was also carried out in ~ 95% D_2O and the rate constant obtained in D_2O, 1.7 (± 0.2) $M^{-1}s^{-1}$, was within experimental error of the rate obtained in H_2O (Table II-6). The lack of an observable deuterium isotope effect on the rates of oxidation or reduction of native Hr does not preclude the presence of a proton in the mechanism of oxidation or reduction (30). However, since good correlations with Marcus theory can be obtained for the oxidation and reduction of native and μ-S^{2-}Hrs, and no deuterium isotope effects can be seen, it may be suggested that the addition or removal of a proton from the μ-oxo bridge in native metHr occurs in a fast (non-rate determining) step.

Oxidation of deoxyMb

In Table II-8, the second order rate constants for oxidation of deoxyMb by met- and μ-S^{2-}metHrs are shown. In the case of the reaction of μ-S^{2-}metHr with deoxyMb, metMb and

Table II-8. Second order rate constants for the oxidations of deoxy Mb and *P.g.* $cytb_5$ by met- and μ-S^{2-}metHrs

Reductant	(E°',mV)	k_{12}met ($M^{-1}s^{-1}$)	$k_{12}\mu$-S^{2-}met ($M^{-1}s^{-1}$)	$k_{12}\mu$-S^{2-}met/ k_{12}met
deoxyMb[a]	(46)[b]	1.22 (± 0.25)	38 (± 4)	31
P.g. $cytb_5$[c]	(7 ±2)[d]	160 (± 10)[d]	8900 (± 600)	56

[a] pH 6.3 (50 mM MES), 0.15 M Na_2SO_4, 25 °C.

[b] Reference 31.

[c] pH 7.5 (10 mM phosphate), 0.15 M Na_2SO_4, 25 °C.

[d] Reference 15.

μ-S^{2-}semi-metHr are produced. The production of metMb can be ascertained by the change in the Soret band from 430 nm in deoxyMb to 411 nm for metMb. The reaction rates of deoxyMb with μ-S^{2-}metHr are linearly dependent upon the concentration of μ-S^{2-}metHr as shown in Figure II-16. The oxidation of deoxyMb by metHr has been previously described by Bradić et al. (14). These workers reported that the reaction of deoxyMb with excess metHr was uniphasic and linearly dependent upon the concentration of metHr. Wilkins obtained a rate constant of 0.25 $M^{-1}s^{-1}$ for P. gouldii metHr, pH 6.3, I = 0.2 M (Na_2SO_4) 25 °C. The rate determining step appears to be reduction of metHr to the semi-met oxidation level with subsequent more rapid reduction to the deoxy level. We obtain a rate constant of 1.22 $M^{-1}s^{-1}$ for the oxidation of deoxyMb with metHr, pH 6.3, 0.15 M Na_2SO_4, 25 °C. The reaction still appears to be uniphasic under our conditions. An EPR spectrum of a sample of a 1:1 mol:mol solution of metHr and deoxyMb frozen in liquid nitrogen after 11 minutes reaction at 25 °C is shown in Figure II-17. This spectrum shows a small steady state level of $(semi\text{-}met)_R$ accompanying the production of metMb. Small amounts of $(semi\text{-}met)_R$ can also be seen in EPR spectra taken at later reaction times (i.e., 45, 165, 225 minutes). These spectra provide additional evidence that the reaction is proceeding through $(semi\text{-}met)_R$. Thus, we are comparing the following reactions:

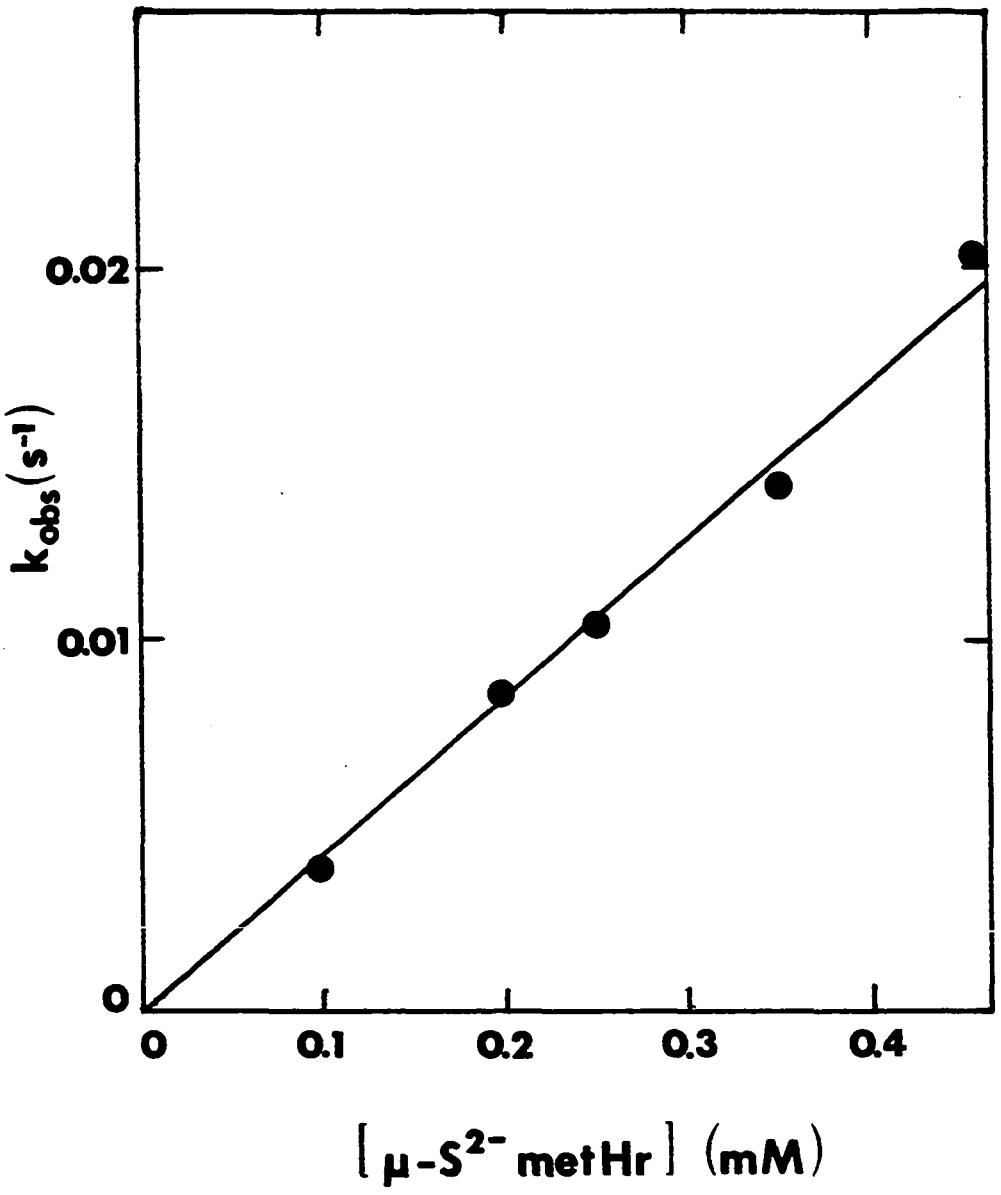

Figure II-16. The dependence of the observed first order rate constants for oxidation of 30 μM deoxyMb upon the concentration of μ-S^{2-}metHr at pH 6.3, (50 mM MES), 0.15 M Na_2SO_4, 25 °C

Figure II-17. EPR spectrum taken during the oxidation of deoxyMb with metHr

EPR spectrum taken during the oxidation of 0.2 mM deoxyMb with 0.2 mM metHr, pH 7.0 (50 mM HEPES), 0.15 M Na_2SO_4, 25 °C. The g-values at 1.94, 1.87 and 1.66 are due to $(semi\text{-}met)_R Hr$. The g-values at 6.0, 3.4, 2.6, 2.25 and 2.1 are due to metMb. The sample was frozen at liquid N_2 temperatures, 11 minutes into the reaction. EPR parameters are: temperature, 4 K;power, 0.2 mW; frequency, 9.46 GHz; modulation, 16 gauss at 100 kHz; time constant 0.2 sec; gain, 1×10^5.

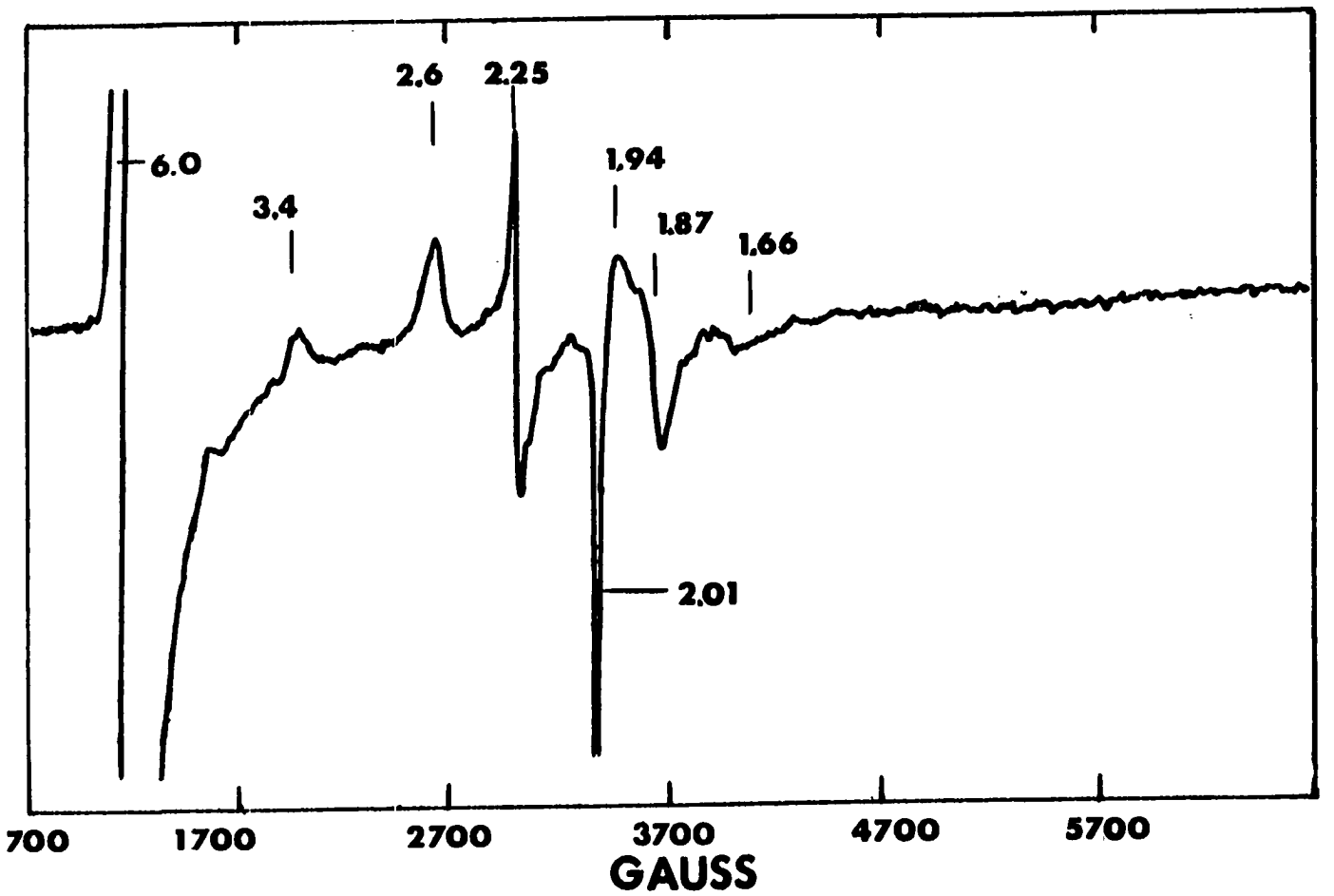
6.0
3.4
2.6
2.25
1.94
1.87
1.66
2.01
700
1700
2700
3700
4700
5700
GAUSS

$$[Fe^{3+},Fe^{3+}](met) + Fe^{2+}Mb \rightarrow [Fe^{2+},Fe^{3+}](semi\text{-}met)_R + Fe^{3+}Mb \quad (4$$

$$[Fe^{3+},Fe^{3+}](\mu\text{-}S^{2-}met) + Fe^{2+}Mb \rightarrow [Fe^{2+},Fe^{3+}](\mu\text{-}S^{2-}semi\text{-}met) + Fe^{3+}Mb \quad (5$$

Here again we assume that the self-exchange rate constants, k_{11}s, of metHr and μ-S^{2-}metHr are essentially identical and that the proteins differ only in their reduction potentials. These assumptions are borne out by the results on reductions of met- and μ-S^{2-}metHrs by inorganic reagents previously discussed. Thus, using Equation 3, we can predict that the second order rate constant for oxidation of deoxyMb by μ-S^{2-}metHr will be ~ 40-fold faster than the second order rate constant for the oxidation of deoxyMb by metHr. In Table II-8, the experimentally determined second order rate constants are listed along with the ratio $k_{12}\mu$-S^{2-}met/k_{12}met. The experimental value of 31 obtained for this ratio for reactions 4 and 5 is in good agreement with Marcus theory, and, therefore, consistent with the above assumptions.

Oxidation of Reduced P. g. $cytb_5$

It is also interesting to compare the rates of the oxidation of reduced P.g. $cytb_5$, a possible physiological reductant of metHr, with the native and the sulfide derivative

of Hr. The reactions carried out are shown in Equations 6 and 7.

$$[Fe^{3+},Fe^{3+}](met) + Fe^{2+}cytb_5 \rightarrow [Fe^{2+},Fe^{3+}](semi\text{-}met)_R + Fe^{3+}cytb_5 \quad (6$$

$$[Fe^{3+},Fe^{3+}](\mu\text{-}S^{2-}met) + Fe^{2+}cytb_5 \rightarrow [Fe^{2+},Fe^{3+}](\mu\text{-}S^{2-}semi\text{-}met) + Fe^{3+}cytb_5 \quad (7$$

The rate constants for reactions 6 and 7 are listed in Table II-8. The linear dependence of the observed first order rate constant upon the concentration of μ-S^{2-}metHr is shown in Figure II-18. The linear dependence of k_{obs} for oxidation of P.g. $cytb_5$ on concentration of metHr is shown elsewhere (15). In Figure II-18, we see a nonzero intercept, indicating the autooxidation of P.g. $cytb_5$. This autooxidation makes impossible any further reduction of Hr past the semi-met level in the absence of additional constituents. Here again, the ratio $k_{12}\mu$-S^{2-}met/k_{12}met for reactions with P.g. $cytb_5$ (Table II-8) shows good agreement with the value of 40 calculated using the simple Marcus relation and assuming identical values of k_{11}. Thus, we have demonstrated that increasing the reduction potential of a metal site in a protein causes an increase in the rate at which the metal site accepts electrons from a metal site in another protein. Furthermore, the

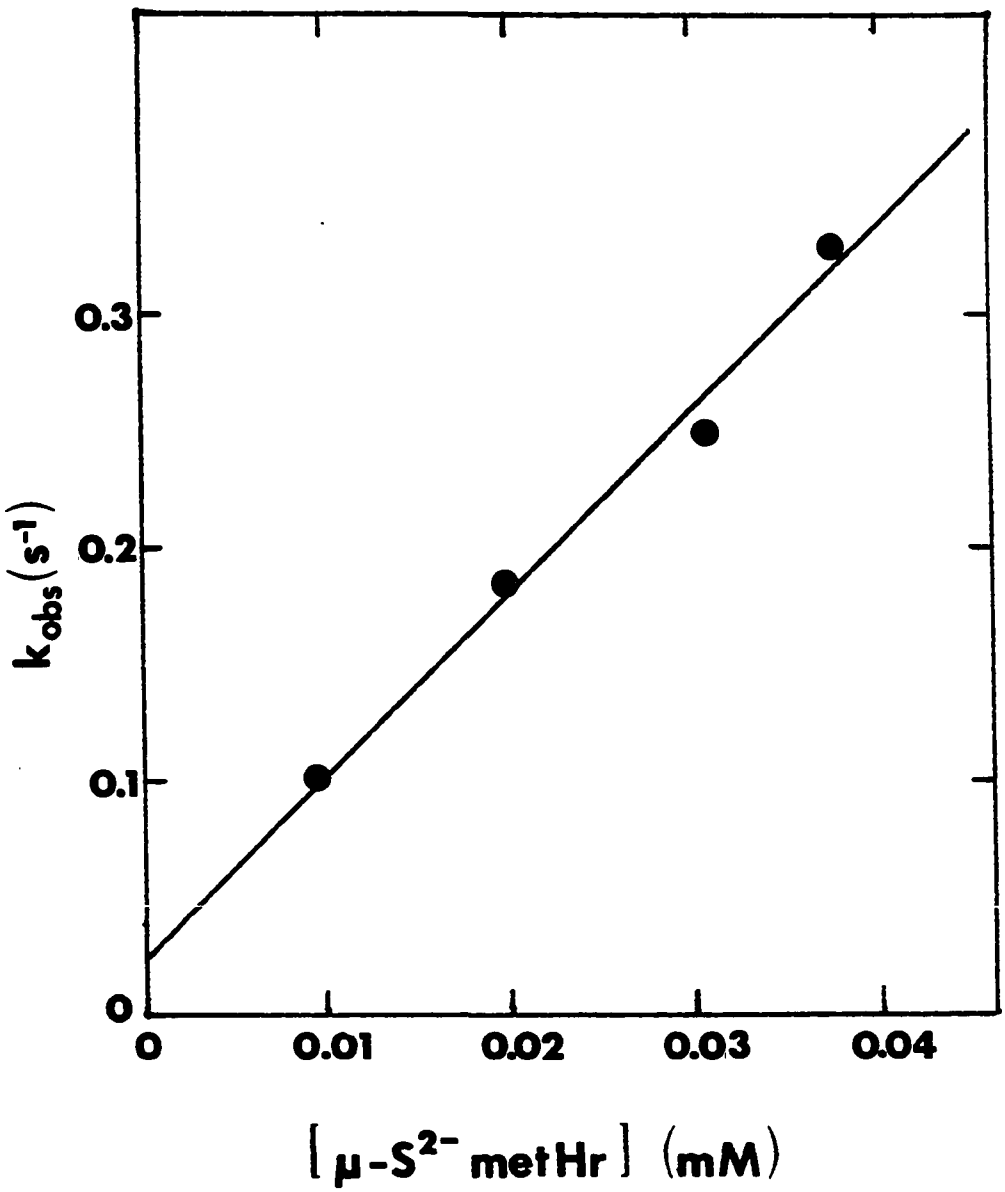

Figure II-18. The dependence of the observed first order rates of oxidation of reduced P.g. $cytb_5$ upon the concentration of μ-S^{2-}metHr at pH 7.5, (10 mM phosphate), 0.15 M Na_2SO_4, 25 °C

increases in rates are in essentially quantitative agreement with those predicted using simple Marcus theory, whether or not electron transfer is the major function of the donor protein.

Comparison of the rates of oxidation of deoxyMb versus P.g. $cytb_5$ by metHr

We also have an opportunity to compare the rates of oxidation of deoxyMb and reduced P.g. $cytb_5$ by metHr.

The second order rate constants for the oxidation of reduced P.g. $cytb_5$ by metHr are pH dependent, and vary by a factor of ~ 5 in the range of pH 6.5-7.5 (15). However, the second order rate constants for the oxidation of deoxyMb by metHr appears to vary little when the pH is raised to 7.5 from pH 6.3. At pH 6.5 (10 mM phosphate), 0.15 M Na_2SO_4, 25 °C, the rate of oxidation of reduced P.g. $cytb_5$ by metHr is 490 $M^{-1}s^{-1}$ (15,16). Under the same conditions, the rate of oxidation of deoxyMb by metHr is 1.22 $M^{-1}s^{-1}$ (Table II-8). According to simple Marcus theory (Equation 3), the $\Delta E°'$ of ~ 40 mV (15,31) between P.g. $cytb_5$ and Mb should lead to a value of ~ 10 for the ratio $k_{12}cytb_5/k_{12}Mb$ whereas, from the values cited above and those in Table II-8, this ratio is observed to be in the range of 150-400 using either metHr or μ-S^{2-}metHr as the oxidant. Thus, the difference in reduction potential between Mb and $cytb_5$ is not enough to account for the

differences in rates of reduction of the iron site in Hr.

In order to provide a frame of reference for this comparison we compared the rates of reduction of P.g. $cytb_5$ and metMb with $Fe(EDTA)^{2-}$. $Fe(EDTA)^{2-}$ was chosen in order to compare the reactivity of P.g. $cytb_5$ with that published for cytochrome b_5 isolated from beef liver. At pH 7.0, μ = 0.2 (phosphate) 25 °C, the second order rate constant was found to be 256 ($\pm$ 20) $M^{-1}s^{-1}$ for the reduction of P.g. $cytb_5$ by a 1000-fold molar excess or higher of $Fe(EDTA)^{2-}$. Using 1 μM P.g. $cytb_5$ it was found that reaction with $Fe(EDTA)^{2-}$ concentrations less than 1 mM did not go to completion. The second order rate constant for the $Fe(EDTA)^{2-}$ reduction of cytochrome b_5 isolated from beef liver was determined to be 186 $M^{-1}s^{-1}$ under the same conditions by Reid and Mauk (32). They also noticed incomplete reduction with concentrations of $Fe(EDTA)^{2-}$ of 0.5 mM or less. It appears that the reactivity as well as many physical properties of P.g. $cytb_5$ (33) is quite similar to those of cytochrome b_5 from other sources. The self-exchange rate constant (k_{11}) is a measure of the inherent reactivity of a redox reagent, which is essentially corrected for the difference in redox potentials. Published values of the electrostatics-corrected self-exchange rate constant, $k_{11}corr$, for bovine liver cytochrome b_5 and Mb are 11 $M^{-1}s^{-1}$ and 1.26 x 10^{-1} $M^{-1}s^{-1}$, respectively at pH 7 and 25 °C using $Fe(EDTA)^{2-}$ as redox partner (34,35). While these

values may not be accurate reflections of the absolute values of the self-exchange rate constants, they are one measure of relative electron transfer reactivity since they represent corrections for differences in both reduction potential and surface charge (24). Because of the similar reactivities and physical properties, we take the self-exchange rate constant for P.g. $cytb_5$ to be the value for bovine liver cytochrome b_5, 11 $M^{-1}s^{-1}$. Thus, according to this analysis, after correcting for differences in potential and electrostatics, P.g. $cytb_5$ should exhibit a 10-fold higher electron transfer reactivity than Mb. This factor of 10 combined with the factor of 10 calculated above for $k_{12}cytb_5/k_{12}Mb$ from differences in reduction potential can account for our experimental range of 150-400 for this ratio.

The activation parameters for the oxidation of P.g. $cytb_5$ by metHr, calculated from an Eyring plot, are $\Delta H^{\ddagger}$ = 35.7 (± 0.1) kJ/mol and $\Delta S^{\ddagger}$ = -35.5 (± 0.3) J/mol·K (15). This value of $\Delta H^{\ddagger}$ is similar to that obtained for reductions of metHr by small molecule metal complexes (Table II-4). However, the activation entropy appears less negative in the protein-protein reaction than values obtained for the small molecule-protein reactions (e. g., $\Delta S^{\ddagger}$ = -137 J/mol·K, $Fe(EDTA)^{2-}$ reduction of metHr; $\Delta S^{\ddagger}$ = -122 J/mol·K, Cr^{2+}/cacodylate reduction of metHr). The more positive value obtained for the protein-protein reaction fits a pattern

observed for cytochrome c and blue copper proteins (36). The trend may result from the more extensive hydration of protein molecules. If the oxidized and reduced forms of the protein differ in the degree of hydration, water rearrangement may play a role in the activation process. At pH 7.2-7.5 and $\mu \leq 0.5$ the rate of oxidation of *P.g.* $cytb_5$ by metHr increases as the ionic strength is lowered (Figure II-19) consistent with formation of an electrostatic complex between these oppositely charged proteins. Dehydration of the protein surface during formation of this precursor complex may contribute to the lower $\Delta S^{\ddagger}$. Both of the factors mentioned above may result in more positive $\Delta S^{\ddagger}$ for the metHr-$cytb_5$ reaction than for the less hydrated small molecule metal complex-Hr reactions. However, any interpretation of activation parameters for protein-protein reactions should be viewed with caution as many unknown factors may contribute. Formation of a stable electron transfer complex between metHr and *P.g.* $cytb_5$, either by chemical cross-linking or by sufficient lowering of the ionic strength might eliminate some of these amibiguities. A stable electron transfer complex has been obtained by both methods in the case of cytc-cytc peroxidase (37,38).

The heme group in $cytb_5$ is known to have a greater exposure to solvent than the heme group in Mb (23% versus 18%) (40). This greater exposure of the heme in $cytb_5$ may lead to a closer approach to the iron site of Hr, and, therefore, to

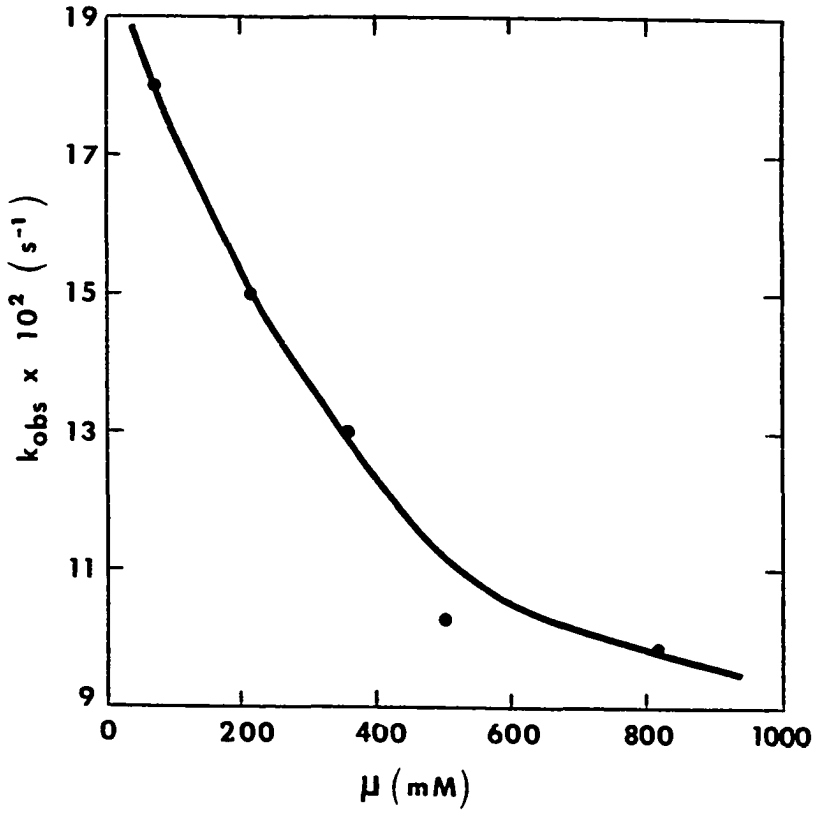

One and two-tenths μM P.g. $cytb_5$; 61 μM metHr; 10 mM phosphate buffer pH 7.5; 25 °C. Ionic strength adjusted by the addition of Na_2SO_4. The solid curve does not represent any theoretical fit of the data.

Figure II-19. Effect of ionic strength on the observed first order rate constant for the oxidation of reduced P.g. $cytb_5$ by metHr (15)

faster rates of electron transfer. Mb also contains a high spin iron while the iron in $cytb_5$ is low spin. A greater reorganizational energy barrier has been suggested to exist in Mb than in low spin heme proteins (40,41,42). Both of these factors may effect the greater rates of electron transfer from *P.g.* $cytb_5$ versus Mb to the iron site of Hr. ^1H NMR studies strongly suggest that the six coordinate iron is the one reduced in semi-metHr (28,29). Significantly, it is this iron (Fe(1) in Figure II-2) that is closer to the outer surface of each subunit within the Hr octamer. It is tempting to speculate that the imidazole side chains of the His residues 73, 77 and 101 provide a "funnel" for electron flow into the iron site. It is possible that electron transfer from both inorganic complexes and from proteins occurs subsequent to binding of the complex or protein to the outer surface of the Hr subunit at a site near the aforementioned His residues.

Conclusion

The replacement of the μ-oxo bridge in native Hr with a μ-sulfido bridge presents a unique opportunity to study the effect of raising the potential of a protein metal site on its electron transfer reactivity. Our physical-chemical studies and reduction kinetics are consistent with little or no change in the protein matrix, upon replacement of the μ-oxo by the

μ-sulfido bridge. In the reduction of metHr versus μ-S^{2-}metHr the simple Marcus correlation, assuming identical values of k_{11}, holds rather well for both small molecule:protein and protein:protein reactions. The kinetic parameters indicate that little is changed between metHr and μ-S^{2-}metHr as far as the electron transfer is concerned with the exception of the reduction potentials of the iron sites. The kinetics of oxidation of μ-S^{2-}semi-metHr and semi-metHr by $Fe(CN)_6^{3-}$ also obey the simple Marcus correlation. The oxidation of $(semi\text{-}met)_R$ and μ-S^{2-}semi-metHrs by $[Co(phen)_3]Cl_3$ does not obey the Marcus relation and the activation parameters suggest different mechanisms for the two oxidations. The difference in mechanism may be due to differing hydrophobic interactions of the phenanthroline groups in $Co(phen)_3^{3+}$ with the two derivatives of Hr.

We have successfully applied Marcus theory to two protein-protein electron transfer reactions and predicted the increases in rates that accompany the rise in reduction potential due to the replacement of a μ-sulfido for a μ-oxo bridge in Hr. These results represent a unique test of Marcus theory for protein-protein electron transfer in that presumably only the active site of Hr has been modified while the protein matrix is relatively unchanged. The only other direct comparison of protein-protein electron transfer rates as a function of exothermicity appear to be those of the

cytc/cytb$_5$ and cytc/cytc peroxidase couples in which the metal ion in cytc is either removed or substituted with Zn (37,43). Our studies extend these comparisons to a heme:non-heme couple and to a system in which the metal site is disrupted to a much smaller extent. We have also shown the first direct comparison of a protein-protein electron transfer reaction involving a low spin heme, P.g. cytb$_5$ versus a high spin heme, Mb. The ratio k_{12}cytb$_5$/k_{12}Mb for oxidations by either metHr or μ-S^{2-}metHr are increased by a factor of 15-40 greater than would be predicted on the basis of differences in reduction potential alone, which is apparently a reflection of the inherently greater ability of cytb$_5$ to transfer electrons as reflected in previously published values of k_{11}corr. One can also compare previously published ratios of heme protein-heme protein reactions using low spin versus high spin hemes. The reaction of Mb with cytochrome c results in rate constant of 2.2×10^3 $M^{-1}s^{-1}$ while cytb$_5$ reacts with cytc to give a bimolecular rate constant of 4×10^7 $M^{-1}s^{-1}$ (43,44,45). Again we see that the high spin heme, cytb$_5$, reacts much more quickly than the low spin heme, Mb.

In the case of Hr, when the relative values of k_{11}corr are taken into account, it appears that specificity of protein-protein interactions need not be invoked to explain the higher rates of the P.g. cytb$_5$/Hr reactions. Thus, if a specific docking site for P.g. cytb$_5$ exists on metHr near His

73, 77 and 101 as suggested above, its function may not be to increase the rate of electron transfer. Alternate possibilities for the function of a specific docking site include the prevention of short-circuiting of electron transfer between the NADH-$cytb_5$ reductase and Hr and partitioning of electron flow, if P.g. $cytb_5$ has more than one electron acceptor within the erythrocyte.

References Cited

1. Kurtz, D. M., Jr.; Sage, J. T.; Hendrich, M.; Drebrunner, P.; Lukat, G. S. J. Biol. Chem. 1983, 258, 2115-2117.

2. Lukat, G. S.; Kurtz, D. M., Jr.; Shiemke, A. K.; Loehr, T. M.; Sanders-Loehr, J. Biochemistry 1984, 23, 6416-6422.

3. Lukat, G. S.; Kurtz, D. M., Jr.; Biochemistry 1985, 24, 3464-3472.

4. Lukat, G. S., Ph.D. thesis, Iowa State University, 1985.

5. Armstrong, F. A.; Harrington, P. C.; Wilkins, R. G. J. Inorg. Biochem. 1983, 18, 83-91.

6. Marcus, R. A. Chem. Phys. 1956, 29, 21.

7. Marcus, R. A.; Sutin, N. Inorg. Chem. 1975, 14, 213.

8. Wherland, S.; Gray, H. B. In "Biological Aspects of Inorganic Chemistry", Addison, A. W.; Cullen, W. R.; Dolphin, D.; James, B. R., Eds. 1977, Wiley-Interscience: New York p. 289-368.

9. Espenson, J. H. In "Chemical Kinetics and Reaction Mechanisms" McGraw-Hill, Inc.: New York, 1981, Chapter

10. Wherland, S.; Holwerda, R. A.; Rosenberg, R. C.; Gray H. B. J. Am. Chem. Soc. 1975, 97, 5260-5262.

11. Klotz, I. M.; Klotz, T. A.; Fiess, H. A. Arch. Biochem. Biophys. 1957, 68, 284-299.

12. Garbett, K.; Darnell, D. W.; Klotz, I. M.; Williams, R. J. P. Arch. Biochem. Biophys. 1969, 103, 419-434.

13. Irwin, M. J.; Duff, L. L.; Shriver, D. F.; Klotz, I. M. Arch. Biochem. Biophys. 1983, 244, 473-478.

14. Bradić, Z.; Harrington, P. C.; Wilkins, R. G. Biochemistry 1979, 18, 889-893.

15. Utecht, R. E. Ph.D. thesis, Iowa State University, 1986.

16. Utecht R. E.; Kurtz, D. M., Jr. manuscript in preparation.

17. Dawson, J. W.; Gray, H. B.; Holwerda, R. A.; Westhead, E. W. Proc. Nat. Acad. Sci. USA 1972, 69, 30-33.

18. Adzamali, J. K.; Henderson, R. A.; Sinclair-Day, J. D.; Sykes, A. G. Inorg. Chem. 1984, 23, 3069-3073.

19. Segal, M. G.; Sykes, A. G. J. Am. Chem. Soc. 1978, 100, 4585-4588.

20. Armstrong, G. D.; Ramasami, T.; Sykes, A. G. Inorg. Chem. 1985, 24, 3230-3234.

21. a) Stenkamp, R. E.; Sieker, L. C.; Jensen, J. H. J. Am. Chem. Soc. 1984, 106, 618-622. b) Stenkamp, R. E.; Sieker, L. C.; Jensen, L. H J. Inorg. Biochem. 1983, 19, 247-253.

22. Stenkamp, R. E.; Sieker, L. C.; Jensen, L. H. J. Mol. Biol. 1978, 126, 457-466.

23. Kerestes-Nagy, S.; Klotz, I. M. Biochemistry 1965, 4, 919-931.

24. Harrington, P. C.; Wilkins, R. G. J. Inorg. Biochem. 1983, 19, 339-344.

25. Espenson, J. H. In "Chemical Kinetics and Reaction Mechanisms" McGraw-Hill, Inc: New York 1981, p. 197-198.

26. Lim, A. R.; Mauk, A. G. Biochem. J. 1985, 229, 765-769.

27. a) Bradic, Z.; Harrington, P. C.; Wilkins, R. G.; Yoneda, G. Biochemistry 1980, 19, 4149-4155. b) Lukat, G. S., personal communication, University of Iowa.

28. Maroney, M. J.; Lauffer, R. B.; Que, L. Q., Jr.; Kurtz, D. M., Jr. J. Am. Chem, Soc. 1984, 106, 6445-6446.

29. Maroney, M. J.; Kurtz, D. M., Jr.; Nocek, J. M.; Pearce, L. L., Que, L. C., Jr. submitted for publication.

30. Jencks, W. P. In "Catalysis in Chemistry and Enzymology" McGraw-Hill: New York, 1969, Chapter 4.

31. Benlke, J.; Scheler, W. Naturwissenschatten 1961, 48, 717-718.

32. Reid, L. S.; Mauk, A. G. J. Am. Chem. Soc. 1982, 104, 841-845.

33. Utecht, R. E.; Kurtz, D. M., Jr. Inorg. Chem. 1985, 24, 4458-4459.

34. Reid, L. S.; Mauk, A. G. J. Am. Chem. Soc. 1984, 106, 2182-2185.

35. Mauk, A. G.; Gray, H. B. Biochem. Biophys. Res. Comm. 1979, 86, 206-210.

36. Sutin, N. Adv. Chem. Ser. 1977, 162, 156-172.

37. Cheung, E.; Taylor, K.; Kornblatt, K. A.; English, A. Proc. Nat. Acad. Sci. USA 1986, 83, 1330-1333.

38. Waldmeyer, B.; Bosshard, H. R. J. Biol. Chem. 1985, 260, 5184-5190.

39. Stellwagen, E. Nature 1978, 275, 73-74.

40. Pasternack, R. F.; Spiro, E. G. J. Am. Chem. Soc. 1978, 100, 968-972.

41. Winkler, J. R.; Nocera, D. G.; Yocum, K. M.; Bordignon, E.; Gray, H. B. J. Am. Chem. Soc. 1982, 104, 5798-5800.

42. Crutchley, R. J.; Ellis, W. R., Jr.; Gray, H. B. J. Am. Chem. Soc. 1985, 107, 5002-5004.

43. McClendon, G.; Miller, J. R. J. Am. Chem. Soc. 1985, 107, 7811-8716.

44. Ataullakhanov, F. A.; Atanasov, B. P.; Postnikova, G. B.; Sadykov, Y. K. Stud. Biophys. 1976, 54, 41.

45. Strittmatter, P. In "Rapid Mixing and Sampling in Biochemistry", Chance, B.; Eisenhardt, R.; Gibson, Q.; Lundberholm, K., Eds. Academics: New York, 1964; p. 71-84.

III. THE OXIDATION OF DEOXYHEMERYTHRIN TO THE SEMI-MET OXIDATION LEVEL BY CHROMATE

Introduction

Chromium(VI) has recently been under investigation as a possible carcinogen in biological systems (1,2). In the form of chromate, Cr(VI) can cross cell membranes, while Cr(III) cannot. Chromate can be reduced in cellular systems and there are many possible reductants available to the cell. Small molecules such as glutathione, present in fairly large quantities (0.8 ~ 8 mM), can reduce chromate to Cr(III). Cr(III) can then bind to DNA, causing problems in replication. Little is known about the interaction of chromate with proteins. Chromate is known to oxidize some heme proteins and some flavoproteins. Not much is known about the mechanism of oxidation of these proteins by chromate, although the involvement of sulfhydryl groups has been suggested (1).

Extensive study has been concentrated on the reduction of chromate by some small molecules which may be found in the cellular environment (3). It has been suggested that the rates of reduction of chromate by carboxylic acids and thiols are very much dependent on the pK_a's of the reducing agents. Protonation of an oxygen atom on chromate to form hydroxide or water, which then functions as a leaving group has been

proposed as the crucial step in the mechanism by Connett and Wetterhahn (3).

The oxidation of deoxyHr has been studied using several oxidizing agents, such as $K_3Fe(CN)_6$ (5). DeoxyHr is rapidly oxidized to the $(semi\text{-}met)_o$ oxidation level by these reagents. The further oxidation of $(semi\text{-}met)_o$ to metHr appears to occur either directly, or by a disproportionation mechanism, depending on pH. At pH 6.3, the oxidation of $(semi\text{-}met)_oHr$ appears to be direct, whereas at pH 8.2 the oxidation is disproportionation-controlled. Since CrO_4^{2-} can penetrate cell membranes, it may be possible to study the oxidation of Hr under close to physiological conditions.

Experimental

Oxidation of hemerythrin-containing erythrocytes by $HCrO_4^-$

Na_2CrO_4 was obtained from Fischer Co. and used without further purification in all reactions.

Hemerythrin-containing erythrocytes were obtained from specimens of P. gouldii by slitting the worms lengthwise and collecting the coelomic fluid. The fluid was then filtered through miracloth and the erythrocytes collected and washed with sea water by several centrifugations. To approximately one ml of packed erythrocytes, solid Na_2CrO_4 was added to give a concentration of 30 - 100 mM. (The concentration of Hr

subunits in the erythrocytes is thought to be ~ 10 mM (6).) The cells and Na_2CrO_4 were incubated together in a vial capped with a septum at 13 °C. At hourly intervals, 100 µL aliquots were removed, placed in anaerobic quartz EPR tubes and frozen in liquid nitrogen. These tubes were then evacuated and flame sealed.

Oxidation of purified deoxyhemerythrin by Na_2CrO_4

OxyHr was prepared by literature methods (7). Live worms of the species Phascolopsis gouldii were obtained from the Marine Biological Laboratory, Woods Hole, Massachusetts, slit and drained of their coelomic fluid. The erythrocytes were then filtered through miracloth and washed with sea water by centrifugation. The cells were lysed by adding 2.5 times their volume of deionized water. The resulting Hr solution was centrifuged at 16,000 g on a Beckman centrifuge for two hours. The Hr was then dialzyed against a 20% ethanol/water solution until crystals of oxyHr formed. The oxyHr crystals were dissolved in 50 mM Tris/acetate buffer, pH 8.2.

DeoxyHr was prepared by dialyzing oxyHr anaerobically against excess dithionite in 50 mM MES (pH 6.0) and 0.15 M Na_2SO_4 for 24-48 hours at 4°C. DeoxyHr was then dialyzed against buffer (50 mM MES, pH 6.0, and 0. 15 M Na_2SO_4) overnight to rid deoxyHr of excess dithionite.

DeoxyHr was transferred anaerobically to deaerated vials

containing a previously weighed amount of solid Na_2CrO_4. The concentration of deoxyHr was determined by exposure to air to form oxyHr. The concentration of oxyHr was determined using ε_{500} = 2200 $M^{-1}cm^{-1}$ (8). The reactions were usually run with a ten-fold or greater molar excess chromate over Hr. Hr concentrations varied from 0.5 - 3.0 mM. EPR samples were prepared as previously described for the erythrocytes. The reactions were usually carried out at 13°C by incubation in a water bath. All reactions were carried out under N_2 scrubbed with two chromous scrubbing towers (see Appendix A).

Reactions with I^- and N_3^-

Excess solid I^- and N_3^- were placed in vials and deaerated. Aliquots of deoxyHr/chromate reaction mixtures, typically 100 µl to 1 ml, were added to these vials. One hundred microliter aliquots were added to EPR tubes and quickly frozen in liquid nitrogen.

Instrumentation

EPR spectroscopy was performed on a Bruker ER-220D spectrometer equipped with an Oxford Instruments liquid helium cryostat. A Perkin-Elmer Model 554 spectrophotometer was used to obtain UV-visible spectra.

Results and Discussion

Erythrocytes and $HCrO_4^-$

When cells were incubated with chromate, the EPR spectra of the type shown in Figure III-1 were observed. Without chromate, EPR signals of this intensity were not observed at this time (Figure III-2). The maximum intensities were observed at 24 hours. The g-values of 1.92, 1.86, and 1.58 are similar to those previously observed in erythrocytes as shown in Figure III-2 (9), and are attributed to a $(semi\text{-}met)_R$ Hr species. The g values for $(semi\text{-}met)_R$ are 1.94, 1.87, and 1.66 at pH 7.0 EPR spectra similar to those found in Figure III-1 and III-2 have also been found in membrane fractions isolated from the erythrocytes. It is possible this semi-met EPR signal is due to membrane bound Hr although the intensity seems greater than previously observed from the cell membrane fractions (6). The EPR signal observed at g = 1.985 is believed to be that of Cr(V) (10,11). The EPR signal at g = 1.94 has been observed in reaction with purified deoxyHr and chromate early on in the reaction as shown in Figure III-3. The exact nature of this signal is unclear at this time.

Oxidation of purified Hr by $HCrO_4^-$

The outcome of the above experiment with Hr erythrocytes led to experiments in which purified deoxyHr was oxidized by

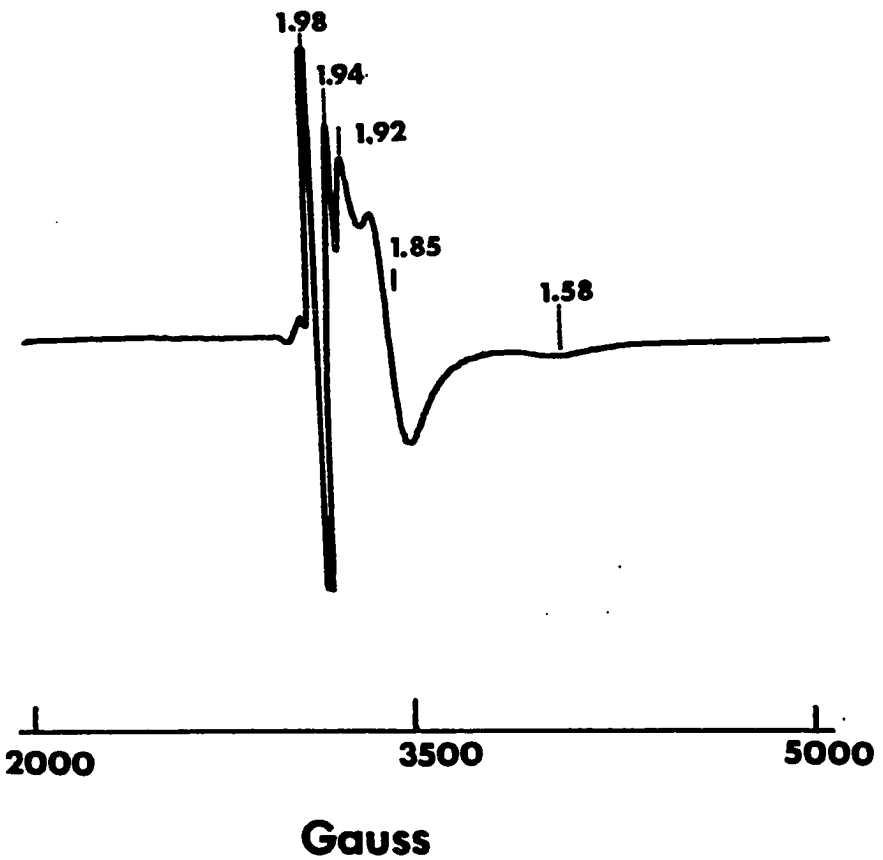

Sample frozen 24 hours after cells were incubated with ~ 30 mM Na_2CrO_4 at 13 °C. Temperature 4K; frequency 9.57 GHz; power 0.2 mW; gain 3.2 x 10^4; modulation 16 G at 100 kHz; time constant 0.15 sec.

Figure III-1. EPR spectrum of P. gouldii erythrocytes incubated with Na_2CrO_4

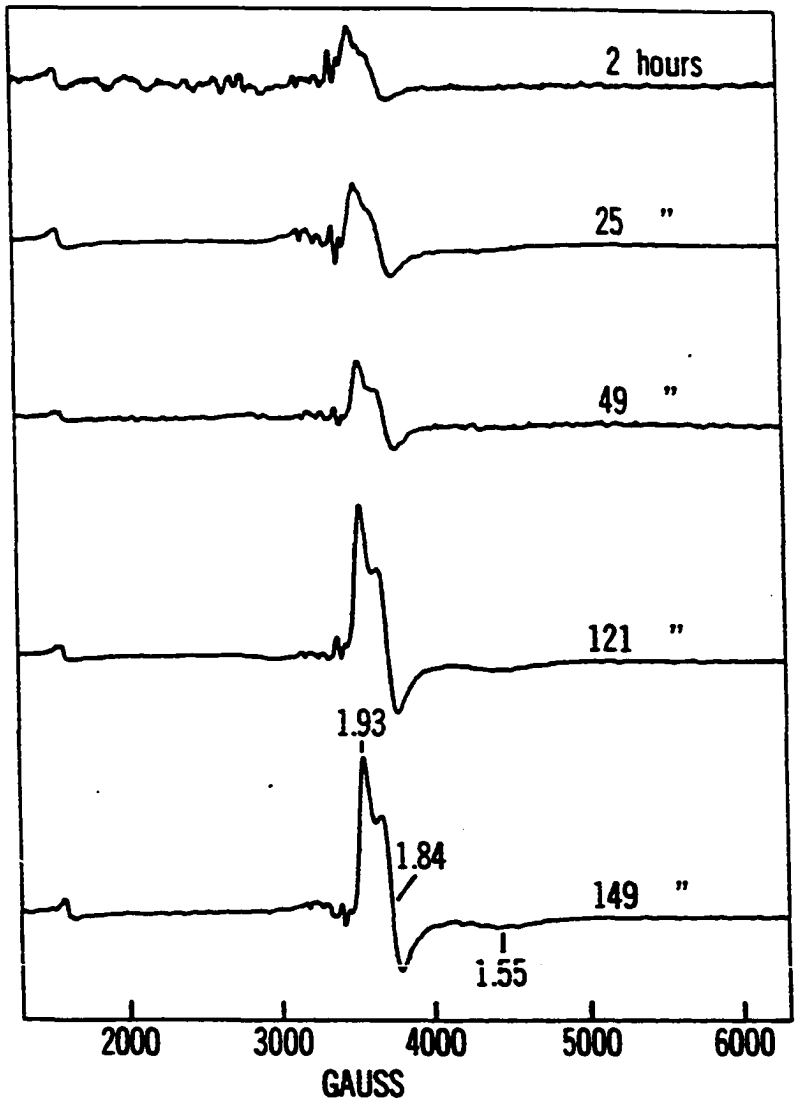

Deoxygenated erythrocytes incubated aerobically at 4 °C. Temperature 4 K; frequency 9.57 GHz; power 0.2 mW; gain 1.6 x 10^5; modulation 16 G at 100 KHz; time constant 0.15 sec.

Figure III-2. EPR spectra of intact erythrocytes (9)

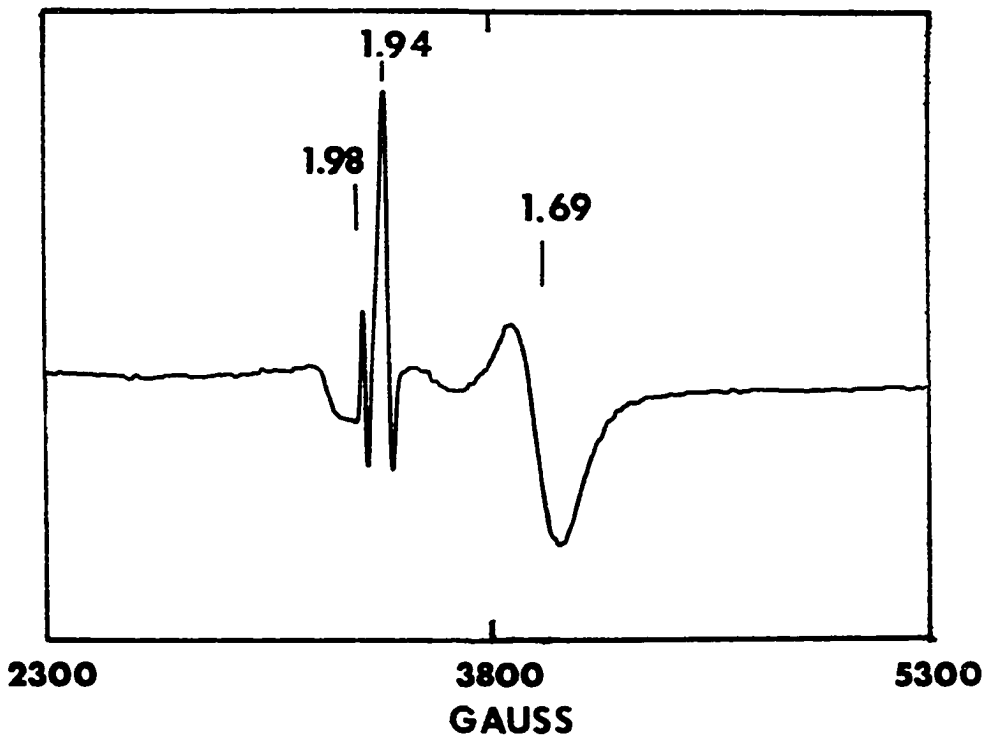

Sample frozen in liquid nitrogen after ~ 10 minutes. Temperature 4 K; frequency 9.42 GHz; power 0.2 mW; gain 8 x 10^4; modulation 16 G at 100 KHz; time constant 0.200 sec.

Figure III-3. EPR spectrum of 1.4 mM deoxyHr incubated at 13 °C with ~ 1.4 mM Na_2CrO_4, pH 6.3, 50 mM HEPES, 0.15 M Na_2SO_4

$HCrO_4^-$. The reaction was difficult to follow by UV-visible absorption due to the precipitation of a small amount of the total concentration of protein after a few hours. Therefore, EPR spectroscopy was used. The kinetic data for the oxidation of deoxyHr are presented in Table III-1. The EPR signal intensities, I, at g = 1.69, were plotted versus time [ln (I_∞ - I_t) versus t(sec)] and a least squares analysis was used to obtain the rate constants from the slope of the line. Reactions were followed for 48 hours. The rates are relatively slow, k_{obs} = 3 (± 1) x 10^{-5} s^{-1} at 13 °C, and essentially independent of chromate concentration and deoxyHr concentration. When sodium perchlorate was added to these reactions, no change was observed in the rate of oxidation of deoxyHr as shown in Table I-1. The EPR signals observed during the course of an oxidation by chromate are shown in Figure III-4. The axially symmetric signal with g-values of 1.94 and 1.68 is recognizable as that of $(semi\text{-}met)_o$. No change in the EPR lineshape was observed when ClO_4^- was added. Signals at g = 1.98 and g = 2.01 can also be observed. The species responsible for the g = 1.98 signal is Cr(V). Cr(V) is known to react quickly with I^- (12). Upon addition of N_3^- and then I^- (I^- will also react with Hr and N_3^- prevents this reaction) the signal at g = 1.98 disappears as shown in Figure III-5. This disappearance is further evidence for its assignment to Cr(V). The g = 2.01 signal has been observed in

Table III-1. Rate constants for oxidation of deoxyHr by chromate at pH 6.0 (50 mM MES, 0.15 M Na_2SO_4) and 13 °C

$k_{obs} \times 10^5$ s^{-1}	[deoxy] (mM)	[Na_2CrO_4] (mM)	[$NaClO_4$] (mM)
3.79	0.73	15	
2.32	1.50	15	
4.67	3.00	30	
3.75	3.00	30	100
3.78	1.60	15	
2.26	1.00	96	
2.10	1.00	24	

Figure III-4. EPR spectra of the incubation of 1.0 mM deoxyHr with 10 mM Na_2CrO_4 at pH 6.0 and 13 °C

pH 6.0, 50 mM MES, 0.15 M Na_2SO_4, with samples frozen at 1/2, 3, 6, 9, 12 and 24 hours. EPR parameters: temperature 4.2 K; frequency 9.57 GHz; power 0.2 mW; gain 3.2×10^4; modulation 16 G at 100 KHz; time constant 0.1 sec.

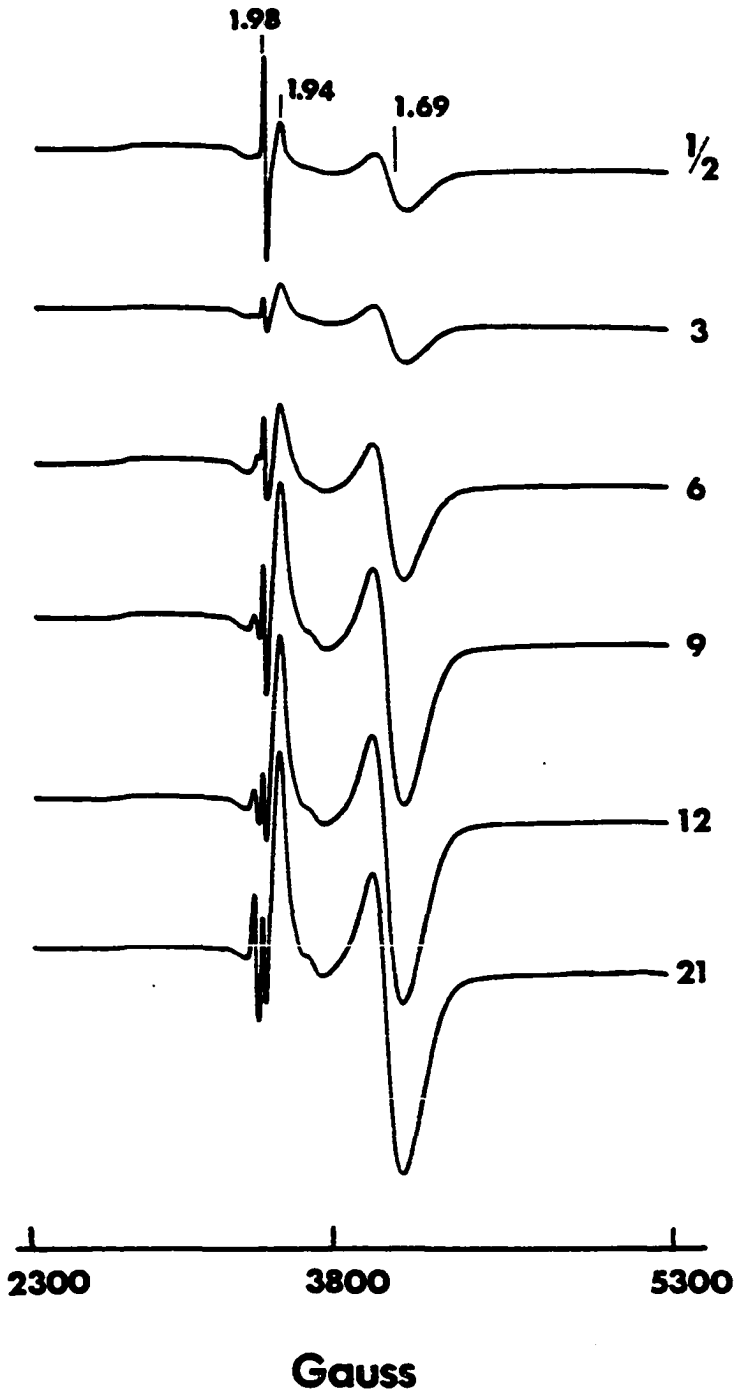
1.98
1.94
1.69
½
3
6
9
12
21
2300
3800
5300
Gauss

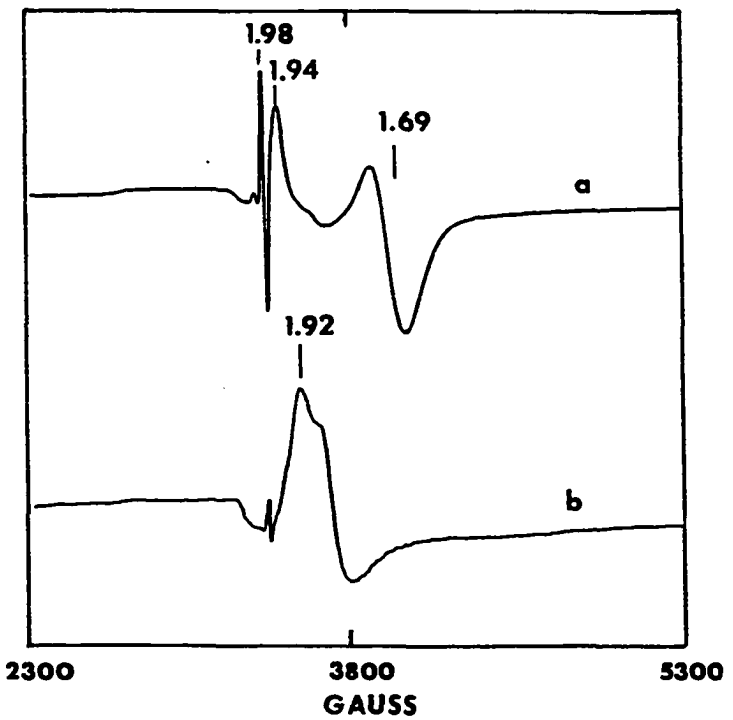

a) 1.4 mM deoxy incubated with 2.8 mM $NaCrO_4$ at 13 °C for 24 hours, gain 3.2 x 10^4.
b) Addition of I^- then N_3^- to a), gain 6.3 x 10^4. EPR parameters: temperature 4 K; frequency 9.243 GHz; power 0.2 mW; modulation 16 G at 100 kHz; time constant 0.200 sec.

Figure III-5. EPR spectra taken before a) and after, b) addition of I^- followed by N_3^- to semi-metHr generated by chromate oxidation

EPR samples of Hr and can be attributed to a sulfur radical due to the lone cysteine in Hr (13). The EPR signal due to $(\text{semi-met})_O\text{Hr}$ persists for up to ~ 60 hours without appreciable loss of intensity.

The above data leads one to propose a mechanism which can be written as follows:

$$CrO_4^{=} + \text{H-S-Hr[Fe(II,II)]}_{\text{deoxy}} \rightarrow O_3\text{-Cr}(=O)\text{....S(H)-Hr[Fe(II,II)]}$$

$$O_3\text{Cr}(O)\text{....S(H)-Hr[Fe(II,II)]} \rightarrow O_3\text{Cr}(OH)\text{....S-Hr[Fe(II,II)]}$$

$$O_3\text{Cr}(OH)\text{....S-Hr[Fe(II,II)]} \rightarrow O_3\text{Cr....S-Hr[Fe(II,II)]} + OH^-$$

$$O_3\text{Cr-S-Hr[Fe(II,II)]} \xrightarrow{k_{obs}} \text{Cr(V)} + \cdot\text{S-Hr[Fe(II,II)]}$$

$$\cdot\text{S - Hr[Fe(II,II)]} \xrightarrow[\text{e-}]{\text{fast}} {}^-\text{S - Hr[Fe(III,II)]}$$

$$H^+ + {}^-\text{S - Hr[Fe(III,II)]} \rightarrow \underset{(\text{semi-met})_O}{\text{HSHr[Fe(III,II)]}}$$

Connett and Wetterhahn have proposed a similar mechanism for the reaction of thiols with chromate (3). The independence of the rate of oxidation of Hr on $[CrO_4^{=}]$ suggests that the thioester linkage is formed rapidly and breakage of the thioester linkage to give Cr(V) and the sulfur radical is the rate-determining step. The sulfur radical so formed can then rapidly oxidize Hr to the semi-met level.

The oxidation of deoxyHr appears to be slower at pH 7.0 than at pH 6.3 and an EPR signal is formed which resembles a mixture of $(semi\text{-}met)_R$ and $(semi\text{-}met)_O$Hrs as shown in Figure III-6. Several explanations are available. At pH 6, there is a mixture of $HCrO_4^-$ and $CrO_4^{=}$ species. The protonated oxygen on $HCrO_4^-$ is known to be more labile and so the formation of the thioester may be more rapid at pH 6.0 than at pH 7.0. It has also been observed that lower pH's stabilize $(semi\text{-}met)_O$ and at pH 7.0 $(semi\text{-}met)_O$ is converted towards $(semi\text{-}met)_R$. At pH 6.0, the $(semi\text{-}met)_O$ signal, generated by the addition of one equivalent of $Fe(CN)_6^{3-}$ to deoxyHr, persists much longer than $(semi\text{-}met)_O$ EPR signals at pH 8.2 (13), and some portion of the signal can still be observed at eight hours, as shown in Figure III-7. At pH 6, it is also possible that $HCrO_4^-$ mimics perchlorate and binds at the same site. Perchlorate also stabilizes $(semi\text{-}met)_O$. When $NaClO_4$ is added to $(semi\text{-}met)_O$Hr at pH 8.0, the EPR signal due to $(semi\text{-}met)_O$ persists for about twice as long as $(semi\text{-}met)_O$ without

Figure III-6. EPR spectra of the incubation of 1.0 mM deoxyHr with 10 mM Na_2CrO_4 at pH 7.0, 13 °C

pH 7.0, 50 mM HEPES, 0.15 M Na_2SO_4, with samples frozen in liquid nitrogen at 2, 4, 6, 8, 10 and 48 hours. EPR conditions: temperature 4.2 K; frequency 9.57 GHz; power 0.2 mW; gain 5 x 10^4; modulation 16 G at 100 KHz; time constant 0.1 sec.

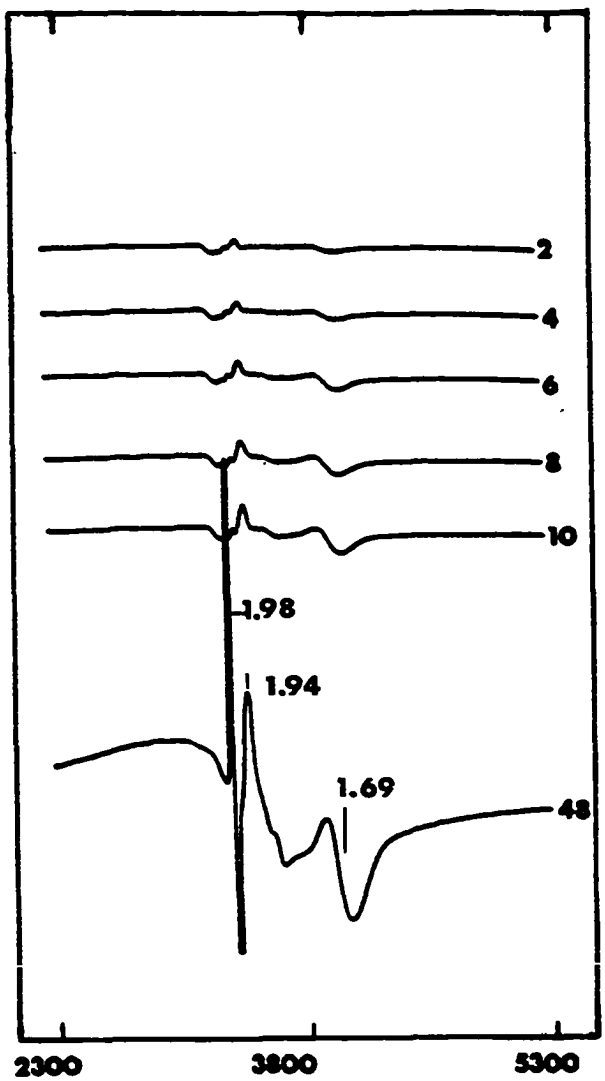
2
4
6
8
10
1.98
1.94
1.69
48
2300
3800
5300
Gauss

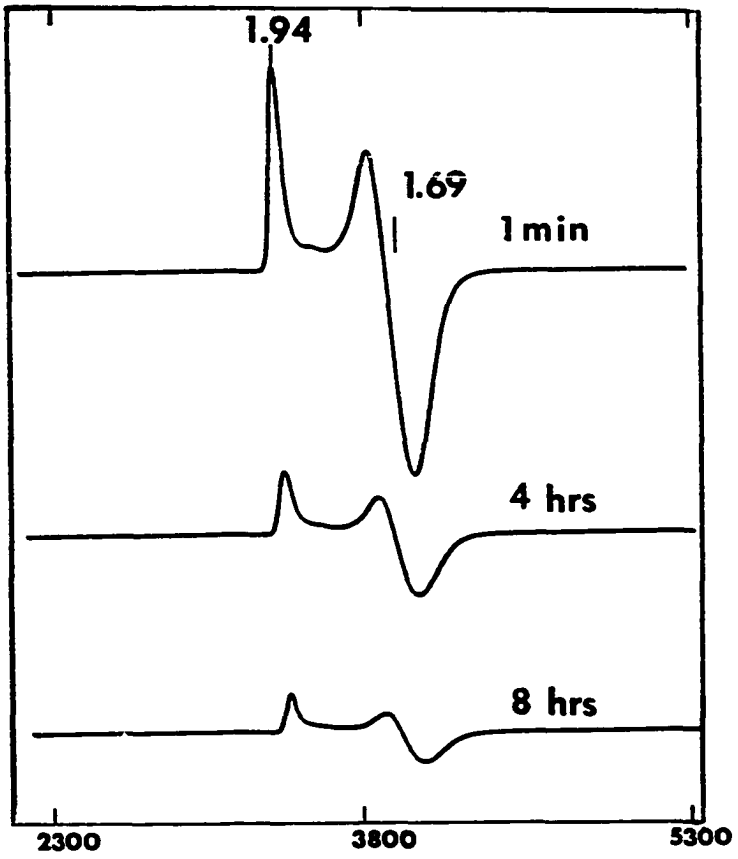

pH 6.3, 50 mM MES, 0.15 M Na_2SO_4, and one equivalent of $K_3Fe(CN)_6$. EPR samples frozen at one minute, four hours, and eight hours. Temperature 4.2 K; frequency 9.57 GHz; power 0.2 mW; gain 3.2 x 10^4; modulation 16 G at 100 KHz; time constant 0.1 sec.

Figure III-7. EPR spectra of 1.0 mM $(semi\text{-}met)_o$ incubated at room temperature at pH 6.3

perchlorate.

Detection of the thioester intermediate seems possible and would provide further evidence for the suggested mechanism. Chromate thioesters absorb in the visible region around 420-440 nm with extinction coefficients of ~ 3000 $M^{-1}cm^{-1}$ (3). If an excess of deoxy over chromate is used, the thioester absorbance may be observable, since there is no absorbance in this region from deoxyHr. If the thioester is not observed, an alternative site for the binding of chromate may be responsible for the observed kinetics.

Using an excess (~ 10 fold) of deoxyHr (~ 0.3 mM) over chromate (~ 0.03 mM) no change in the UV-visible absorbance spectrum from 400-450 nm was observed over the period of an hour at 25 °C. Under similar conditions, the formation of a thioester is observed in two minutes during the reaction of chromate with excess glutathione (3). This would indicate that no thioester is formed initially. Unless further evidence can be found, it must then be assumed that the reaction must proceed by an alternate mechanism. This alternate mechanism may account for the length of the reaction.

A mechanism may be written as follows:

$$HCr(VI)O_4^- + Hr[Fe(II,II)] \rightarrow \underset{\underset{OH}{|}}{Cr(VI)O_3^-}...Hr[Fe(II,II)]$$

$$\underset{\underset{OH}{|}}{Cr(VI)O_3^-}...Hr[Fe(II,II)] \xrightarrow{k_{obs}} Cr(V)...Hr[Fe(II,III)]$$

$$Cr(V)...Hr[Fe(II,II)] \longrightarrow Cr(V) + Hr[Fe(II,III)]$$

Cr(V) may be further reduced to Cr(III) by deoxyHr. In essence, it can be suggested that a binding site for chromate, other than the single thiol group, exists on Hr. The binding of chromate at this alternate site may also account for the stability of the $(semi\text{-}met)_oHr$ produced by chromate oxidation of deoxyHr. The lengthy oxidation of deoxyHr may be due to the use of an alternate pathway for electron transfer other than the cysteine thiol group.

The resulting stable $(semi\text{-}met)_oHr$ from the oxidation of deoxyHr by chromate may be the best candidate to obtain ^1H NMR of $(semi\text{-}met)_oHr$. $(Semi\text{-}met)_oHr$ prepared by $Fe(CN)_6^{3-}$ oxidation appears to disproportionate too quickly at the temperatures necessary to obtain good ^1H NMR spectra (~ 40 °C). This is an obvious area of continuing research.

Another area of research suggested by this work is the

mechanism of oxidation of intracellular Hr by chromate. The very different EPR signals obtained in Figures III-1 versus III-3 to III-5 suggest different semi-met products of oxidation of intracellular versus purified Hr.

References Cited

1. Connett, P. H.; Wetterhahn, K. E. Structure and Bonding 1983, 54, 94-122.

2. Wetterhahn-Jennette, K. J. Am. Chem. Soc. 1982, 104, 874-875.

3. Connett, P. H.; Wetterhahn, K. E. J. Am. Chem. Soc. 1985, 107, 4282-4288.

4. Sjoberg, B.; Graslund, A. Adv. Inorg. Biochem. 1983, 5, 87-110.

5. Bradić, Z.; Harrington, P. C.; Wilkins, R. G.; Yoneda, G. Biochemistry 1980, 19, 4149-4155.

6. Utecht, R. E. Ph. D. thesis, Iowa State University, 1986.

7. Klotz, I. M.; Klotz, T. A.; Fiess, H. A. Arch. Biochem. Biophys. 1957, 68, 284-299.

8. Garbett, K.; Darnall, D. W.; Klotz, I. M.; Williams, R. J. P. Arch. Biochem. Biophys. 1969, 135, 419-434.

9. Utecht, R. E.; Kurtz, D. M., Jr. Inorg. Chem. 1985, 24, 4458-4459.

10. Russev, P.; Mitewa, M.; Bontchev, P. R. J. Inorg. Nucl. Chem. 1981, 43, 55-40.

11. Kon, H. J. Inorg. Nucl. Chem. 1963, 25, 933-944.

12. Espenson, J. H. J. Am. Chem. Soc. 1964, 86, 5101-5107.

13. Lukat, G. S., Ph. D. thesis, Iowa State University, 1985.

GENERAL CONCLUSIONS

A variety of approaches has been used in this study to examine some of the electron transfer properties of Hr. In Section I, the reduction of met to deoxyHr is examined using not only kinetic studies but in depth physical characterization of the products at intermediate stages of reduction. EPR, UV-visible, ^{1}H NMR and Mössbauer spectroscopies have provided evidence for a new mechanism of reduction of metHr to the deoxy oxidation level. The mechanism, proposed in Section I seems to resolve the controversy recently generated in the literature concerning the reduction mechanisms of metHrs from the two species T. zostericola and P. gouldii. It has long been noted that P. gouldii semi-metHr disproportionates only 10-20% while the T. zostericola species disproportionates completely to 1/2 met and 1/2 deoxy. The mechanism proposed takes these facts into account and yet a similar mechanism for both proteins can be envisaged. In brief, a similar conformational change is proposed to occur for both species of Hr at the semi-met level, perhaps involving a reversal of oxidation states, i. e. Fe(III),Fe(II) $\rightleftharpoons$ Fe(II),Fe(III). The conformational change appears to be the rate determining step which then allows quick reduction of P. gouldii semi-metHr to the deoxy level (with a slight amount of disproportionation) while T.

zostericola semi-metHr appears to disproportionate to a larger extent after a similar conformational change.

The two species of Hr have similar amino acid compositions but are only approximately 80% homologous. A crystal structure of T. zostericola Hr has not been obtained as of this date as P. gouldii and other species of Hr have been easier to crystallize. It would be interesting if such a structure was available to try to determine what aspects of the structure of T. zostericola Hr allow a greater degree of disproportionation.

It has also been proposed that conformational changes figure largely in the mechanism of reduction of both species of Hrs. Indeed, the rate determining step of the third stage is proposed to consist of a conformational change of met' to metHr. A number of other reactions of Hr are also dependent upon conformational changes such as the $Fe(CN)_6^{3-}$ oxidation of $(semi\text{-}met)_O Hr$ at pH 8.2 (see Table 4). Conformational changes may determine the rate of several electron transfer reactions in Hr. Not the least of these conformational changes is the O → R conversion. Further elucidation of the physical characteristics of these two conformations has not been forthcoming and is an area of continuing research. The new results presented here suggest that one difference between O and R may be the reversal of iron oxidation states. The present study indicates that the iron which is closer to the

Table 4. Reactions of Hr dominated by a first order conformational change (20)

Protein form	Reactant (pH)	Rate Constant s^{-1}
octameric(P.gouldii) metHr	acid⟷base interconversion (pH 8.2)	3.3×10^{-3}
	SCN^- (9.0)	5.0×10^{-3}
	$S_2O_4^{2-}$(9.0)	2.7×10^{-3}
	thiol reagents (9.0)	2.0×10^{-3}
	SDS (7.8)	2.11×10^{-3}
semi-metHr	O→R forms and $Fe(CN)_6^{3-}$ oxidation (pH8.2)	1.3×10^{-3}
semi-metHr	intramolecular disproportionation pH 8.2	2.2×10^{-3}
monomer (T.zostericola) metmyoHr	acid-base interconversion (7.0)	7.2×10^{-3}
	SCN^-	3.2×10^{-3}
	$S_2O_4^{2-}$(8.2)	3.5×10^{-3}
semi-metmyoHr	O→R forms (8.2)	1.0×10^{-2}

protein surface is easier to reduce in an outer sphere fashion than the iron which is more buried within the protein matrix (the more buried iron binds oxygen). An intrasubunit shuttling of electrons and the reordering of the tertiary structure of Hr is a possible key to the O R conformational conversions. The results in Section I provide a context for examinations of reduction of metHr by the presumed physiological reducing agent, cytochrome b_5.

Section II applies Marcus theory to Hr redox reactions using inorganic reagents and heme proteins. Many research groups have applied Marcus theory to proteins using inorganic reagents and proteins. The usual approach is to use inorganic redox reagents with various reduction potentials and compare the experimentally obtained rate constant with that calculated by use of Marcus theory. Wilkins et al. (20) have used several free radical reducing agents and obtained a good correlation with the Marcus theory in the reduction of metHr to the semi-met oxidation level. Few research groups have changed the reduction potential of a protein (21) with presumably little change in protein matrix, as has been done here with μ-S^{2-}metHr versus native Hr. Good agreement with the Marcus relation is obtained in the reducing direction, met to semi-met when using both inorganic reagents and heme proteins as reducing reagents. Good agreement with theory in the oxidizing direction is obtained with $Fe(CN)_6^{3-}$.

The use of a presumably physiologically relevant protein, P.g. $cytb_5$ (19), versus Mb as a reducing agent also has some further implications for physiological electron transfer reactions in general. The fact that the Marcus relation can account for the increase in rates observed when P.g. $cytb_5$ is used as a reducing agent with met- and μ-S^{2-}metHrs versus those with deoxyMb, implies that the use of a physiologically relevant protein in biological electron transfer reactions does not increase the rate of electron transfer over what would be expected from the Marcus relation (22). This "nonspecificity" in electron transfer protein-protein reactions has been observed by other workers most notably Gray and co-workers. If binding occurs between Hr and P.g. $cytb_5$, possibly electrostatic in nature, it is not to increase the rate of electron transfer.

The last section of this study concerns the oxidation of deoxyHr to the semi-met oxidation level. A stable $(semi\text{-}met)_O$ product is formed which may enable future researchers to obtain good ^1H NMR of $(semi\text{-}met)_O$. If ^1H NMR spectra of $(semi\text{-}met)_R$ can also be obtained, these spectra would aid in understanding the nature of the differences existing between these two conformations of Hr. The initial chromate reaction appears to produce a form of Hr which has not been previously observed. Further study of the products and mechanism of the chromate oxidation of deoxyHr may provide insight into the

carcinogenicity of chromate as well as provide more information about the redox properties of Hr within the erythrocytes.

LITERATURE CITED FOR GENERAL INTRODUCTION AND GENERAL CONCLUSION

1. Wilkins, R. G.; Harrington, P. C. Adv. Inorg. Biochem., 1983, 5, 51-85.

2. Klotz, I. M.; Kurtz, D. M., Jr. Acc. Chem. Res. 1984, 17, 16-22.

3. DePhillips, H. A. Arch. Biochem. Biophys. 1971, 144, 122-126.

4. Groskopf, W. R.; Holleman, J. W.; Margoliash, E.; Klotz, I. M. Biochemistry 1966, 5, 3783-3796.

5. Clarke, S. E.; Sieker, L. C.; Stenkamp, R. E.; Loehr, J. S. Biochemistry 1979, 18, 684-689.

6. Keresztes-Nagy, S.; Klotz, I. M. Biochemistry 1965, 4, 919-931.

7. a) Stenkamp, R. E.; Jensen, L. H. Inorg. Biochemistry 1979, 1, 219-233. b) Stenkamp, R. E.; Sieker, L.; Jensen, L. H. J. Am. Chem. Soc. 1984, 106, 618-622.

8. Stenkamp, R. E.; Sieker, L. C.; Jensen, L. H.; McCallum, J. D.; Sanders-Loehr, J. Proc. Natl. Acad. Sci. USA 1985, 82, 713-716.

9. Okamura, M. Y.; Klotz, I. M.; Johnson, C. E.; Winter, M. R. C.; Williams, R. J. P. Biochemistry 1969, 8, 1951-1958.

10. Garbett, K.; Johnson, C. E.; Klotz, I. M.; Okamura, M. Y.; Williams, R. J. P. Arch. Biochem. Biophys. 1971, 142, 574-583.

11. Lukat, G. S.; Kurtz, D. M., Jr.; Shiemke, A. K.; Loehr, T. M.; Sanders-Loehr, J. Biochemistry 1984, 23, 6416-6422.

12. Kurtz, D. M., Jr.; Sage, T. J.; Hendrich, M.; Debrunner, P. G.; Lukat, G. S. J. Biol. Chem. 1983, 258, 2115-2118.

13. Maroney, M. J.; Kurtz, D. M., Jr.; Nocek, J. M.; Pearce, L. L.; Que, L., Jr. submitted to J. Am. Chem. Soc.

14. Bradić, Z.; Wilkins, R. G. Biochemistry 1983, 22, 5401-5409.

15. Garbett, K.; Darnell, D. W.; Klotz, I. M.; Williams, R. J. P. Arch. Biochem. Biophys. 1969, 135, 419-434.

16. Loehr, J. S.; Loehr, T. M.; Mauk, A. G.; Gray, H. B. J. Am. Chem. Soc. 1980, 102, 6992-6996.

17. Muhoberac, B. B.; Wharton, D. C.; Babcock, L. M.; Harrington, P. C.; Wilkins, R. G. Biochem. Biophys. Acta 1980, 626, 337-345.

18. Olivas, E.; deWaal, D. J.; Wilkins, R. G. J. Inorg. Biochem. 1979, 11, 205-212.

19. Utecht, R. E.; Kurtz, D. M., Jr. Inorg. Chem. 1985, 24, 4458-4459.

20. Bradić, Z.; Tsukahara, K.; Wilkins, P. C.; Wilkins, R. G. in "Frontiers in Bioinoganic Chemistry" Xavier, A. V., Ed. 1986, VCH Publishers: Deerfield Beach, FL p. 336-344.

21. Lim, A. R.; Mauk, A. G. Biochem. J. 1985, 229, 765-769.

22. Wherland, S.; Gray, H. B. in "Biological Aspects of Inorganic Chemistry" Addison, A. W.; Cullen, W. R.; Dolphin, D.; James, B. R., Eds. 1977, Wiley-Interscience: New York, p. 289-368.

APPENDIX A: $Cr^{2+}(aq)$ SCRUBBING TOWERS

A $Cr^{2+}(aq)$ scrubbing tower used to remove trace amounts of oxygen from nitrogen is shown in Figure A-1. Two towers are normally employed in series. Bubble nitrogen through towers until solution is a baby blue color. Replace Zn/amalgam and solution when color changes.

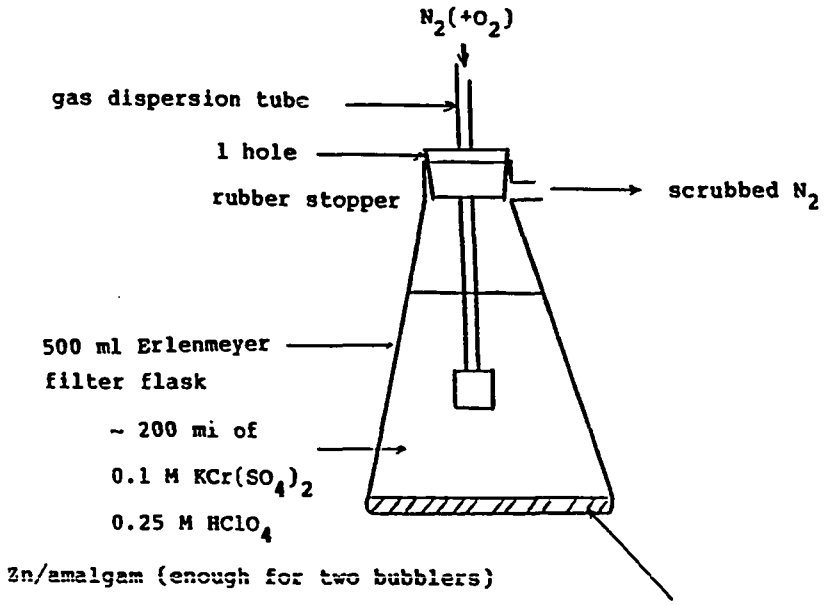

1) Clean 120 g of zinc metal in dilute HCl (0.1 M) for 10 minutes.
2) Dissolve 3.6 g of HgO in ~ 5 ml of concentrated HCL.
3) Wash HCl off of the cleaned zinc with distilled water. Leave Zn in enough water to cover it and add the HgO solution while stirring.
4) Drain off amalgamated Zn twice, then dry amalgamated Zn on paper towel.

Figure A-1. $Cr^{2+}(aq)$ scrubbing tower

APPENDIX B: CALIBRATION OF EPR CRYOSTAT TEMPERATURE

Using Equation 1,

$$\ln R + K/\ln R = A + B/T \qquad (1$$

where A, B and K are constants, R is the resistance, and T is the temperature in K. A standard curve for a resistor was determined by measurement of the resistor at three fixed temperatures. Once constants A, B and K are determined by this procedure, the resistance of the resistor in the operating cryostat could be measured, and, thus, the temperature could be calculated.

A 1/8 W Allen Bradley resistor (room temperature resistance 560 Ω) was used. Magnesium wire with 12.4 Ω/foot was used for leads to voltmeter, v, and ampmeter, I, (Figure B-1). Separate current and voltage leads were soldered to the 560 Ω resistor. The 560 Ω resistor was placed in an EPR tube and surrounded with glycerol.

Figure B-1. Circuit diagram for cryostat temperature determination

One MΩ resistor was placed in power supply circuit to keep the measuring current constant, at slightly under 10 μA. The voltage and current were then measured at three fix points (liquid He, 4 K; liquid nitrogen, 77 K; ice water, 273 K) and the resistance calculated using Equation 2.

$$V = IR \qquad (2$$

A, B and K in Equation 1 were determined by solving three simultaneous equations using the temperatures and calculated resistances above. The voltage and current were then measured with the resistor in the EPR tube placed in the operating EPR cryostat and the resistance, R, calculated using Equation 2. Using the previously determined values of A, B and K, the calculated resistance from the EPR cryostat and substituting these values into Equation 1, the temperature at the sample position in the operating cryostat was determined.